DYNAMICAL MODEL OF THE Σ

Thesis by

Boris Jules Kayser

In Partial Fulfillment of the Requirements

For the Degree of

Doctor of Philosophy

California Institute of Technology

Pasadena, California

1964

(Submitted May 20, 1964)

ACKNOWLEDGEMENTS

iii

ABSTRACT

In the spirit of the bootstrap hypothesis, a dynamical model is developed for the Σ hyperon, taking into account the $\pi\Lambda$ and $\pi\Sigma$ channels. Born amplitudes for the exchange of Λ, Σ, Y_1^* (1385 Mev), Y_o^* (1405 Mev), and ρ form the inputs to dynamical calculations which utilize an extension of the matrix ND^{-1} method. The properties of all particles other than the Σ are taken from experiment, or, where they are experimentally uncertain, estimated on the basis of current theoretical ideas and then varied in the calculations. The cutoff which governs the damping of the input amplitudes at high energies is also varied. It is found that quite a few combinations of the experimental unknowns and the cutoff do lead to a self-consistent $\frac{1}{2}^+$, $I = 1$ $\pi\Lambda-\pi\Sigma$ bound state, identified as the Σ, with reasonable values for the mass M_Σ and couplings $g^2_{\pi\Lambda\Sigma}/4\pi$ and $g^2_{\pi\Sigma\Sigma}/4\pi$. These results favor the conjecture that the Σ is a composite particle.

TABLE OF CONTENTS

I. INTRODUCTION

The bootstrap idea is that the family of strongly interacting particles generates itself. Each particle is a composite object, being a bound or resonant state of all the multi-particle systems with which the various conservation laws allow it to communicate. The binding forces come from exchange of the strongly interacting particles themselves; hence the self-generation. In the mathematics corresponding to this idea, one has equations which, hopefully, can eventually be built up to the point where they determine all the masses and coupling strengths of the strongly interacting particles, and possibly their quantum numbers as well. These relations are based simply on the self-consistency requirement that the particles producing the forces be the same as the particles these forces produce.

In practice, a realistic calculation involving all of the baryons and mesons (stable and unstable) simultaneously would be out of the question. One therefore looks for situations where a small number of particles (e.g., one or two) are expected to support themselves, largely without outside help or interference. An illustration is the early bootstrap of the ρ meson.[1] The ρ was pictured as primarily a ππ resonance; other "channels" with which

the ρ can communicate, such as $\pi\omega$, were neglected. Having
tentatively decided what a dynamical ρ is made of, one has
to find out what forces operate between the constituents,
and verify that the forces are indeed attractive and pro-
duce the ρ resonance. The forces which the pions feel
come from the exchange of various objects between them,
and one hopes that the most important forces will be the
long-range ones caused by the exchange of light objects.
The least massive system that two pions can exchange is
a pion pair. Since pion pairs exhibit the very prominent
ρ resonance, one can try to approximate the influence of
the exchanged pion pair by finding instead the force pro-
duced by an exchanged ρ. The latter force does indeed
turn out to be attractive in the p-wave, $I=1$ $\pi\pi$ state,
where the ρ resonance appears. And a dynamical calcula-
tion with the ρ force as input, neglecting all shorter
range effects, does show that a $\pi\pi$ resonance with the ρ
quantum numbers is produced. Variation of the input ρ
mass and width until consistency between these quantities
and the corresponding outputs is achieved yields a mass
of 350 Mev and $\rho\pi\pi$ coupling of $\frac{Y^2_{\rho\pi\pi}}{4\pi} = 2.4$. These numbers
do not compare well with the actual values of 750 Mev
and .5, but the calculation is still qualitatively success-
ful in that the dominant force turns out to be attractive
and does produce a self-consistent resonance.

The present work is a dynamical explanation of the Σ hyperon along the lines of the bootstrap philosophy. The Σ is pictured as partly a $\pi\Lambda$ and partly a $\pi\Sigma$ bound state. To the extent that multi-particle exchanges can be approximated by resonance exchanges, all long and medium long range forces are taken into account. Actually, quite a number of particles contribute forces which influence the properties of the Σ. Since it would be impractical to bootstrap all of these particles simultaneously with the Σ, the properties of the other particles have been taken from experiment, or from some other theory. In other words, we have tried to show that in a universe where all particles other than the Σ already exist with their observed properties, the Σ should also exist as a dynamically produced bound state.

The purposes of the calculation are twofold. First, to shed light on the question of whether the Σ in particular is a composite object, and hence to increase our information on the question of whether all the strongly interacting particles are composite. Secondly, to study the detailed techniques of the bootstrap theory as applied in a somewhat new and more elaborate way than previously.

II. THE MODEL OF THE Σ

A Σ can be made up out of $\pi\Lambda$, $\pi\Sigma$, $2\pi\Lambda$, $\overline{K}N$, $2\pi\Sigma$, πY_1^*, etc. The physical scattering thresholds of these

TABLE 2.1. Thresholds of channels which can

couple to the Σ

Channel	Threshold (Mev)
$\pi\Lambda$	1255
$\pi\Sigma$	1330
$2\pi\Lambda$	1395
$\overline{K}N$	1440
$2\pi\Sigma$	1470
πY_1^*	1525

channels are indicated in Table 2.1. Intuitively, one
expects the channel with the lowest threshold, $\pi\Lambda$, to
be the most important. Furthermore, if one thinks of
the other channels as coming in through virtual tran-
sitions of the Σ state between its $\pi\Lambda$ mode and its higher
threshold modes, then one expects the influence of a
given channel to be smaller the further its threshold
is from that of the $\pi\Lambda$ channel, because of the greater
violation of energy conservation involved. Also, because
of the existence of the baryon and meson resonances, it
can tentatively be hoped that the main effects of a three

particle channel such as $2\pi\Lambda$ will come from situations in which the $2\pi\Lambda$ system is in a two-particle state like πY_1^* or $\rho\Lambda$. This is because two-particle phase space is larger than that for three particles, so that transitions to a two-particle state are more likely. Thus the effective $2\pi\Lambda$ threshold is 1525 Mev, not 1395 Mev.

The simplest thing to try is a model in which only the $\pi\Lambda$ channel is included. Table 2.1 makes it clear, however, that the neglect of the other channels, particularly $\pi\Sigma$, is likely to be a very bad approximation. Indeed, calculations based on the $\pi\Lambda$ channel alone have shown severe sensitivity of the results to the crudely represented high-energy effects.[2]

Thus it is evident that a treatment of the Σ must take into account the lowest two channels, at the very least, and probably should include more. Beyond two channels, however, the amount of electronic computing time involved becomes prohibitive, so it was decided to try to build a model of the Σ based on the $\pi\Lambda$ and $\pi\Sigma$ states.

Suppose the two-channel treatment is successful in predicting that the Σ is a dynamical particle. Could this conclusion be changed by the inclusion of the first omitted channel, $\bar{K}N$? When three channels are included the Σ will spend part of its time in a $\pi\Lambda$ or $\pi\Sigma$ state, in which,

as we shall see, the forces are attractive, and the rest
in a $\bar{K}N$ state. If the forces in the $\bar{K}N$ state are wildly
repulsive, then the inclusion of the $\bar{K}N$ channel could
drastically affect our results. If, on the other hand,
the forces in the $\bar{K}N$ channel are attractive and of moderate
strength, then they are just like the forces which the Σ
already encounters in the $\pi\Lambda$ and $\pi\Sigma$ channels, and thus
they can hardly destroy the bound state.

The principal forces in the $\bar{K}N$ channel are expected
to come from ρ, ω, and φ exchange:

$$\bar{K} \quad N$$
$$\rho, \omega, \phi$$
$$\bar{K} \quad N$$
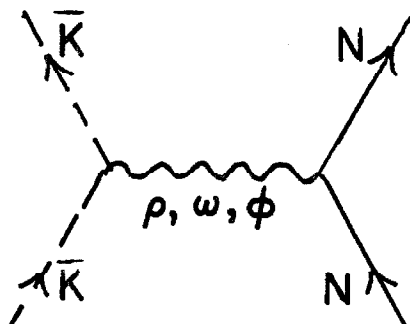
(Baryon exchange is impossible because the baryon would
have to have strangeness +1.) If the ρ couples univer-
sally to the isospin current, then the ρ force will be
repulsive in the $I = 1$ state (which is the state of
interest because the Σ has $I = 1$), where the $\bar{K}$ and N
isospins are parallel. As for the ω and φ, presumably
some combination of them, ω_B, couples to the baryon
current, while the orthogonal combination, ω_Y, couples
to the hypercharge current. ω_B makes no contribution

because the $\bar{K}$ is not a baryon, but m_Y will produce an attractive force, since the $\bar{K}$ and N hypercharges have opposite sign. Together, the ω and φ thus produce an attraction.

By looking at KN scattering, where the ρ and $\omega - \varphi$ exchange contributions are simply related to the corresponding forces in the $\bar{K}N$ case, Dalitz verified the above conjectures about the signs of the forces, and found that the $\omega - \varphi$ contribution is more than 3 times stronger than that of the ρ.[3] Thus the force in the I = 1 state of the $\bar{K}N$ channel is attractive, and the inclusion of the $\bar{K}N$ channel is not likely to wipe out the bound state predicted on the basis of the two-channel model, although it could cause significant changes in the numerical results obtained there.

By now it is quite well-established that the relative $\Sigma\Lambda$ parity is even,[4] so we shall look for the Σ as a $p_{\frac{1}{2}}$, I = 1 $\pi\Lambda-\pi\Sigma$ bound state.

The particle exchanges which lead to forces in the $\pi\Lambda$ and $\pi\Sigma$ channels, as well as to $\pi\Lambda - \pi\Sigma$ transitions, are shown in Fig. 2.1. Multi-particle exchanges are approximated by resonance exchanges; hopefully the non-resonant contributions thus omitted are small. All established particles with masses up to about 1400 Mev are taken into account as possible sources of force.

FORCES IN πΛ CHANNEL
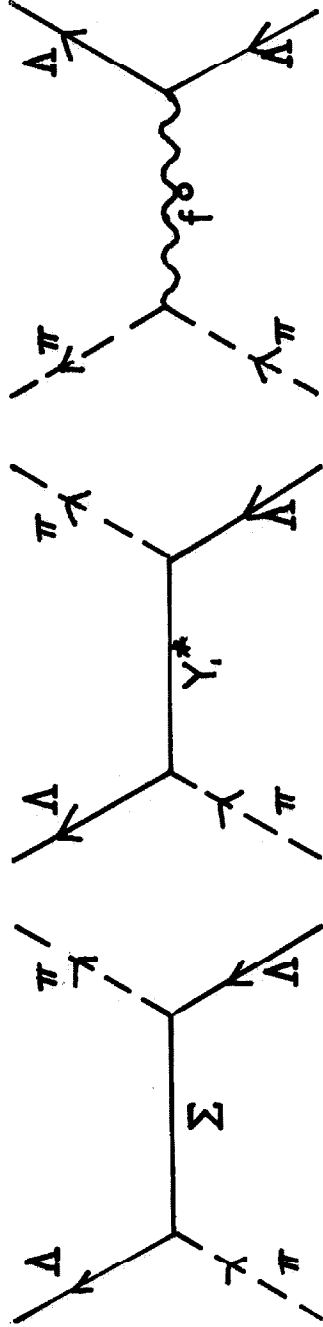
πΛ→πΣ TRANSITIONS MEDIATED BY PARTICLE EXCHANGE
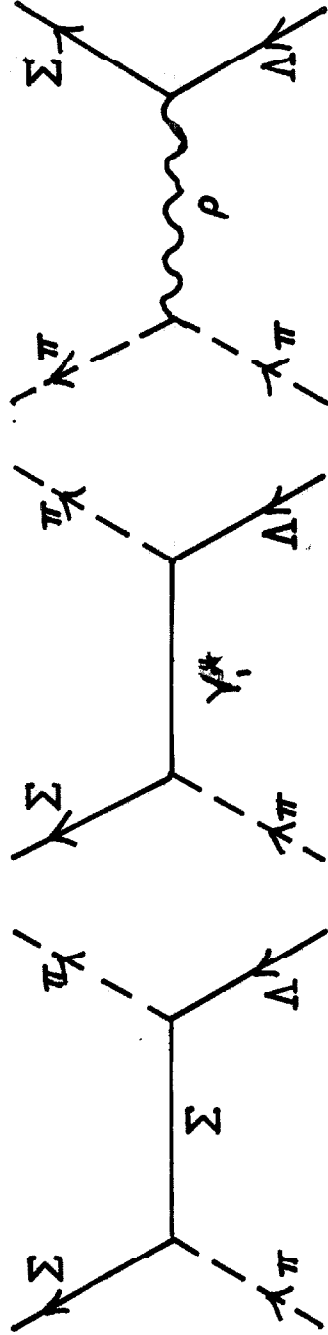
(a)

FORCES IN $\pi\Sigma$ CHANNEL

(b)

Figure 2.1. $\pi\Lambda$ and $\pi\Sigma$ forces, and $\pi\Lambda - \pi\Sigma$ transitions due to particle exchange. The diagrams for $\pi\Sigma \to \pi\Lambda$ transitions are the same as those shown for $\pi\Lambda \to \pi\Sigma$ transitions upside down. The Y_1^* and Y_0^* referred to are the 1385 Mev and 1405 Mev resonances.
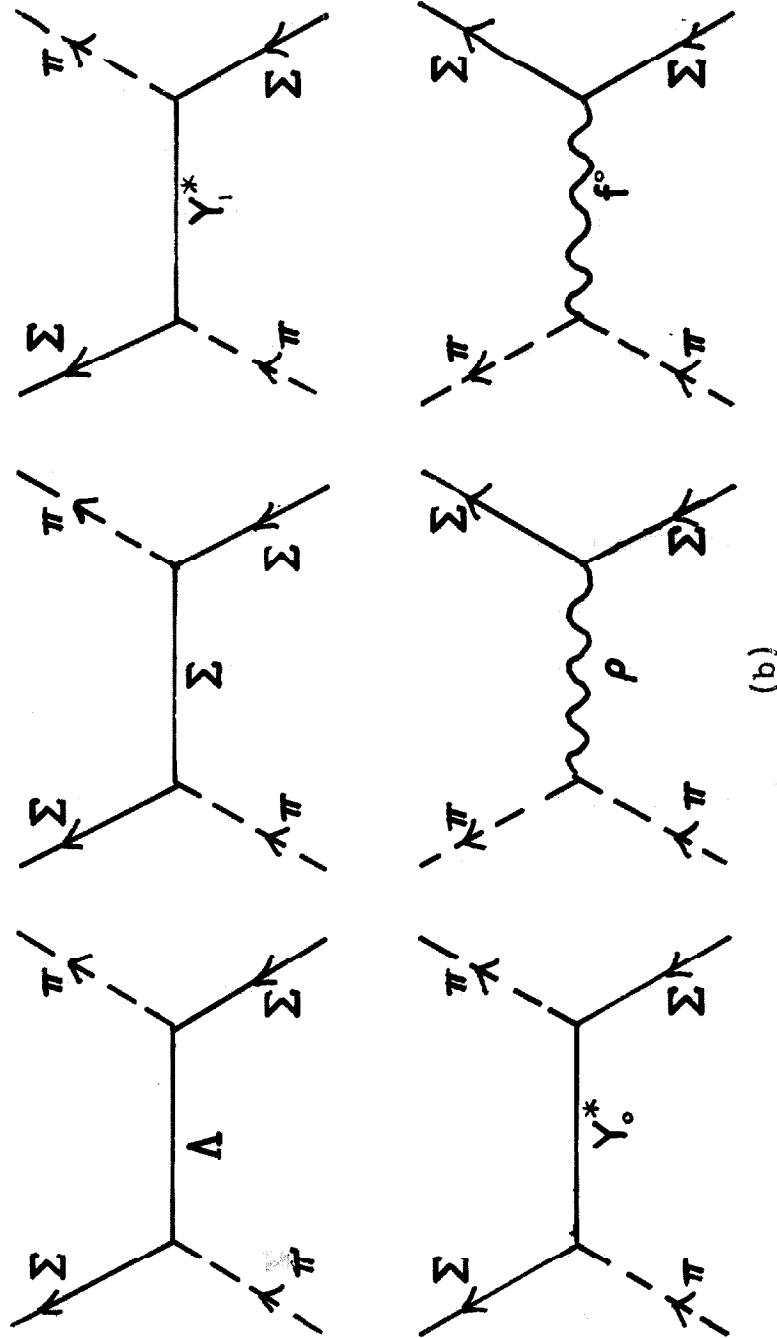
It would be pointless to include higher mass exchanges
explicitly, since we are already neglecting the high-
energy effects associated with the channels above $\pi\Sigma$.

To substantiate our model of the Σ as a $\pi\Lambda - \pi\Sigma$
bound state, we must verify that the forces we've listed
add up to a net attraction, and, by putting these forces
into some dynamical scheme which plays the role assumed
by Schrodinger's equation in simple problems, we have to
show that these forces in fact produce a bound state. We
also hope to be able to make this bound state self-con-
sistent, so that the Σ which emerges as an output has
identically the same properties as the Σ which entered
as an input.

Of course, as the reader realizes, some of the
properties of the particles which appear here are experi-
mentally uncertain (e.g., spin and parity, widths). As
discussed in detail in Section V, these uncertain quanti-
ties have been estimated on the basis of both current
theoretical ideas and any available experimental evidence,
and have been varied in the calculations, so that our
results can be stated for quite a wide range of values
of the things we don't yet know too well.

III. S-MATRIX THEORY AND THE ND^{-1} METHOD

The dynamical calculations will be done with the dispersion techniques based on the unitarity and analyticity of the S-matrix. The Σ bound state will be sought for as a pole in the matrix of $p_{\frac{1}{2}}$, $I = 1$ $\pi\Lambda$-$\pi\Sigma$ scattering amplitudes. If we call the $\pi\Lambda$ system channel 1 and the $\pi\Sigma$ channel 2, then the ij element of this 2 x 2 matrix is just the $\frac{1}{2}^{+}$, $I = 1$ partial wave amplitude for scattering (inelastically if $i \neq j$) from channel j to channel i. Symbolically:

$$\text{Scattering Matrix} = \begin{pmatrix} \mathcal{Q}(\pi\Lambda \to \pi\Lambda) & \mathcal{Q}(\pi\Sigma \to \pi\Lambda) \\ \mathcal{Q}(\pi\Lambda \to \pi\Sigma) & \mathcal{Q}(\pi\Sigma \to \pi\Sigma) \end{pmatrix}.$$

Because of time-reversal invariance, the phases of the states can be so chosen that the 12 and 21 amplitudes are equal; we will choose them to achieve this equality. Each amplitude in the partial wave scattering matrix is assumed to be a real analytic function in the complex plane of the total center-of-mass energy W, except for the unitarity and force cuts discussed below.

In detail, the particular amplitudes we shall work with are defined in terms of the usual S-matrix as follows. For a transition from state i to state f, we write the S-matrix element in the form[5]

$$S_{fi} = \delta_{fi} - i(2\pi)^4 \delta^{(4)}(p_f + q_f - p_i - q_i) \cdot$$

$$\cdot \sqrt{\frac{M_i M_f}{4 E_f E_i^{(1)} f^{(1)}_i}} \; \bar{u}_f T u_i , \qquad (3.1)$$

where M, p, E, u are the mass, 4 - momentum, total energy, and Dirac spinor for the initial or final baryon, depending on the index, and q, ω are the corresponding 4 - momentum and total energy of the initial or final pion.[6] The matrix T can always be written as

$$T = -A + i\not{Q}B; \quad Q = \frac{q_i + q_f}{2} , \qquad (3.2)$$

in which A and B are functions of the usual invariants s, t, u, and also depend on the initial and final charge states ($\not{Q} \equiv \gamma_\mu Q_\mu$). In the center-of-mass frame, we define f_1 and f_2, simply related to the spin-flip and non-flip amplitudes, by expressing the barycentric differential cross section, for specific initial and final spin states, in the form ($\vec{\sigma}$ is the Pauli spin matrix)

$$\left(\frac{d\sigma}{d\Omega}\right)_{fi} = \frac{q_f}{q_i} \left| \left\langle f \left| f_1 + \frac{\vec{\sigma} \cdot \vec{q_f}}{q_f} \frac{\vec{\sigma} \cdot \vec{q_i}}{q_i} f_2 \right| i \right\rangle \right|^2 . \qquad (3.3)$$

$\vec{q}$ and q (f or i) now refer to the pion momentum and its magnitude in the center-of-mass. By comparison, the cross section is related to $\bar{u}_f T u_i$ by

$$\left(\frac{d\sigma}{d\Omega}\right)_{fi} = \left| -\sqrt{\frac{q_f}{q_i}} \sqrt{\frac{M_i M_f}{4\pi W}} \; \bar{u}_f T u_i \right|^2 . \tag{3.4}$$

Writing $\bar{u}_f T u_i$ out in terms of Pauli spinors and matrices, one finds that

$$f_1 = \frac{\sqrt{(E_i + M_i)(E_f + M_f)}}{8\pi W} \left[A + \left(W - \frac{M_i + M_f}{2} \right) B \right]$$

$$f_2 = \frac{\sqrt{(E_i - M_i)(E_f - M_f)}}{8\pi W} \left[-A + \left(W + \frac{M_i + M_f}{2} \right) B \right] \tag{3.5}$$

Denote by $S_{\ell\pm}$ the S-matrix element between states of definite orbital angular momentum ℓ, and definite total angular momentum $J = \ell \pm \frac{1}{2}$. The customary partial wave amplitudes $f_{\ell\pm}$ are then defined by

$$f_{\ell\pm} = \frac{(S - 1)_{\ell\pm}}{2i \sqrt{q_i q_f}} . \tag{3.6}$$

In terms of these partial wave amplitudes, f_1 and f_2 are

$$f_1 = \sum_{\ell = 0}^{\infty} f_{\ell +} \; P'_{\ell + 1}(\cos \theta) - \sum_{\ell = 2}^{\infty} f_{\ell -} \; P'_{\ell - 1}(\cos \theta)$$

(3.7)

$$f_2 = \sum_{\ell = 1}^{\infty} (f_{\ell -} - f_{\ell +}) \; P'_{\ell} (\cos \theta).$$

(Here $P'_{\ell} (\cos \theta)$ is the derivative of the usual Legendre polynomial.) The inverse relations are

$$f_{\ell \pm} = \tfrac{1}{2} \int_{-1}^{1} d(\cos \theta) \left[f_1 P_{\ell} (\cos \theta) + f_2 P_{\ell \pm 1}(\cos \theta) \right].$$

(3.8)

We shall assume, in accordance with the Mandelstam representation and with the indications from perturbation theory, that the Lorentz-invariant amplitudes A and B can be written in terms of s, t, and u alone, with no dependence on quantities like $\sqrt{s}$. In that case, it follows from (3.5) and (3.8) that the $f_{\ell \pm}$, as functions of W, have the MacDowell reflection property:

$$f_{\ell +} (-W) = - f_{(\ell + 1) -}(W).$$

(3.9)

This says that the two amplitudes for the same J but opposite parity are simply reflections of each other through $W = 0$, apart from a minus sign.

The $p\frac{1}{2}$ amplitude $f_1 - (\equiv f_{p\frac{1}{2}})$ as defined above has a number of purely kinematical singularities and zeroes which we would like to eliminate. This is both so that kinematical singularities will not be confused with the dynamical singularities of interest, and so that the important general features of the true scattering amplitude will automatically be maintained by the approximation techniques to be introduced. In removing the kinematic singularities, we would like to leave the present asymptotic behavior of $f_{p\frac{1}{2}}$, which goes to 0 as $\frac{1}{W}$ or faster at large W, unaffected, for reasons which will become clear.

Working in the W plane, the properties to be "corrected" are (1) Threshold zeroes: It follows from the assumption that A and B satisfy the Mandelstam representation that $f_{p\frac{1}{2}} \propto (q_i q_f)$ (more generally $f_{\ell\pm} \propto (q_i q_f)^\ell$), not only at the physical scattering threshold, where we expect such behavior, but also at all positive energies W where either q_i or q_f has a zero. From the formulae in Appendix A, these points are $(M_i \pm \mu)$, $(M_f \pm \mu)$. By the MacDowell reflection rule, $f_{p\frac{1}{2}}(W)$ will then go like $(q_i q_f)^0 = $ constant at the negatives of these points.

(2) Double pole at $W = 0$: Due to the factors

$$\frac{\sqrt{(E_i \pm M_i)(E_f \pm M_f)}}{W} = \frac{1}{W^2}\sqrt{\frac{((W \pm M_i)^2 - u^2)}{2}\frac{((W \pm M_f)^2 - \mu^2)}{2}}$$

in f_1 and f_2, (3.5), the amplitude $f_{\ell\pm}$ will have a second-order pole at $W = 0$.

Speaking now of the $p_{\frac{1}{2}}$ amplitude, and suppressing the $\ell\pm$ subscripts, we define the amplitude we shall be working with, h, by

$$h_{fi} = \frac{f_{fi}}{\rho_{fi}} \quad ; \quad \rho_{fi} = \sqrt{\left(\frac{E_f - M_f}{W}\right)\left(\frac{E_i - M_i}{W}\right)} . \quad (3.10)$$

With the observation that, for $j = 1$ or 2 referring to either channel,

$$\frac{q_j}{\sqrt{\frac{E_j - M_j}{W}}} \propto \text{constant near positive energies}$$

W where $q_j \rightarrow 0$, and that

as $W \rightarrow - W$, $\rho_{fi} \rightarrow \sqrt{\left(\frac{E_f + M_f}{W}\right)\left(\frac{E_i + M_i}{W}\right)}$, and that

$$\frac{E_j - M_j}{W} \rightarrow \tfrac{1}{2} \quad \text{as } W \rightarrow \infty,$$

we see that division of f_{fi} by ρ_{fi} cancels all the kine-
matical zeroes, and removes the double pole at $W = 0$, with-
out disturbing either the constant behavior at all the
"thresholds" in the left-hand plane, or the asymptotic
behavior.

We remark that the decision to work in the W plane,
rather than in the $s = W^2$ plane, is motivated by the fact
that as a function of s, $f_{\ell\pm}$ would have a branch point at
$s = 0$, due to the presence of $W = \sqrt{s}$ in (3.5).

Now we can discuss the unitarity and singularities
of the $p_{\frac{1}{2}}$ amplitude h. Figure 3.2 shows the singularities.
In the first place, each amplitude h_{ij} (i and j run from
1 to 2) has the usual "physical" cut on the real W axis
running from the physical threshold of the process $i \leftarrow j$
up to ∞. The physical threshold is the $\pi\Lambda$ threshold for
$\pi\Lambda \rightarrow \pi\Lambda$; for the other three reactions the $\pi\Sigma$ threshold
is the physical threshold. The physical scattering ampli-
tude at energy W for $i \leftarrow j$ is the value of h_{ij} just above
the cut, $h_{ij} (W + i\varepsilon)$. The two-channel unitarity condition
for the amplitudes h_{ij} in their respective physical
regions is

$$\text{Im } h_{ij} (W) = \sum_{k=1}^{2} h^*_{ik} (W) \, \Theta_k (W) \, h_{kj} (W) \; ;$$

where $i,j = 1,2,$ $W \geq$ physical threshold

for $i \leftarrow j$, and is taken <u>above</u> the cut,   (3.11)

and $\theta_k (w) = q_k (w) \rho_{kk} (w) \theta_k (w)$.

Here $\theta_k (w)$ is the unit step function which is 1 above the threshold for channel k and o below. This set of relations is just the two-channel analogue of the familiar statement for a one-channel problem that the partial wave amplitude $\dfrac{S_{\ell\pm} - 1}{2i}$ has the form $\sin \delta_{\ell\pm} e^{i\delta_{\ell\pm}}$ with a <u>real</u> phase shift $\delta_{\ell\pm}$. In writing (3.11), the symmetry of the scattering matrix, $h_{ij} = h_{ji}$, which follows from time-reversal invariance, has been assumed.

It is frequently assumed that the relations represented by (3.11) are true, not only above the physical thresholds, but everywhere above the threshold of the lowest channel ($\pi\Lambda$), for all ij. For $h_{12} = h_{21}$ and h_{22}, this represents an extension of the unitarity condition into the region between $(M_\Lambda + \mu)$ and $(M_\Sigma + \mu)$. Below $\pi\Sigma$ threshold, the unitarity equation for h_{12} or h_{22} does not have the physical significance of a statement of conservation of probability, because we are at unphysical values of W. Consequently, the validity of the extended unitarity conditions cannot be taken for granted, but must be established by looking at perturbation theory or by a procedure of analytic continuation.[7] Let us assume for the

moment that conditions in the present problem are such
that the proofs which have been given apply. Then,
collecting all the amplitudes h_{ij} into a matrix h, and
defining a diagonal matrix Θ (w) with diagonal element
Θ_k (w), we can write

$$\text{Im } h = h^* \Theta h, \text{ at all } W + i\epsilon, W \text{ real, with } W \geqslant \pi\Lambda$$
$$\text{threshold.} \tag{3.12}$$

Since the real analytic function h_{ij} (w) now has a non-
vanishing imaginary part all along the real axis from
$+ \infty$ down to $\pi\Lambda$ threshold, it has a branch cut extending
down to this point. This cut, which goes below the
physical cut except for h_{11}, will be called the unitarity
cut.

By the MacDowell reflection rule, (3.9), there
is also a "unitarity cut" in the left-hand plane, running
from $W = - (M_\Lambda + \mu)$ to $W = - \infty$. Plugging the rule into
the unitarity relation for the right unitarity cut, one
finds that if the definition of the Θ matrix is extended
so that for all (real) W,

$$\Theta(W) = \begin{pmatrix} q_1(|W|)\left(\dfrac{E-M}{W}\right)_1 \theta_1(|W|) & 0 \\ \\ 0 & q_2(|W|)\left(\dfrac{E-M}{W}\right)_2 \theta_2(|W|), \end{pmatrix} \tag{3.13}$$

then above the left unitarity cut we again have

$$\text{Im } h = h^* \Theta h. \tag{3.14}$$

Apart from the unitarity cut, there remain the driving or input cuts, which correspond to processes in which one or more particles are exchanged between the scattering particles. In the elastic amplitudes, h_{11} and h_{22}, these exchanges represent attractive or repulsive forces, while in h_{12} they simply correspond to transitions between the channels mediated by particle exchange. Frautschi and Walecka [8] discuss in detail the locating of the driving cuts by looking at the assumed Mandelstam representation of the invariant amplitudes A and B. Their analysis shows that the exchange cuts can be found simply by locating the singularities of the propagators for the exchanged objects. The exchange of a mass m_e carrying "energy" u(or t) leads to a factor $\dfrac{1}{u - m_e^2}$ (or $\dfrac{1}{t - m_e^2}$)

in the amplitudes A and B for the exchange process. In projecting out the partial waves, we will thus encounter expressions of the form

$$a_\ell(s) = \tfrac{1}{2} \int_{-1}^{1} d(\cos\theta) \; \frac{P_\ell(\cos\theta)}{u - m_e^2} \; .$$

From Appendix A, we have

$$u - m_e^2 = 2q_i q_j \left[\frac{(2\omega_i\omega_j - 2\mu^2) - (s + m_e^2 - \Sigma_{ij})}{2q_i q_j} - \cos\theta \right].$$

Let

$$x_s^e = \frac{(2\omega_i\omega_j - 2\mu^2) - (s + m_e^2 - \Sigma_{ij})}{2q_i q_j} \; , \qquad (3.15)$$

so that

$$u - m_e^2 = 2q_i q_j \left[x_s^e - \cos\theta \right].$$

Then $a_\ell(s)$ becomes

$$a_\ell(s) = \tfrac{1}{2} \int_{-1}^{1} d(\cos\theta) \; \frac{P_\ell(\cos\theta)}{2q_i q_j (x_s^e - \cos\theta)} = \frac{1}{2q_i q_j} Q_\ell(x_s^e) \; .$$

$Q_\ell(x)$ is the Legendre function of the second kind, and has a branch cut running between $x = \pm 1$. (The branch

points associated with the factor $q_i q_j$ are taken care of when the kinematical singularities are eliminated.) In terms of s, the points $x_s^e = \pm 1$ correspond to

$$s = \tfrac{1}{2}\left[(\Sigma_{ij} - m_e^2) + \frac{\sqrt{\beta_i \beta_j}}{m_e^2}\right] \pm$$

(3.16)

$$\tfrac{1}{2}\sqrt{\left[(\Sigma_i - m_e^2) - \frac{\beta_i}{m_e^2}\right]\left[(\Sigma_i - m_e^2) - \frac{\beta_i}{m_e^2}\right]}$$

and to $s = 0, -\infty$.

The notation here is

$$\Sigma_i = 2(u^2 + M_i^2), \quad \beta_i = (M_i^2 - u^2), \quad \Sigma_{ij} = 2u^2 + M_i^2 + M_j^2.$$

Note the complete symmetry of (3.16) in i and j, which is necessary if the matrix h is to be symmetric. For elastic scattering (j = i), (3.16) reduces to

$$s = (\Sigma_i - m_e^2), \frac{\beta_i}{m_e^2} \quad ;$$

(3.16a)

$$s = 0, -\infty.$$

A given exchange thus leads to two cuts in the s plane,
one from $-\infty$ to 0, the other connecting the two finite
points determined by (3.16). In the W ($= \sqrt{s}$) plane, the
first of these appears as a cut running the entire length
of the imaginary axis, while the second becomes a pair
of relatively short cuts symmetrically placed on either
side of the imaginary axis. The complete set of cuts
resulting from all u exchanges is found by letting m_e
vary over the entire range of effective masses which
can be exchanged. For h_{11}, m_e can be M_Σ (Σ exchange),
or anything from $(M_\Lambda + \mu)$ to ∞ ($\pi\Lambda$ or $\pi\Sigma$ exchange); for
h_{22}, M_Λ, M_Σ and $(M_\Lambda + \mu)$ to ∞; and for h_{12}, M_Σ and
$(M_\Lambda + \mu)$ to ∞.

Completely parallel remarks apply to the t ex-
changes. The $\frac{1}{t - m_e^2}$ pole corresponding to exchange of
a mass m_e in the t channel again leads to Q_ℓ functions
in the partial wave amplitudes, this time with argument
x_s^e given by

$$x_s^e = \frac{2\omega_i\omega_j - 2\mu^2 + m_e^2}{2q_iq_j} \; ; \; t - m_e^2 = -2q_iq_j\left[x_s^e - \cos\theta\right]. \tag{3.17}$$

The branch points in the s plane are now at

$$s = \tfrac{1}{2}(\Sigma_{ij} - m_e^2) \pm \tfrac{1}{2}\sqrt{\frac{m_e^2 - 4\mu^2}{m_e^2}\left[m_e^2 - (M_i + M_j)^2\right]\left[m_e^2 - (M_i - M_j)^2\right]},$$ (3.18)

and at $s = 0, -\infty.$

For elastic scattering in channel i, this reduces to

$$s = \tfrac{1}{2}(\Sigma_i - m_e^2) \pm \tfrac{1}{2}\sqrt{(m_e^2 - 4\mu^2)(m_e^2 - 4M_i^2)};$$ (3.18a)

$$s = 0, -\infty.$$

Of course, formulae for the branch points do not completely determine the connecting cuts; furthermore, I have not said which of the four points in (3.18) correspond to $x_s^e = +1$, and which to $x_s^e = -1$, so we don't even know which pairs of points to try to join. To locate the cuts in detail, one must see where s goes when x_s^e goes from -1 to $+1$. As an illustration, consider ρ exchange in $\pi\Sigma$ elastic scattering. Omitting the index $i = 2$ from kinematical quantities, we have

$$x_s^\rho = \frac{2\omega^2 - 2\mu^2 + m_\rho{}^2}{2q^2} = 1 + \frac{m_\rho{}^2}{2q^2} \quad .$$

Writing out the right hand side explicitly in terms of s, and then solving for s in terms of x_s^ρ, one obtains

$$s = \frac{\left[\Sigma + \frac{2m_\rho{}^2}{x_s^\rho - 1}\right] \pm \sqrt{\left[\Sigma + \frac{2m_\rho{}^2}{x_s^\rho - 1}\right]^2 - 4\beta}}{2} \quad . \tag{3.19}$$

This shows explicitly that there are two points s for every point x_s^ρ, so that the branch cut running along the real axis from -1 to $+1$ in the x_s^ρ plane maps into two branch cuts in the s plane, corresponding to the two signs in (3.19). As x_s^ρ goes from -1 to $+1$, s traverses the curve in Figure 3.1a, if we pick the upper sign, and that in Figure 3.1b, if we pick the lower. Together these two branch cuts add up to the configuration in Figure 3.1c. With reference to (3.18a), we now know which branch points in s correspond to which value of x_s^ρ (the two points given by the non-trivial formula in (3.18a) are the ends of the circular arcs in Figures 3.1a and 3.1b).
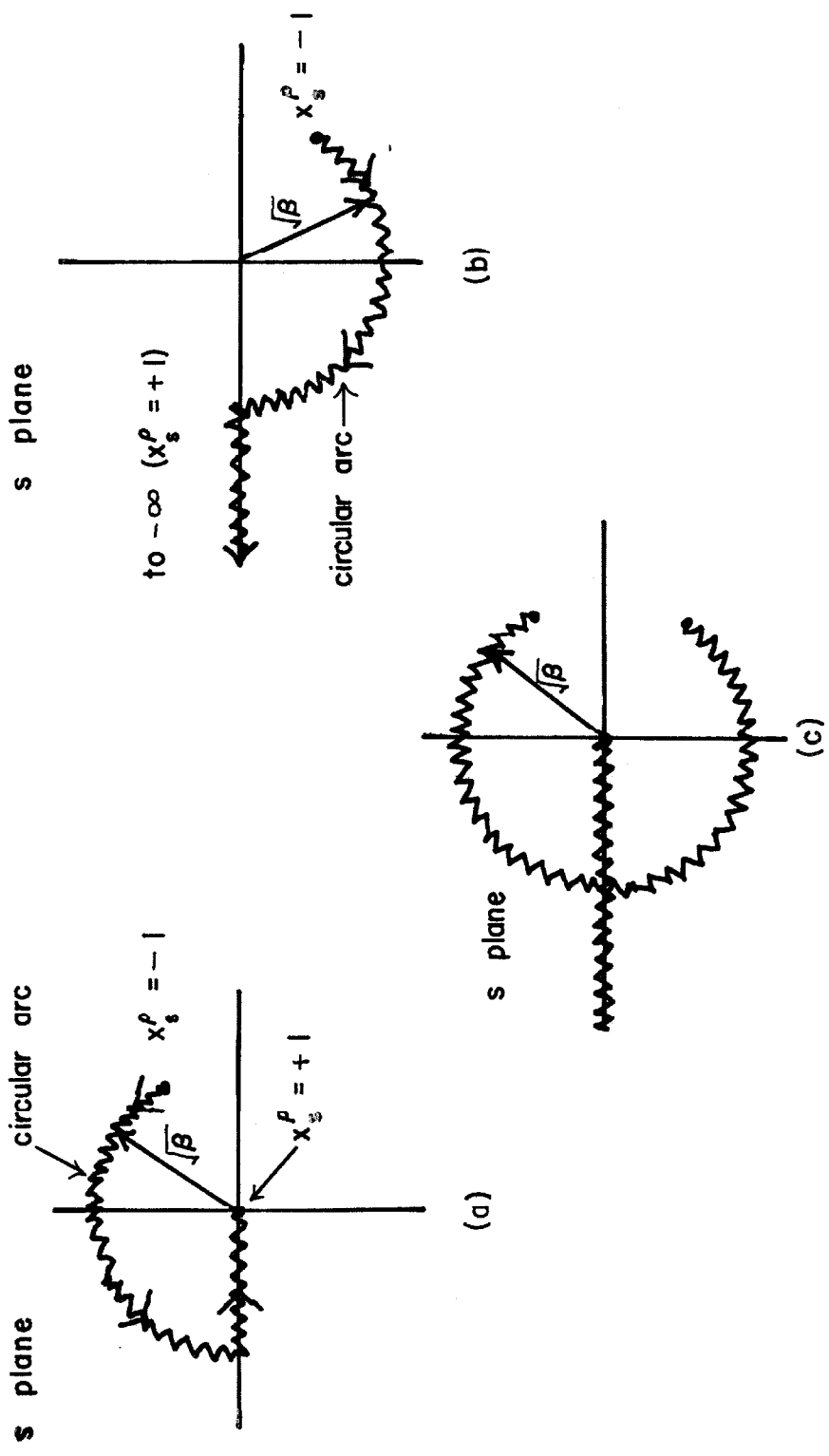
Figure 3.1. Branch cuts associated with ρ exchange. The cut joining -1 to +1 in the x_s^ρ plane maps into the two cuts shown in (a) and (b), which together give the singularities depicted in (c).

It is now clear how the exchange cuts arise, and how they can be located in the s or the W plane. In the $\pi\Lambda \rightarrow \pi\Lambda$ amplitude, h_{11}, we have the following collection of cuts (in the W plane):

(1) u - exchanges

    a) From Σ exchange, a pair of short cuts on the real axis with $\dfrac{(M_\Lambda^2 - \mu^2)}{M_\Sigma} \leq |W| \leq \sqrt{2(M_\Lambda^2 + \mu^2) - M_\Sigma^2}$, and a cut along the entire imaginary W axis, from $-i\infty$ to $+i\infty$.

    b) From $\pi\Lambda$, or other multi-particle exchange, a real cut $-(M_\Lambda - \mu) \leq W \leq (M_\Lambda - \mu)$, and a cut along the whole imaginary axis.

(2) t - exchanges

    a) No single stable particle exchanges are possible.

    b) From $\pi\pi$, or other multi-particle exchange, a circular cut with radius $\sqrt{M_\Lambda^2 - \mu^2}$, and again a cut along the whole imaginary axis.

These cuts are drawn in Figure 3.2.
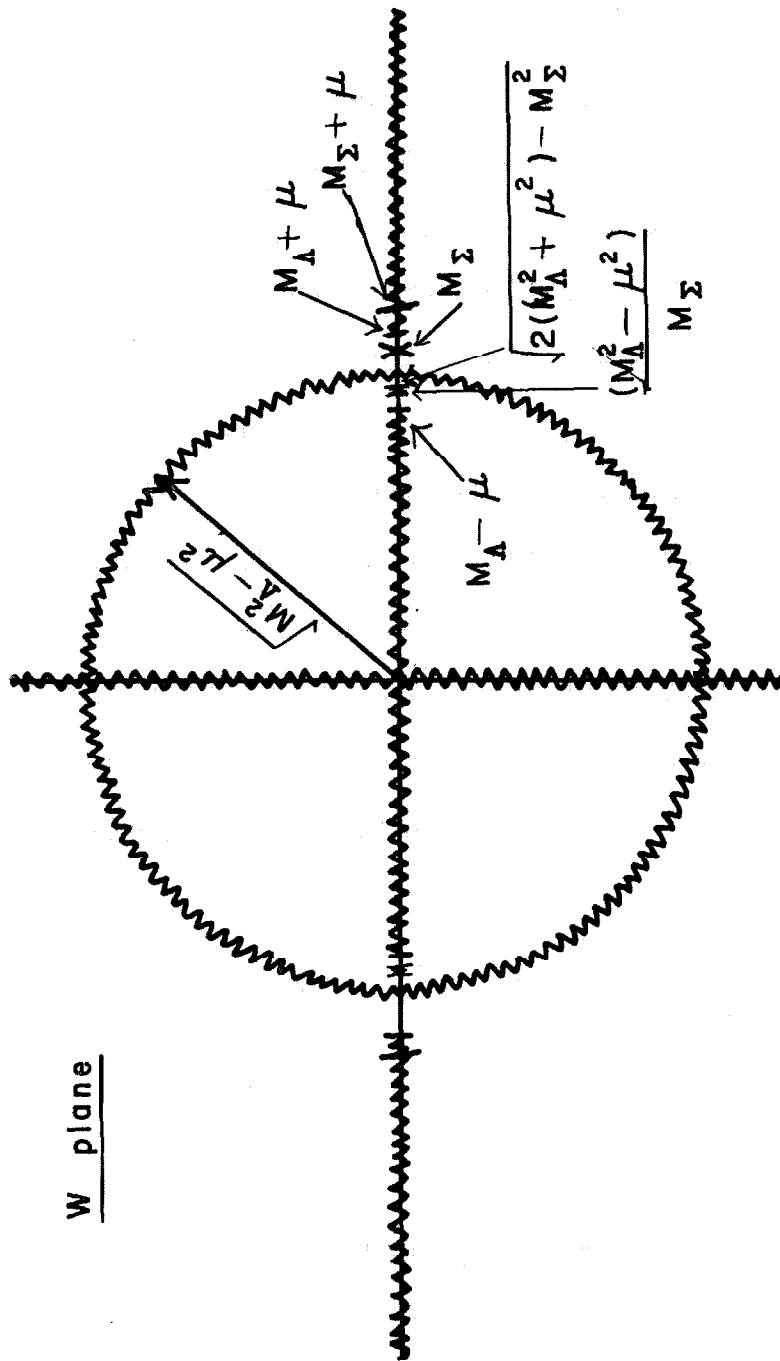
Figure 3.2. Singularities of the $p\frac{1}{2}$ $\pi\Lambda \to \pi\Lambda$ elastic scattering amplitude in the complex W plane. Except for the Σ pole X at M_Σ, all singularities in the right half-plane have mirror images in the left half-plane. The cuts beginning at $|W| = M_\Lambda + \mu$ are the right and left unitarity cuts; the remaining cuts represent forces acting between the π and Λ.

The singularities of the $\pi\Lambda\leftrightarrow\pi\Sigma$ and $\pi\Sigma\rightarrow\pi\Sigma$ $p_{\frac{1}{2}}$, $I = 1$ amplitudes are very similar in structure to those of the corresponding $\pi\Lambda\rightarrow\pi\Lambda$ amplitude, so it is unnecessary to deal with them in detail. Each amplitude has a unitarity cut and an array of driving cuts in the right half W plane, and reflected cuts on the left. Each $p_{\frac{1}{2}}$, $I = 1$ amplitude also has a pole at $W = M_\Sigma$, as discussed below.

It should, however, be noted that in $\pi\Sigma$ elastic scattering, there is an anomalous threshold. Because $M_\Sigma^2 > M_\Lambda^2 + \mu^2$, there are diagrams, involving Λ exchange, in the process $\pi\pi\rightarrow\Sigma\bar{\Sigma}$ which have anomalous thresholds in the variable t, which is the energy for $\pi\pi\rightarrow\Sigma\bar{\Sigma}$. The anomalous region extends down to

$$ t_o = 2(M_\Sigma^2 + \mu^2) - M_\Lambda^2 - \frac{(M_\Sigma^2 - \mu^2)^2}{M_\Lambda^2} \, , \qquad (3.20) $$

whereas the normal t threshold is $4\mu^2$.[9] The spectral representation of the full $\pi\Sigma\rightarrow\pi\Sigma$ amplitude now involves values of t down to t_o, so that in locating the singularities of the $\pi\Sigma\rightarrow\pi\Sigma$ partial waves, we must let the effective exchanged mass m_e go all the way down to $m_e^2 = t_o$, to use the language of the preceding analysis. If

we replace m_e^2 by t_o and x_s^e by x_s^o in (3.19) and again
follow the s cuts given by this formula, we find that
there is a cut on the real s axis which runs from M_Λ^2
until just <u>above</u> the $\pi\Lambda$ threshold $(M_\Lambda + u)^2$. In effect,
then, the unitarity cut appears to run without interrup-
tion from ∞ down to M_Λ^2, instead of stopping at the
"normal" place, $(M_\Lambda + u)^2$, so one speaks of the unitarity
cut as having an anomalous threshold.

On the other hand, we will be approximating multi-
particle exchanges by resonance exchanges, and neglecting
the non-resonant "background" contributions. Since the
anomalous threshold in $\pi\Sigma \longrightarrow \pi\Sigma$ comes from such a back-
ground process, it will not appear once the resonance
approximation is made, and hence, will cause no practical
difficulties. From now on we will, therefore, assume
that there is complete separation between the unitarity
cut and the driving cuts in each amplitude h_{ij}.

Although all the partial waves for a given process
$i \longleftarrow j$ have the same branch cuts, the $P_{\frac{1}{2}}$, $I = 1$ amplitude
has in addition the Σ pole at $W = M_\Sigma$, corresponding to
$i \longleftarrow j$ via an intermediate state consisting of just a Σ.
From the point of view of scattering theory, the question
of whether the Σ is a dynamically produced particle or

not is just the question of whether this pole follows
from the other singularities already present, or not.
In other words, if the amplitudes in the scattering
matrix h are required to have certain specified driving
cuts, are they then forced into also having a pole at
$W = M_\Sigma$ in order to satisfy the general properties of
scattering amplitudes? If so, the Σ is a dynamical con-
sequence of the driving forces, and as an intermediate
state in reactions, can be pictured in exactly the same
way as one pictures the compound nucleus which is formed
in reactions in nuclear physics.

THE ND^{-1} METHOD

The ND^{-1} method[10] is a manageable technique for
making approximate calculations of partial wave scattering
matrices, such as h, with two important features. First,
the approximate h which results from an "N over D" com-
putation will automatically possess the main general
properties required of it: it will be exactly unitary,
have cuts in the right places, be analytic where it should
be, and be symmetric. Other properties will be main-
tained as well. Secondly, in the ND^{-1} method, it is
possible to specify an approximate set of driving cuts

(forces), and see if the h possessing these cuts has a dynamically produced pole as well.

Let us assume that the two-channel scattering matrix h can be represented in the form

$$h(W) = N(W)D^{-1}(W), \qquad (3.21)$$

where $N(W)$ and $D(W)$ are real analytic 2 x 2 matrices, and D has cuts only where h has unitarity cuts, while N has cuts only where h has driving cuts. (Within the permitted regions, the various D_{ij} and N_{ij} can have cuts in different places.) In the one-channel case, this assumption can be rigorously justified by actually displaying formulae for N and D in terms of the phase shift.[11] For the multi-channel case no such explicit proof exists as yet, but the multi-channel generalization is very plausible, and a partial proof has been given.[12]

The unitarity condition $\text{Im } h = h^{*}\Theta h$, obeyed by h above both left and right unitarity cuts (U cuts), can be rewritten as

$$\text{Im} (h^{-1}) = -\Theta, \quad \text{above U cuts.} \qquad (3.22)$$

This is obtained using the fact that for a complex matrix
A, $\text{Im}(A^{-1}) = -A^{-1*}(\text{Im}A)A^{-1}$.

If $h = ND^{-1}$ is to be unitary, we must have, above
the U cuts,

$$\text{Im}D = \text{Im}(h^{-1}N) = \text{Im}(h^{-1})N = -\Theta N \qquad (3.23)$$

(Recall that N is real in the "unitarity region"). Also,
if h is to have driving cuts (F cuts) with a specified
discontinuity disc h, we must have

$$\text{disc }N = (\text{disc }h)\,D \qquad (3.24)$$

in the region of the F cuts (where D is analytic). Note:
Since we are dealing with real analytic functions and the
U cuts are on the real axis, the discontinuity across
these cuts is just 2i times the imaginary part above the
cuts. However, the driving cuts are not restricted to
the real axis, so for these cuts, the discontinuities do
not amount to the imaginary parts.

We now wish to obtain more explicit represen-
tations for $N(W)$ and $D(W)$. To this end we define a matrix
$B(W)$ as the dispersion integral over <u>just</u> the driving
cuts of h:

$$B\ (W)\ =\ \frac{1}{2\pi i}\ \int_F \frac{disc\ h(W')}{W'\ -\ W}\ dW'\ . \qquad (3.25)$$

$\int_F$ means, of course, the integral over the F cuts. (3.24) now becomes

$$disc\ N\ =\ (disc\ B)D\ ;\quad F\ cuts. \qquad (3.24a)$$

Then across the F cuts,

$$disc\ (N\ -\ BD)\ =\ (disc\ B)D\ -\ (disc\ B)D\ =\ 0,$$

so that $(N\ -\ BD)$ is singular only on the U cuts, above which

$$Im\ (N\ -\ BD)\ =\ -\ B\ Im\ D\ =\ B\Theta N. \qquad (3.26)$$

Next we write dispersion relations for D and for $(N\ -\ BD)$, making the minimum number of subtractions needed in order to get a convergent, consistent set of equations. This involves the simplest assumptions one can make about the asymptotic behavior of N and D. It is easy to show that if $B(W) \rightarrow \frac{1}{W}$ as $W \rightarrow \pm \infty$, as our approximate B will (after being damped), no subtractions will not work, but one

subtraction in D, with none in (N - BD), is sufficient. Because h is being represented as a "quotient", ND^{-1}, there is obviously a multiplicative freedom in the specific choice of N and D, which we utilize by normalizing D to the unit matrix I at the subtraction point W_o. Then, denoting by $\int_U$ an integral above both left and right U cuts, we have

$$D(W) = I - \frac{W - W_o}{\pi} \int_U \frac{\Theta(W')\ N(W')\ dW'}{(W' - W)(W' - W_o)} , \qquad (3.27)$$

and

$$N(W) - B(W)D(W) = \frac{1}{\pi} \int_U \frac{B(W')\Theta(W')N(W')\ dW'}{W' - W} \equiv J(W). \qquad (3.28)$$

Substituting the dispersion relation for D into (3.28), we obtain

$$N(W) = B(W) + \frac{1}{\pi} \int_U dW' \left[B(W') - \frac{W - W_o}{W' - W_o} B(W) \right] \frac{\Theta(W')N(W')}{W' - W}, (3.29)$$

which is a linear integral equation for N, given B.
These equations are identical in form to those for the
single-channel case,[13] except that now N, D, etc. are
matrices, so one has to keep the order of multiplication
straight. The ranges of integration which appear in
(3.27) - (3.29) are actually controlled by the step
functions in the Θ matrix, as given in (3.13). Some
integrals start at $|W| = M_\Lambda + \mu$, others only extend to
$|W| = M_\Sigma + \mu$.

Now the point is that if we have some reasonable
approximation for B(W), we can use the basic relations
(3.29), then (3.27), then (3.21), to calculate a corre-
sponding approximate h(W), and this h will be <u>exactly</u>
unitary, will have precisely the driving cuts and dis-
continuities implicitly specified by giving B, and will,
as we shall show, be properly behaved in several other
respects as well. And all this is independent of the
approximation made for B. The unitarity results simply
from our maintaining the relation ImD = - ΘN above the
U cuts, so that there

$$Im(h^{-1}) = Im(DN^{-1}) = (ImD)N^{-1} = - \Theta NN^{-1} = - \Theta.$$

And h will have the prescribed driving cuts, i.e., the cuts of B, because we calculate N in such a way that across the F cuts disc N = (disc B)D, so that there

$$\text{disc } h = \text{disc } (ND^{-1}) = (\text{disc } N)D^{-1} = \text{disc } B.$$

In terms of the elements of D,

$$D^{-1} = \frac{1}{\Delta} \begin{pmatrix} D_{22} & -D_{12} \\ -D_{21} & D_{11} \end{pmatrix} \equiv \frac{\bar{D}}{\Delta} \quad ; \quad \Delta \equiv \text{determinant of } D. \quad (3.30)$$

If the forces represented by the driving cuts result in a $\pi\Lambda - \pi\Sigma$ bound state, the corresponding pole in h will show up as a zero of Δ.

The additional properties which the matrix ND^{-1} has, whether calculated with the true B or with some approximate B as input, are as follows:

A) Symmetry

Bjorken and Nauenberg[14] proved that if N and D both satisfy unsubtracted dispersion relations, and if the input B is symmetric, then the output h = ND^{-1} will be also, and will thus satisfy the requirement of time reversal invariance. Their argument, which also applies

to the present case, where D is somewhat more divergent
at ∞ and requires a dispersion relation with one subtraction, is reproduced here for completeness.

Consider the matrix function

$$A(W) = D^T(h - h^T)D = D^T(ND^{-1} - (D^{-1})^T N^T)D$$
$$= D^T N - N^T D , \qquad (3.31)$$

where D^T is the transpose of D, etc. A can be singular
only where h is. On the driving cuts,

$$\text{disc } A = D^T (\text{disc } B - \text{disc } B^T)D = 0, \qquad (3.32)$$

since the input matrix B is assumed to be symmetric. On
the unitarity cuts,

$$\text{ImA} = (\text{ImD}^T) N - N^T(\text{ImD}) = - N^T \Theta^T N + N^T \Theta N = 0, \quad (3.33)$$

since the diagonal matrix Θ is its own transpose. If h
has a dynamical pole somewhere because the determinant
of D is zero, this will not produce a pole in $A = D^T N - N^T D$.

At infinity, if the input B goes like $\frac{1}{W}$, N will also
(as can be shown from (3.29)), and D cannot diverge
as fast as W or the once-subtracted dispersion relation
for it would be wrong. Thus, A goes to zero at infinity,
and is not singular anywhere in the finite plane, so it
must be identically zero. Hence, h is a symmetric matrix,

$$h = h^T .$$

(3.34)

B) Threshold Behavior

The h being represented as ND^{-1} was deliberately
chosen not to have threshold zeroes, which the ND^{-1}
method cannot be expected to produce when an approximate
B is used as input. Threshold zeroes would have to
come from zeroes in the N matrix, which will hardly come
out of the integral equation (3.29) regardless of the
approximations in B. However, when the h is so chosen
that there are no threshold zeroes required, one can say,
if one wants to put it this way, that the correct thres-
hold behavior is guaranteed.

C) Reality of the Coupling Constants

If, as anticipated, the input forces result in
a zero of $\Delta = \det D$ at some energy $W = M$ in the region
$0 < W < (M_\Lambda + \mu)$, so that we have a dynamical bound state,
h near the pole will look like

$$h = ND^{-1} = \frac{N\bar{D}}{\Delta} \cong \frac{N(M)\bar{D}(M)}{\Delta'(W)\big|_M (W - M)} \equiv \frac{R}{W - M} .$$

$$(3.35)$$

Here $\Delta'(W)\big|_M$ is the derivative of $\Delta(W)$ at $W = M$. As we
shall see, the elements of the residue matrix R at a
single (stable) particle pole are real coupling constants
multiplied by real coefficients, so the R which results
from an approximate ND^{-1} calculation had better be real,
if this approximation scheme is to be sensible.

That R will be real is easy to see. In the region
of interest, D(hence $\bar{D}$ and Δ) is real. Thus $\Delta'(W)\big|_M$ is
real, and we only need to show that $N(M)\bar{D}(M)$ is real.
Noting that $D\bar{D} = \Delta$, we see that near the pole

$$\text{Im}(N\bar{D}) = (\text{Im}N)\bar{D} = (\text{Im}B)D\bar{D} = (\text{Im}B)\Delta .$$

$$(3.36)$$

At the pole Δ is zero, so $\text{Im}(N\bar{D})$ vanishes. In fact, re-
calling that the integral equation for N can be written
as in (3.28):

$$N = BD + J ,$$

we see that

$$N\bar{D} = BD\bar{D} + J\bar{D} = B\Delta + J\bar{D} . \qquad (3.37)$$

Hence, at the bound state pole,

$$N\bar{D} = J\bar{D} . \qquad (3.38)$$

The integral $J(W)$ is clearly real below the $\pi\Lambda$ threshold, so this relation shows explicitly that $N\bar{D}$ is real at the pole, and will be useful in the numerical calculations.

D) Independence of the Subtraction Point

Since it is not transparent from (3.29) and (3.27) that ND^{-1} is completely independent of the subtraction point W_o used in calculating it from some approximate B, we will demonstrate this explicitly. Instead of dealing with (3.29), it is simpler to use the equivalent (3.28). Suppose, then, that $N(W)$ and $D(W)$ are the solution of the set of equations

$$N(W) = B(W)D(W) + \frac{1}{\pi} \int_U \frac{B(W')\Theta(W')N(W')}{W' - W} \, dW' \qquad (3.39a)$$

$$D(W) = I - \frac{W - W_o}{\pi} \int_U \frac{\Theta(W') \; N(W') \; dW'}{(W' - W)(W' - W_o)} . \qquad (3.39b)$$

Using two other subtraction points W_1 and W_2, we can also write for <u>this same D</u>,

$$D(W) = D(W_i) - \frac{W - W_i}{\pi} \int_U \frac{\Theta(W')N(W')dW'}{(W' - W)(W' - W_i)} ,$$

$$(3.40)$$

$$i = 1, 2.$$

Now define the matrices $N_i(W)$ and $D_i(W)$ by

$$N_i(W) = N(W) \; D^{-1}(W_i)$$

$$(3.41)$$

$$D_i(W) = D(W) \; D^{-1}(W_i) .$$

Then multiplication of (3.39a) and (3.40) by $D^{-1}(W_i)$ yields

$$N_i(W) = B(W)D_i(W) + \frac{1}{\pi} \int_U \frac{B(W')\Theta(W')N_i(W')dW'}{W' - W}$$

$$\left.\begin{array}{c} \\ \\ \\ \\ \\ \\ \end{array}\right\} i = 1,2. \quad (3.42)$$

$$D_i(W) = I - \frac{W - W_i}{\pi} \int_U \frac{\Theta(W')N_i(W')dW'}{(W' - W)(W' - W_i)}$$

For each value of i, these are the usual equations of the ND^{-1} method, corresponding to a subtraction point W_i, with D normalized to I at the subtraction point. And by construction, their solutions differ only by a constant matrix A which cancels out of ND^{-1}:

$$N_2(W) = N_1(W)\ A,$$

and $\qquad\qquad\qquad\qquad\qquad\qquad\qquad\qquad\qquad$ (3.43)

$$D_2(W) = D_1(W)\ A,$$

so that

$$N_2 D_2^{-1} = N_1 D_1^{-1} . \qquad\qquad\qquad (3.44)$$

By way of comparison, we should mention at this point the lowest order determinantal method. This technique, which is computationally vastly less involved than the full ND^{-1} method employed here, may be viewed as the lowest order in an iteration solution to the ND^{-1} equations. Effectively, the integral equation for N, (3.29),

is replaced by the approximation $N(W) = B(W)$, and then
D is calculated from N by the usual dispersion relation,
(3.27).[15] By comparison with the full ND^{-1} method, the
determinantal approximation yields an output matrix
which is not symmetric and is not independent of the
subtraction point. Furthermore, if the output pole
happens to lie on top of one of the input driving cuts,
the output coupling constants will be complex, which is
nonsense. In the present problem, if a self-consistent
bound state can be found, the output Σ pole will lie
right in the middle of one of the cuts coming from Σ
exchange in the $\pi\Sigma$ channel (Put $i = 2$ and $m_e^2 = M_\Sigma^2$ in
$(3.16a)$ to see this.). Thus, the determinantal method
will never lead to a self-consistent Σ with real coupling
constants, and for this reason alone it cannot be used
here.

THE OVERLAPPING CUT

We have been assuming that the driving cuts are
completely separate from the unitarity cuts in each of
the amplitudes h_{ij}. In fact, however, this is not the
case. The source of the difficulty is the Λ exchange
force in the $\pi\Sigma \to \pi\Sigma$ amplitude (see Fig. 2.1). The

reader may be familiar with the fact that an exchange graph of this type cannot lead to a cut in the physical region (i.e., above the $\pi\Sigma$ threshold) unless the Σ is so heavy that it is unstable for decay into π and Λ, to which particles it is coupled at each vertex. This is verified by (3.16a). However, in the $\pi\Sigma$ elastic scattering amplitude, the _unitarity_ cut extends below the physical region down to the $\pi\Lambda$ threshold, and there is nothing to stop the short cut associated with a process like Λ exchange from creeping above the _unitarity_ threshold at $W = (M_\Lambda + \mu)$, even though no physical instability is involved. Indeed, application of (3.16a) shows that for the experimental mass values, the right hand short cut coming from Λ exchange does lie between the $\pi\Lambda$ and $\pi\Sigma$ thresholds. This situation is illustrated in Fig. 3.3. A mirror-image arrangement is, of course, simultaneously present in the left half W plane, but for simplicity we shall speak in terms of what is happening in the right half plane near the actual physical region; it will be clear that the steps taken apply as well to the reflected overlap.

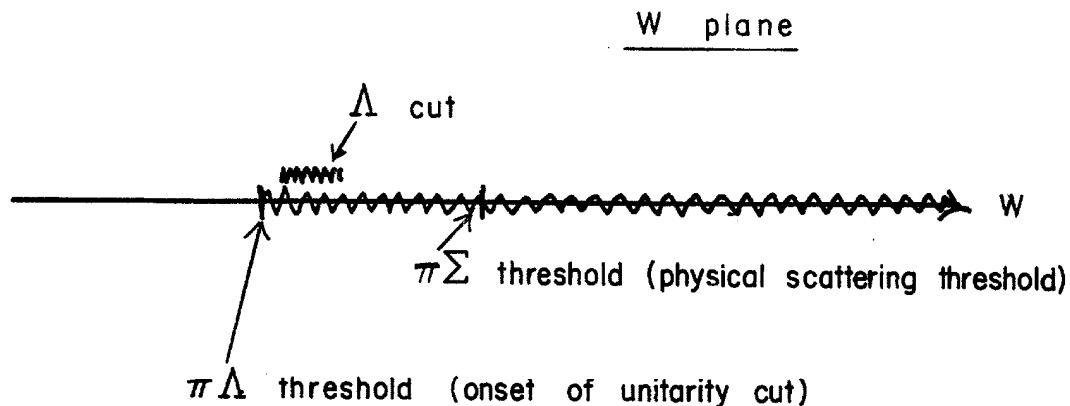Now that a force cut overlaps the unitarity cut in the unphysical region in one of the h_{ij}, the problem

W plane

Figure 3.3. The overlapping cuts in h_{22}. In this view
of the real axis in the right half W plane, the unitarity
cut extends from $\pi\Lambda$ threshold to ∞, with the overlapping
Λ cut lying between the $\pi\Lambda$ and $\pi\Sigma$ thresholds. For
clarity, the Λ cut is drawn slightly above the axis.

is to find out what becomes of the extended unitarity

condition, (3.12)[16], and to try to find a practical

computational scheme which still works when the "usual"

unitarity relation no longer applies.

Let us pretend that the Λ is a little heavier

than it really is, so that the overlapping cut recedes

to a less troublesome position below $\pi\Lambda$ threshold.[17]
In this situation, which is represented in Figure 3.4,
the usual unitarity relation, (3.12), is assumed to be
correct, and the ND^{-1} formalism previously discussed
applies. Imagine that the Λ is now made lighter, so
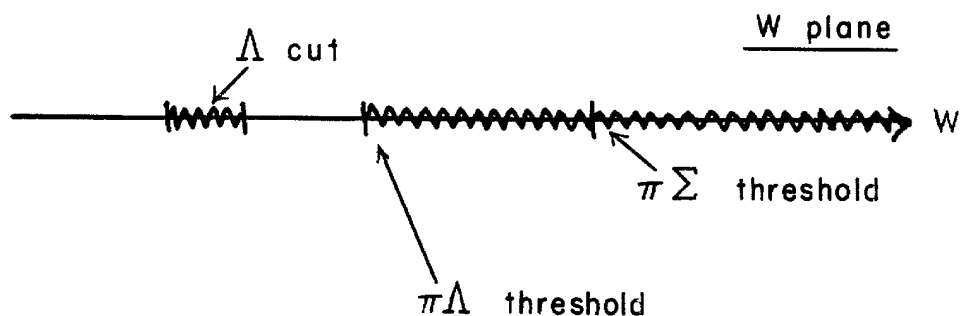
Figure 3.4. The Λ and unitarity cuts in h_{22} when the
masses are so related that there is no overlap.

that the Λ cut obtrudes into the unitarity region. Since
the crossing of the $\pi\Lambda$ threshold by the Λ cut is not
associated with any actual physical occurrence, such as
the Σ becoming unstable for $\pi\Lambda$ decay,[18] one expects the
scattering amplitudes h_{ij} (W) to vary smoothly as the Λ
mass is decreased. Thus, one would like to find some
explicit way of analytically continuing the matrix h(W)

in the Λ mass, from values where there is no overlap to values where there is.

We have at hand the means for achieving this analytic continuation in a trivial way: namely, the ND^{-1} method itself. To make this clear, we rewrite the basic equations used to calculate N and D in the non-overlap case, explicitly indicating the channel indices.

$$N_{ij}(W) = B_{ik}(W) \left[I_{kj} - \frac{W - W_o}{\pi} \int_U \frac{\theta_k(W')N_{kj}(W')dW'}{(W'- W)(W'- W_o)} \right]$$

$$(3.45a)$$

$$+ \frac{1}{\pi} \int_U \frac{B_{ik}(W')\theta_k(W')N_{kj}(W')dW'}{W' - W}, \quad i,j = 1,2;$$

$$D_{ij}(W) = I_{ij} - \frac{W - W_o}{\pi} \int_U \frac{\theta_i(W')N_{ij}(W')dW'}{(W'- W)(W'- W_o)}, \quad i,j = 1,2. \quad (3.45b)$$

Table 3.1 shows the range over which each function $N_{ij}(W)$ is integrated in this pair of equations, this range being common to both.

TABLE 3.1. Energy ranges over which the $N_{ij}(W)$ are integrated in the N and D equations, (3.45a, b). Each function is integrated in the region from the lower limit listed to $+\infty$ as well as in the reflected region at negative energies. $W_{\pi\Lambda}$ and $W_{\pi\Sigma}$ denote the $\pi\Lambda$ and $\pi\Sigma$ thresholds.

N Function	Threshold of Region of Integration
$N_{11}(W)$	$W_{\pi\Lambda}$
$N_{12}(W)$	$W_{\pi\Lambda}$
$N_{21}(W)$	$W_{\pi\Sigma}$
$N_{22}(W)$	$W_{\pi\Sigma}$

TABLE 3.2. Energy regions where the input functions $B_{ij}(W)$ are required in order to solve the integral equation for N. We assume the input is symmetric: $B_{12}(W) = B_{21}(W)$. The notation is as in Table 3.1.

Input Function	Threshold of Region where Required
$B_{11}(W)$	$W_{\pi\Lambda}$
$B_{12}(W) = B_{21}(W)$	$W_{\pi\Lambda}$
$B_{22}(W)$	$W_{\pi\Sigma}$

Now we vary the Λ mass so as to bring the Λ cut up above the $\pi\Lambda$ threshold, and see what happens to the N and D equations.[19] To solve the N equation, one need only consider the various $N_{ij}(W)$ in the energy regions over which they are integrated. In the first term of (3.45a), which amounts to $B_{ik}(W)D_{kj}(W)$, $B_{22}(W)$ will enter only the equations for $N_{21}(W)$ and $N_{22}(W)$, but in these equations, one is only dealing with energies W above $\pi\Sigma$ threshold, so the Λ cut between the two thresholds will not be involved. Similarly, in the last term of (3.45a), B_{22} will always stand next to a θ_2, so that integrals over B_{22} will start at the $\underline{\pi\Sigma}$ threshold. Thus, the obtruding cut in B_{22} actually does not appear when one is solving (3.45a), so this equation can still be used to define a matrix of real analytic functions $N_{ij}(W)$, and these functions will be analytic continuations (in the Λ mass) of those for the non-overlap case.

Due to the $B_{ik}(W)D_{kj}(W)$ term in (3.45a), the $N_{21}(W)$ and $N_{22}(W)$ defined by this equation will be singular on the Λ cut of B_{22}, between the two thresholds. In the D equation, however, the range of integration for N_{ij} begins at the threshold for channel i, so no cuts have crept into the integrands of this dispersion relation

either, and it can serve to define real analytic functions $D_{ij}(W)$ which are analytic continuatious of the D_{ij} for the non-overlap situation.

Finally, we can put these N_{ij} and D_{ij} together to form a real analytic scattering matrix $h = ND^{-1}$, which will be the analytic continuation of the h we had before. And since we have been able to achieve this by a simple extension of the computational formalism we had before, no new difficulties will be encountered in practical calculations because of the overlapping cuts[20].

From the extended equations (3.45a, b), it follows that the discontinuities of N and D are given by the same relations as previously:

$$\text{disc } N = (\text{disc } B)D \qquad \text{F cuts} \qquad (3.46a)$$

$$\text{Im } D = - \rho N \qquad \text{U cuts.} \qquad (3.46b)$$

Now, however, there is an "F" cut in the unitarity region, and (3.46a) holds for this singularity as well as for all the other "F" cuts.

Using the extended ND^{-1} formalism, we can now find out what has happened to the usual unitarity condition, $\text{Im } h = h*\rho h$. Except on the A cut, the N matrix is

real throughout the unitarity region, so, using (3.46b),
we have as before

$$\text{Im } (h^{-1}) = \text{Im } (DN^{-1}) = (\text{Im}D)N^{-1} = -\Theta NN^{-1} = -\Theta. \qquad (3.47)$$

On the overlapping Λ cut, however, both N and D are com-
plex, so that

$$\text{Im}(h^{-1}) = \text{Im}(DN^{-1}) = (\text{Im}D)\text{Re}(N^{-1}) + (\text{Re}D)\text{Im}(N^{-1}) \quad (3.48)$$

In working this out, it is important to note that on the
Λ cut

$$\Theta(\text{Im}B) = (\text{Im}B)\Theta = 0. \qquad (3.49)$$

This is because these matrices, in this region, have the
form

$$\Theta = \begin{pmatrix} \Theta_1 & 0 \\ 0 & 0 \end{pmatrix}, \quad \text{Im}B = \begin{pmatrix} 0 & 0 \\ 0 & \text{Im}B_{22} \end{pmatrix}. \qquad (3.50)$$

Since $\text{Re}(N^{-1}) = N^{-1}(\text{Re}N)N^{-1*}$, the first term of (3.48) is
(applying (3.46b))

$$- \Theta N \left[N^{-1}(ReN)N^{-1*} \right] = - \Theta(N* + i\,ImN)N*^{-1}. \qquad (3.51)$$

From (3.46a),

$$\Theta(ImN) = \Theta(ImB)D = 0,$$

so we are left with

$$(ImD)Re(N^{-1}) = - \Theta . \qquad (3.52)$$

For the second term of (3.48), we have

$$ReD = D* + i(ImD)* = D* - i\Theta N* , \qquad (3.53)$$

and

$$Im(N^{-1}) = - N^{-1*}(ImN)N^{-1} = - N^{-1*}(ImB)DN^{-1}$$
$$= - N^{-1*}(ImB)h^{-1} . \qquad (3.54)$$

Then

$$(ReD)Im(N^{-1}) = - (D* - i\Theta N*)N^{-1*}(ImB)h^{-1}$$
$$= -\left[h^{-1*} - i\Theta \right](ImB)h^{-1} = - h^{-1*}(ImB)h^{-1}, \qquad (3.55)$$

using (3.49). Consequently, on the overlapping cut,

$$\text{Im}(h^{-1}) = - \rho - h^{-1*}(\text{Im}B)h^{-1} . \qquad (3.56)$$

In view of (3.47), this relation is also true in the
rest of the unitarity region, where ImB = 0. Inverting,
we find that the unitarity condition has become

$$\text{Im}h = h^*\rho h + \text{Im}B. \qquad (3.57)$$

In the search for a self-consistent Σ, the
input Σ mass will be varied, with the Λ and π masses
held fixed. Situations will therefore arise where
the Σ is lighter than the Λ, in which case overlapping
may be expected in the $\pi\Lambda \rightarrow \pi\Lambda$ amplitude, coming from
the diagram
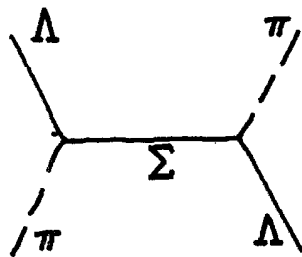
This circumstance, however, is completely identical
to that just discussed, except for the roles of channels
1 and 2 being interchanged, and the previous solution
applies. On the other hand, if one were to take for
the input Σ mass a value outside the range $(M_\Lambda - \mu) <$
$M_\Sigma < (M_\Lambda + \mu)$, then either the Σ or the Λ would be un-
stable for decay into the other baryon plus a pion.
If the Σ is unstable, then
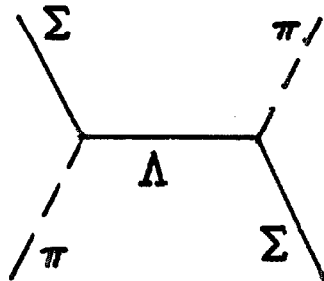
has a cut in the physical region of the $\pi\Sigma$ elastic
scattering amplitude; that is, above the $\pi\Sigma$ threshold.
If it is the Λ which is unstable, then Σ exchange leads
to a cut in the physical region of the $\pi\Lambda$ scattering
amplitude. In either case, the previous analysis no
longer applies. The question of what happens when there
is actual physical instability is a matter of current
debate. In any case, it seems probable that major
computational complications will be involved, and so

it was decided to restrict attention here to input Σ
masses between $M_\Lambda \pm \mu$. The "window" thus defined
extends from 975 Mev to 1255 Mev, the actual Σ mass
being 1193 Mev. As long as one stays within this
window, the method just developed, which allows for
overlap in the unphysical unitarity region of the
elastic amplitude with the higher physical threshold,
is perfectly adequate. From (3.16) one may verify
that for M_Σ within the window, no cut from any of the
possible exchange processes in the inelastic amplitude
ever wanders into the unitarity region. In fact, as
$M_\Sigma \to M_\Lambda - \mu$, a short cut from
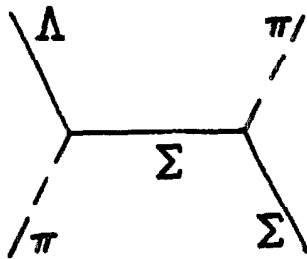
comes exactly up to the lower ($\pi\Sigma$) threshold, but then
retreats.

IV. THE BORN AMPLITUDES

The input forces pictured in Figure 2.1 will be represented in the dynamical calculations by the corresponding Born amplitudes, whose singularities will be the driving cuts. Because of the dispersion denominators $\frac{1}{W' - W}$ in the equations we work with, the singularities near the region of interest (W around M_Σ) are weighted more heavily than the more distant singularities. Now the light mass exchanges lead to the nearest driving cuts, so if one approximates each $B_{ij}(W)$ by the sum of the Born diagrams (suitably damped) for $i \leftarrow j$ in Figure 2.1, the important nearby cuts will be quite accurately treated, although the far-off singularities will be only crudely represented.

If a Born amplitude is calculated for exchange of a mass M in, say, the u channel by using Feynman's rules, the invariant amplitudes A and B will come out in the form

$$A(s,u) = \frac{g(s,u)}{u - M^2} \quad . \tag{4.1}$$

Expanding $g(s,u)$ in powers of $(u - M^2)$,

$$g(s,u) = g(s,M^2) + a(s,M^2)(u - M^2)$$

$$+ b(s,M^2)(u - M^2)^2 + \ldots,$$

one can write A as

$$A(s,u) = \frac{g(s,M^2)}{u - M^2} + a(s,M^2) + b(s,M^2)(u - M^2) + \cdots \quad (4.2)$$

Only the first term here is singular at $u = M^2$; the remaining terms, which we shall refer to as the off-mass-shell parts of A, do not have a pole at $u = M^2$. These off-shell parts of A and B lead to terms in the partial wave amplitudes which have no dynamical cuts. On the other hand, the $B_{ij}(W)$ which are to be approximated by adding up the $i \longleftarrow j$ Born amplitudes are just dispersion integrals over the driving cuts, (3.25), with no extra "cut-less" terms. Therefore, any off-shell pieces in the A and B for some Born diagram should be dropped when computing this diagram's contribution to the relevant $B_{ij}(W)$[21]. There generally are ambiguities in the off-shell pieces of A's and B's calcu-

lated from Feynman's rules (but _not_ in the on-shell parts), stemming from the lack of uniqueness of the interaction Hamiltonian appropriate to a given vertex. These ambiguities are eliminated when the off-shell pieces are dropped. It should also be mentioned that in the only instances in the present work where the computations were so done that the A and B of a particular diagram involved off-shell pieces at first (ρ exchange, with $\sigma_{\mu\nu}k_{\nu}$ coupling to the baryons, in $\pi\Sigma \to \pi\Sigma$ and $\pi\Lambda \to \pi\Sigma$), the rejection of these pieces resulted in a mere $\sim 6\%$ change in the partial wave projections of the diagram, at $\pi\Sigma$ threshold.

The calculation of the Born amplitudes is greatly facilitated by extensive use of the crossing relations. Disregarding isospin, crossing the outgoing and incoming pions in a given Feynman diagram, as in Figure 4.1, corresponds to the interchange $q_i \leftrightarrow -q_f$, or $s \leftrightarrow u$. Thus, the invariant amplitudes for the crossed graph, A^c, B^c, are related to those for the uncrossed ("direct") graph, A^d, B^d, by

$$A^c(s,u) = A^d(u,s) \qquad (4.3a)$$

$$B^c(s,u) = -B^d(u,s). \qquad (4.3b)$$
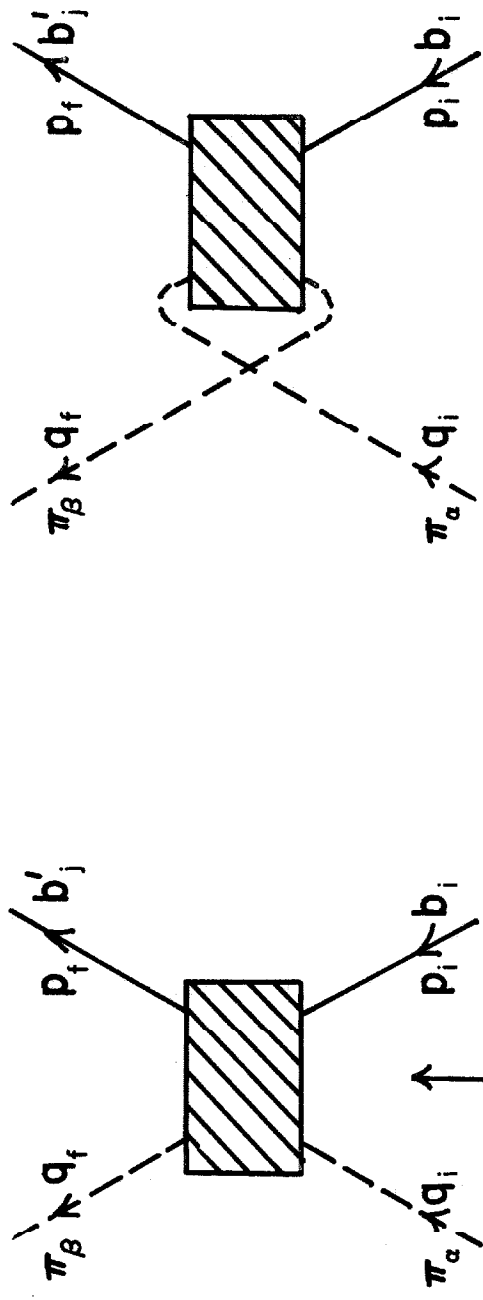
Given Graph

Crossed Graph

$$s = -(p_i + q_i)^2$$
$$u = -(p_i - q_f)^2$$

Figure 4.1. Relation of crossed and uncrossed Feynman graphs. The "grey box" is an arbitrary collection of vertices and internal lines. b and b' may be either a Λ or a Σ; if either is a Λ, its isospin index should be suppressed.

These follow from (3.1) - (3.2), and the fact that $Q = \dfrac{q_i + q_f}{2}$ changes sign under crossing.

As for the isospin, the $\pi\Lambda$ system can only have $I = 1$, while $\pi\Sigma$ can have $I = 0, 1, 2$. Labeling the pions and sigmas by Cartesian isospin indices $(\pi^+ = \dfrac{\pi_1 + i\pi_2}{\sqrt{2}}$, etc.), the $\pi\Lambda$ states of total isospin $I = 1$ and $I_\alpha = 0$ are just

$$|\pi\Lambda;\ I = 1;\ I_\alpha = 0\rangle = |\pi_\alpha\Lambda\rangle \,, \qquad (4.4)$$

while the corresponding $\pi\Sigma$ states are

$$|\pi\Sigma;\ I = 1,\ I_\alpha = 0\rangle = \left| i\left(\dfrac{\vec{\pi} \times \vec{\Sigma}}{\sqrt{2}}\right)_\alpha \right\rangle. \qquad (4.5)$$

The possibly odd-looking choice of phase for the $I = 1$ $\pi\Sigma$ states is necessary to having a symmetric scattering matrix h. Later we shall also use the following representations for $\pi\Sigma$ states with $I = 0$ and $I = 2$:

$$|\pi\Sigma;\ I = 0,\ I_z = 0\rangle = \left| \dfrac{\vec{\pi} \cdot \vec{\Sigma}}{\sqrt{3}} \right\rangle \qquad (4.6a)$$

$$\left| \dfrac{\pi\Sigma;\ I = 2,\ I_z = 2 - \pi\Sigma;\ I = 2,\ I_z = -2}{\sqrt{2}} \right\rangle$$

$$= \left| \ i \ \frac{\pi_x \Sigma_y + \pi_y \Sigma_x}{\sqrt{2}} \right> \ . \tag{4.6b}$$

Although we are after amplitudes corresponding to definite (conserved) total isotopic spin, Feynman's rules will be used to calculate amplitudes for processes of the form $\pi_\alpha \Sigma_i \longrightarrow \pi_\beta \Sigma_j$. The connection between these two types of amplitudes is conveniently discussed together with the isospin crossing matrices.

For $\pi \Lambda \longrightarrow \pi \Lambda$ scattering the isospin is trivial; the amplitude for $\pi_\alpha \Lambda \longrightarrow \pi_\alpha \Lambda$ is also the $I = 1$ amplitude, and the crossing relations (4.3) can be used as they stand.

In $\pi \Sigma \longrightarrow \pi \Sigma$ scattering, the isospin conserving amplitude for $\pi_\alpha \Sigma_i \longrightarrow \pi_\beta \Sigma_j$ can be expressed in terms of three independent functions. Let $a_{\beta j \longleftarrow \alpha i}(s,u)$ stand for either of the invariant amplitudes A and B for some diagram in which $\pi_\alpha \Sigma_i \longrightarrow \pi_\beta \Sigma_j$. A convenient choice of the three functions is defined by writing

$$a_{\beta j \longleftarrow \alpha i}(s,u) = a(s,u)\delta_{\alpha i}\delta_{\beta j} + b(s,u)\delta_{\alpha \beta}\delta_{ij} + c(s,u)\delta_{\alpha j}\delta_{\beta i}. \tag{4.7}$$

The relation between a, b, c and the usual isospin amplitudes for the same process is established by writing the latter in terms of the former with the aid of the representations for the isospin states, (4.5) and (4.6). The relation is

$$a_2 = b + c$$
$$a_1 = b - c \qquad\qquad (4.8)$$
$$a_0 = 3a + b + c$$

where a_i is the amplitude for isospin i.

The isospin dependence of $\pi\Sigma$ scattering diagrams will be summarized by writing their amplitudes as column vectors, in the form

$$a = \begin{pmatrix} a_2 \\ a_1 \\ a_0 \end{pmatrix}. \qquad\qquad (4.9)$$

As far as charge is concerned, crossing of the incoming and outgoing pions corresponds to $\alpha \leftrightarrow \beta$ (see Fig.4.1). If the amplitudes $a^d_{\beta j \leftarrow \alpha i}(s,u)$ and $a^c_{\beta j \leftarrow \alpha i}(s,u)$ for a direct and the corresponding cross graph are both expressed as in (4.7), it is obvious that

$$a^c(s,u) = c^d(u,s)$$

$$b^c(s,u) = b^d(u,s) \tag{4.10}$$

$$c^c(s,u) = a^d(u,s)$$

(the kinematical minus sign in (4.3b) being temporarily disregarded). The restatement of (4.10) in terms of the isospin amplitudes yields the isospin crossing matrix X:

$$X = \begin{pmatrix} 1/6 & 1/2 & 1/3 \\ 5/6 & 1/2 & -1/3 \\ 5/3 & -1 & 1/3 \end{pmatrix} . \tag{4.11}$$

The full crossing relations for the invariant amplitudes A and B are

$$A^c(s,u) = XA^d(u,s) \quad ; \quad B^c(s,u) = -XB^d(u,s), \tag{4.12}$$

where A^c, etc., are understood to be vectors as in (4.9).

In the $\pi\Lambda \longrightarrow \pi\Sigma$ transitions, our phase convention on the $\pi\Sigma$ states is such that

$$a_{\beta j \longleftarrow \alpha\Lambda}(s,u) = \frac{i}{\sqrt{2}} \, \epsilon_{\alpha\beta j} \, a_1(s,u) \, . \tag{4.13}$$

Here $Q_{\beta j \leftarrow \alpha \Lambda}(s,u)$ stands for the A and B of some diagram in which $\pi_\alpha \Lambda \rightarrow \pi_\beta \Sigma_j$, and $Q_1(s,u)$ is the corresponding normalized isospin amplitude (Only $I = 1 \rightarrow I = 1$ transitions are possible). $\epsilon_{\alpha \beta j}$ is the usual totally anti-symmetric object. Since $\epsilon_{\alpha \beta j}$ changes sign under $\alpha \rightarrow \beta$, there is an isospin crossing factor $X = -1$, and the full crossing relations for the $I = 1$ A's and B's are

$$A_1^c(s,u) = -A_1^d(u,s) \; ; \; B_1^c(s,u) = + B_1^d(u,s). \qquad (4.14)$$

The Born diagrams of Figure 2.1 were calculated in three different ways. (1) Feynman's rules were used to obtain the amplitudes for the stable baryon exchanges; in this way the amplitudes are expressed in terms of coupling constants with which people will be familiar from Hamiltonian field theory. Since the Λ and Σ direct (s - pole) graphs are also needed (the Λ in future research), the procedure for the Λ and Σ diagrams was to calculate first the direct graph from Feynman's rules, and then to use the crossing relations to obtain the exchange amplitude. (2) The meson exchanges were computed directly from Feynman's rules. (3) The unstable baryon exchange amplitudes were obtained using only the
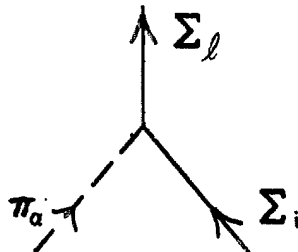
crossing relations and the general formulae for partial wave decomposition. Feynman's rules are unnecessary when one only desires to express the force strength in terms of the experimental width of the force carrier, and not in terms of some arbitrarily defined coupling constants which would be completely unfamiliar parameters. Furthermore, in the case of the diagrams involving the spin $3/2$ Y_1^*, the use of Feynman's rules would require vastly more labor than is involved in simply exploiting the crossing relations.

To illustrate method (1), I will calculate the diagrams involving an internal Σ in $\pi\Sigma \rightarrow \pi\Sigma$ (Fig. 4.2). The $\pi\Sigma\Sigma$ coupling constant will be defined by writing the $\pi\Sigma\Sigma$ interaction Hamiltonian density in terms of field operators as

$$ H = g_{\pi\Sigma\Sigma}(\vec{\Sigma} \times \gamma_5\vec{\Sigma}) \cdot \vec{\pi} , \qquad (4.15) $$

where the vector symbols refer to isospin space. This H corresponds to a vertex factor in Feynman's rules of

$$ g_{\pi\Sigma\Sigma}\gamma_5\epsilon_{\alpha\ell i} \qquad (4.16) $$
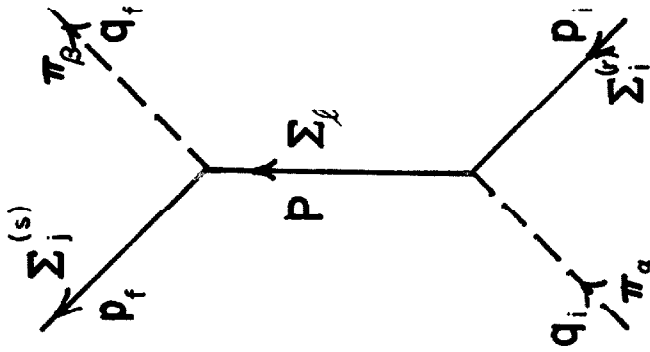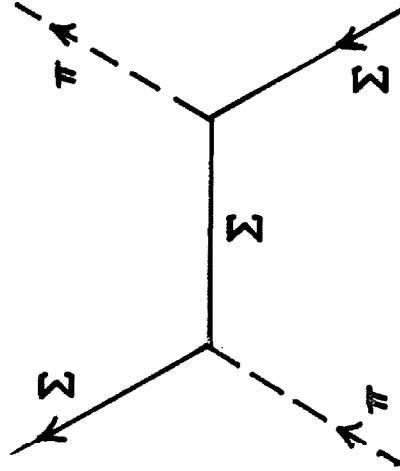
Direct   Exchange

Figure 4.2. Direct and exchange Σ diagrams in $\pi\Sigma \to \pi\Sigma$ scattering. In the direct graph, the momenta and isospin indices used in the calculation are indicated. The superscripts (r) and (s) specify the spin states of the initial and final Σ's.

The rules then give for the S - matrix element of the direct graph (after some manipulation)

$$S_{fi} = -i(2\pi)^4 \delta^{(4)} (p_f + q_f - p_i - q_i) \sqrt{\frac{M_\Sigma^2}{4\omega_i \omega_f E_i E_f}} \cdot$$

$$\cdot g_{\pi\Sigma\Sigma}^2 \frac{\bar{u}^{(s)}(\vec{p_f}) i \not{q} u^{(r)}(\vec{p_i})}{s - M_\Sigma^2} (\delta_{\alpha j}\delta_{\beta i} - \delta_{\alpha\beta}\delta_{ij}).$$

(4.17)

We thus have (see (3.2))

$$A_{\beta j \leftarrow \alpha i} = 0, \quad B_{\beta j \leftarrow \alpha i} = \frac{g_{\pi\Sigma\Sigma}^2}{s - M_\Sigma^2} (\delta_{\alpha j}\delta_{\beta i} - \delta_{\alpha\beta}\delta_{ij}). \quad (4.18)$$

The amplitudes for definite isospin are then, by (4.8),

$$A = 0, \quad B = \begin{pmatrix} 0 \\ 2 \\ 0 \end{pmatrix} \frac{-g_{\pi\Sigma\Sigma}^2}{s - M_\Sigma^2} \cdot \quad (4.19)$$

Hence, by (3.5),

$$f_{1,2} = \begin{pmatrix} 0 \\ 2 \\ 0 \end{pmatrix} \frac{-g_{\pi\Sigma\Sigma}^2}{4\pi} \frac{(E \pm M_\Sigma)}{2W} \frac{(W \mp M_\Sigma)}{s - M_\Sigma^2} \quad , \quad (4.20)$$

and finally, from (3.8), the partial wave with the Σ pole, $f_{p_{\frac{1}{2}}}$, is

$$f_{p_{\frac{1}{2}}} = \begin{pmatrix} 0 \\ 2 \\ 0 \end{pmatrix} \frac{-g^2_{\pi\Sigma\Sigma}}{4\pi} \frac{E - M_\Sigma}{2W} \frac{1}{W - M_\Sigma} \; ; \qquad \qquad . \quad (4.21)$$
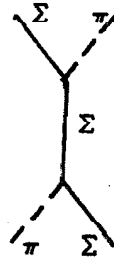
(Except for the partial wave with the same spin and oppo-
site parity, $f_{s_{\frac{1}{2}}}$, all the other partial wave amplitudes
are zero.)

From the present point of view, Feynman's rules
may be thought of as essentially a powerful machinery
for automatically keeping track of the conservation of
various quantities at vertices where states are coupled
together, and for handling some of the kinematics. They
need not be connected with the existence of any "fields",
although I shall always quote the conventional Hamiltonian
which corresponds to my definition of some coupling con-
stant, in order to make the definition clear in familiar
terms. Neither need the particles dealt with be elemen-
tary; (4.21), for example, applies equally well whether
the Σ is composite or elementary. Thus, if the Σ turns
up as a dynamically produced pole in the scattering
matrix h (defined by (3.10)), we see from (4.21) that
the "output" value of the coupling strength $g^2_{\pi\Sigma\Sigma}/_{4\pi}$ is

related to the 22 element of the residue matrix R

(cf.(3.35)) by

$$\frac{g^2_{\pi\Sigma\Sigma}}{4\pi} = - R_{22} \quad . \qquad (4.22)$$

Turning now to the calculation of the Σ exchange graph, we obtain the A and B for this diagram by applying the crossing relations, (4.12), to the direct A and B, (4.19):

$$A^c = 0, \quad B^c = \begin{pmatrix} 1 \\ 1 \\ -2 \end{pmatrix} \frac{g^2_{\pi\Sigma\Sigma}}{u - M_\Sigma^2} \quad . \qquad (4.23)$$

Since $u - M_\Sigma^2 = 2q^2 \ (x_s^\Sigma - \cos\theta)$, $\qquad (4.24)$

where

$$x_s^\Sigma = 1 - \frac{s + M_\Sigma^2 - \Sigma}{2q^2} \quad , \qquad (4.25)$$

it follows that

$$f^c_{1,2} = \begin{pmatrix} 1 \\ 1 \\ -2 \end{pmatrix} \frac{g^2_{\pi\Sigma\Sigma}}{4\pi} \ \frac{1}{4Wq^2} \ (E \pm M_\Sigma)(W \mp M_\Sigma)\frac{1}{x_s^\Sigma - \cos\theta} \quad .(4.26)$$

Projecting out the partial waves by (3.8), we obtain (suppressing the "c")

$$f_{\ell\pm} = \begin{pmatrix} 1 \\ 1 \\ -2 \end{pmatrix} \frac{g^2_{\pi\Sigma\Sigma}}{4\pi} \frac{1}{4Wq^2} \left[(E + M_{\Sigma})(W - M_{\Sigma})Q_{\ell}(x^{\Sigma}_s) \right.$$

$$\left. + (E - M_{\Sigma})(W + M_{\Sigma})Q_{\ell\pm 1}(x^{\Sigma}_s) \right],$$

(4.27)

for
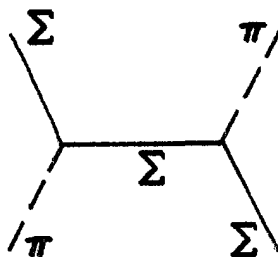
The contribution of Σ exchange to the driving function $B_{22}(W)$, (3.25), is then obtained (aside from the damping explained at the end of this section) by dividing f_{1-} for $I = 1$ by the $p_{\frac{1}{2}}$ kinematical factor ρ_{22}, (3.10).

The other stable baryon exchange amplitudes are arrived at in identical fashion, and on the way, the relations between the output couplings and the remaining residue matrix elements $R_{12} = R_{21}$ and R_{22} are found.

An example of the direct use of Feynman's rules to obtain the meson exchange amplitudes is the calculation of the ρ exchange diagram in $\pi\Lambda \longrightarrow \pi\Sigma$, Figure 4.3.
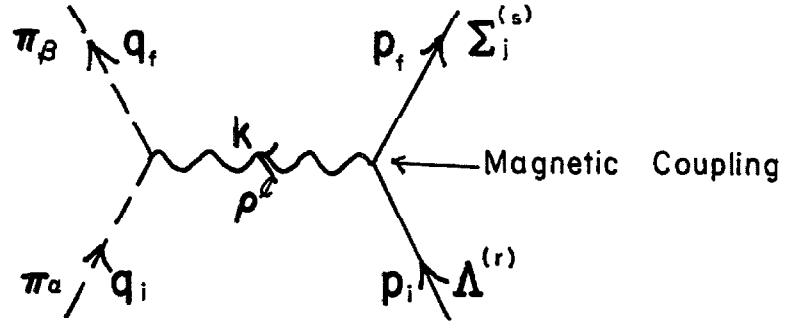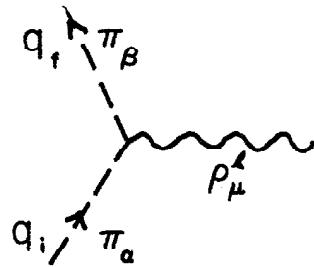
Figure 4.3. The ρ exchange diagram in $\pi\Lambda \to \pi\Sigma$.

The ρ can couple to a pair of baryons such as the Λ and Σ in two independent ways, corresponding to the fact that both the $^3S_1$ and $^3D_1$ $\overline{\Lambda\Sigma}$ states have the quantum numbers of the ρ: $J^{\pi} = 1^-$, $I = 1$. The independent couplings can be taken as the familiar γ_μ (charge) and $\sigma_{\mu\nu}k_\nu$ (magnetic moment) types, where k_ν is the momentum transfer carried by the ρ. Here we shall calculate only the part of the ρ exchange amplitude which corresponds to the $\sigma_{\mu\nu}k_\nu$ coupling.

The $\rho\pi\pi$ coupling constant will be defined as the strength with which the ρ couples to the pion isospin current. Thus we write the $\rho\pi\pi$ interaction Hamiltonian as

$$H = -g_{\rho\pi\pi}\ \vec{\rho_\mu} \cdot (\vec{\pi} \times \partial_\mu \vec{\pi})\ . \tag{4.28}$$

This leads to a vertex factor of
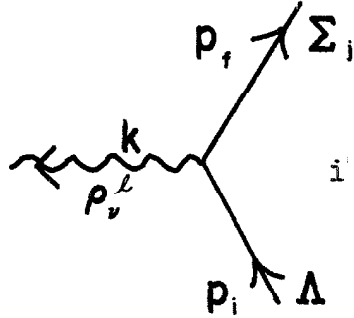
$$ig_{\rho\pi\pi}\varepsilon_{\ell\alpha\beta}(q_i + q_f)_\mu\ , \tag{4.29}$$

where the μ and ℓ on the ρ are its 4 - vector and isospin indices, respectively.

To define the magnetic $\rho\Lambda\Sigma$ coupling constant, $g'_{\rho\Lambda\Sigma}$, we write for the magnetic part of the $\rho\Lambda\Sigma$ interaction

$$H_{mag} = \frac{g'_{\rho\Lambda\Sigma}}{2(M_\Lambda + M_\Sigma)}\ (\bar{\Lambda}\sigma_{\mu\nu}\vec{\Sigma} + \vec{\bar{\Sigma}}\sigma_{\mu\nu}\Lambda) \cdot (\partial_\mu \vec{\rho_\nu} - \partial_\nu \vec{\rho_\mu})\ , \tag{4.30}$$

corresponding to a vertex factor of

$$i \frac{g'_{\rho\Lambda\Sigma}}{(M_\Lambda + M_\Sigma)} \sigma_{\nu\lambda} k_\lambda \delta_{\ell j} \cdot \qquad (4.31)$$

Application of Feynman's rules to the diagram of Figure 4.3 then yields for the S – matrix element

$$S_{fi} = -i(2\pi)^4 \delta^{(4)}(q_f + p_f - q_i - p_i) \sqrt{\frac{M_\Lambda M_\Sigma}{4\omega_i \omega_f E_i E_f}} \cdot \qquad (4.32)$$

$$\cdot \frac{g_{\rho\pi\pi} g'_{\rho\Lambda\Sigma}}{M_\Lambda + M_\Sigma} \frac{\bar{u}_\Sigma^{(\ell_s)}(\vec{p_f}) \left[(q_i + q_f)_\mu \sigma_{\mu\lambda} k_\lambda\right] u_\Lambda^{(r)}(\vec{p_i})}{k^2 + m_\rho^2} \epsilon_{j\alpha\beta} \cdot$$

To analyze the spinology, we first note that

$$\bar{u}_\Sigma(\vec{p_f}) \left[\sigma_{\mu\lambda} (p_i - p_f)_\lambda\right] u_\Lambda(\vec{p_i}) \qquad (4.33)$$

$$= \bar{u}_\Sigma(\vec{p_f}) \left[2\bar{M}\gamma_\mu + i(p_i + p_f)_\mu\right] u_\Lambda(\vec{p_i}),$$

where

$$\bar{M} \equiv \frac{M_\Lambda + M_\Sigma}{2} \quad . \tag{4.34}$$

Then, since $k = p_i - p_f$,

$$\bar{u}_\Sigma(\vec{p_f}) \left[(q_i + q_f)_\mu \sigma_{\mu\lambda} k_\lambda \right] u_\Lambda(\vec{p_i})$$

$$= \bar{u}_\Sigma(\vec{p_f}) \left[4\bar{M} \not{q} + i (q_i + q_f)(p_i + p_f) \right] u_\Lambda(\vec{p_i}) . \tag{4.35}$$

$(q_i + q_f) \cdot (p_i + p_f)$ being equal to $(u - s)$, we have, in the notation of (3.1),

$$T = \frac{g_{\rho\pi\pi} g'_{\rho\Lambda\Sigma}}{2\bar{M}} \left[\frac{-(u - s) + 4\bar{M} i \not{q}}{t - m_\rho^2} \right] i\epsilon_{j\alpha\beta} \quad . \tag{4.36}$$

From (4.13), the amplitudes A_1 and B_1 for $I = 1$ are thus

$$A_1 = \sqrt{2} \frac{g_{\rho\pi\pi} g'_{\rho\Lambda\Sigma}}{2\bar{M}} \frac{u - s}{t - m_\rho^2} \tag{4.37a}$$

$$B_1 = \sqrt{2} \frac{g_{\rho\pi\pi} g'_{\rho\Lambda\Sigma}}{2\bar{M}} \frac{4\bar{M}}{t - m_\rho^2} \quad . \tag{4.37b}$$

$\dfrac{u - s}{t - m_\rho{}^2}$, when written in terms of s and t alone, is

$$\frac{u - s}{t - m_\rho{}^2} = \frac{\Sigma_{12} - 2s - m_\rho{}^2}{t - m_\rho{}^2} - 1 \; , \qquad (4.38)$$

so we see that A_1 involves one of those off-shell pieces discussed previously. We will keep this piece temporarily to show what it leads to, and drop it at the end. From (3.5),

$$f_{1,2} = \sqrt{2} \; \frac{g_{\rho\pi\pi} g'_{\rho\Lambda\Sigma}}{4\pi} \; \frac{1}{2\bar{\bar{M}}} \; \frac{\sqrt{(E_\Lambda \pm M_\Lambda)(E_\Sigma \pm M_\Sigma)}}{2W} \; .$$

$$\cdot \left[\pm (\Sigma_{12} - 2s - m_\rho{}^2) + (W \mp \bar{M}) 4\bar{M} \right] \frac{1}{t - m_\rho{}^2}$$

$$+ \sqrt{2} \; \frac{g_{\rho\pi\pi} g'_{\rho\Lambda\Sigma}}{4\pi} \; \frac{1}{2\bar{\bar{M}}} \; \frac{\sqrt{(E_\Lambda \pm M_\Lambda)(E_\Sigma \pm M_\Sigma)}}{2W} \left[\mp 1 \right]. \quad (4.39)$$

Writing

$$t - m_\rho{}^2 = -2q_1 q_2 \left[x^\rho_s - \cos\theta \right] \; ; \; x^\rho_s = \frac{2\omega_1 \omega_2 - 2\mu^2 + m_\rho{}^2}{2q_1 q_2} \quad (4.40)$$

we find that the partial wave amplitudes are

$$
f^{I\,=\,1}_{\ell\pm} = -\sqrt{2}\;\frac{g_{\rho\pi\pi}g'_{\rho\Lambda\Sigma}}{4\pi}\;\frac{1}{M_\Lambda + M_\Sigma}\;\frac{1}{4Wq_1q_2}\,.
$$

$$
\cdot\left[\sqrt{(E_\Lambda + M_\Lambda)(E_\Sigma + M_\Sigma)}\left\{-2s+2(M_\Lambda + M_\Sigma)W - 2(M_\Lambda M_\Sigma - \mu^2)-m_\rho^2\right\}Q_\ell(x^\rho_s)\right.
$$

$$
\left.+\sqrt{(E_\Lambda - M_\Lambda)(E_\Sigma - M_\Sigma)}\left\{2s+2(M_\Lambda + M_\Sigma)W + 2(M_\Lambda M_\Sigma - \mu^2)+m_\rho^2\right\}Q_{\ell\pm1}(x^\rho_s)\right]
$$

$$
-\sqrt{2}\;\frac{g_{\rho\pi\pi}g'_{\rho\Lambda\Sigma}}{4\pi}\;\frac{1}{M_\Lambda + M_\Sigma}\;\frac{1}{2W}\left[\sqrt{(E_\Lambda + M_\Lambda)(E_\Sigma + M_\Sigma)}\,\delta_{\ell,0}\right. \qquad (4.41)
$$

$$
\left.-\sqrt{(E_\Lambda - M_\Lambda)(E_\Sigma - M_\Sigma)}\;\delta_{\ell\pm1,0}\right].
$$

The last line of this expression is the contribution of the off mass-shell part of A_1; it evidently has no dynamical singularities, and is to be disregarded when applying (4.41) to the calculation of the approximate $B_{12}(W)$.

Method (3) for getting Born exchange amplitudes
will be illustrated by the treatment of the Y_1^* exchange
force in $\pi\Lambda \rightarrow \pi\Lambda$ scattering (Fig. 4.4). We are after
the mass-shell parts of the invariant amplitudes for the
crossed (force) process, and to obtain these it is
sufficient to know the on-shell parts of the correspond-
ing amplitudes for the direct (resonance) process. These,
in turn, could be found if we knew all the partial waves
for the direct process near the resonance pole. But
these we do know; the only non-zero partial wave ampli-
tude, $f_{p_{3/2}}$, [22] is given near the resonance position by
the Breit - Wigner formula:

$$
f_{p_{3/2}} = \frac{-\Gamma(Y_1^* \rightarrow \pi\Lambda)\,\dfrac{M_{Y_1^*}}{q^*}}{s - M_{Y_1^*}^2 + i\,\Gamma_{tot}(Y_1^*)M_{Y_1^*}} \qquad . \qquad (4.42)
$$

Here $\Gamma_{tot}(Y_1^*)$ is the full width at half-maximum of the
Y_1^* resonance, $\Gamma(Y_1^* \rightarrow \pi\Lambda)$ is the partial width for $\pi\Lambda$
decay, q^* is the center of mass momentum for the $\pi\Lambda$ system
when the center of mass energy is $M_{Y_1^*}$, and $M_{Y_1^*}$ is of
course the Y_1^* mass. The zero-width approximation will
be made for the positions of all the resonances to be
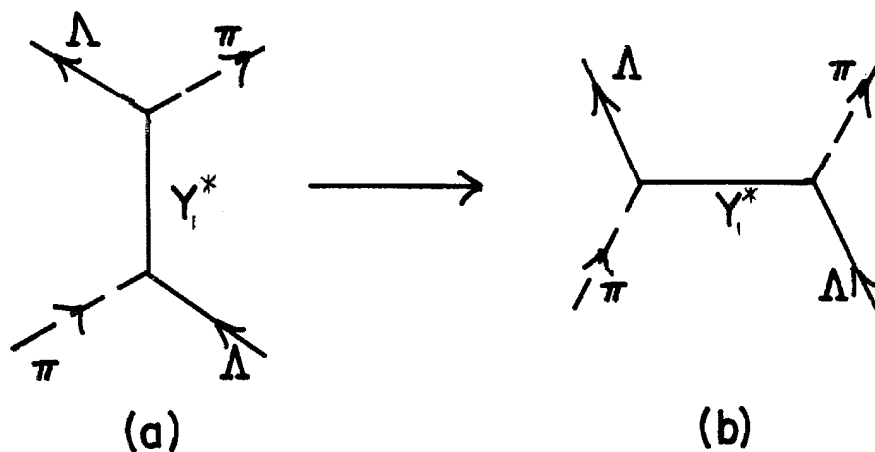
Figure 4.4. Crossing of the Y_1^* resonance pole (a)
to obtain the Y_1^* exchange force in $\pi\Lambda$ scattering (b).

dealt with; in this approximation (4.42) becomes

$$f_{P_{3/2}} = \frac{-\Gamma(Y_1^* \to \pi\Lambda)\frac{M^*}{q^*}}{s - M^{*2}} \equiv \frac{-R}{s - M^{*2}} , \qquad (4.43)$$

where $M_{Y_1^*}$ has been abbreviated to M^*.

Adding up the partial waves, we obtain for f_1
and f_2 near $W = M^*$

$$f_1 = f_{P_{3/2}} P_2'(\cos\theta) = 3\cos\theta\, f_{P_{3/2}} \qquad (4.44a)$$

$$f_2 = -f_{P_{3/2}} \, P_1'(\cos \theta) = -f_{P_{3/2}} \; , \qquad (4.44b)$$

with $f_{P_{3/2}}$ given by (4.43), and where

$$\cos \theta = 1 - \frac{u + M^{*2} - \Sigma}{2q^{*2}} \qquad (4.45)$$

when $W = M^*$. From the relations inverse to (3.5), the on-shell invariant amplitudes are then

$$\frac{A}{4\pi} = \left[\frac{M^* + M_\Lambda}{E^* + M_\Lambda} \, 3 \cos \theta + \frac{M^* - M_\Lambda}{E^* - M_\Lambda} \right] \frac{-R}{s - M^{*2}} \qquad (4.46)$$

$$\frac{B}{4\pi} = \left[\frac{3 \cos \theta}{E^* + M_\Lambda} - \frac{1}{E^* - M_\Lambda} \right] \frac{-R}{s - M^{*2}} \; , \qquad (4.47)$$

where E^* is the total energy of the Λ when $W = M^*$.

The mass-shell parts of the invariant amplitudes A^c, B^c for the Y_1^* exchange graph are now easily obtained by applying the crossing relations (4.3) to (4.46)-(4.47):

$$\frac{A^c}{4\pi} = \left[\frac{M^* + M_\Lambda}{E^* + M_\Lambda} \, 3x_u{}^* + \frac{M^* - M_\Lambda}{E^* - M_\Lambda} \right] \frac{-R}{u - M^{*2}} \qquad (4.48a)$$

$$\frac{B^c}{4\pi} = -\left[\frac{3x_u{}^*}{E^* + M_\Lambda} - \frac{1}{E^* - M_\Lambda}\right]\frac{-R}{u - M^{*2}} \ ; \qquad (4.48b)$$

$$x_u{}^* = \left| \ - \ \frac{s + M^{*2} - \Sigma}{2q^{*2}} \right. \qquad (4.49)$$

being the crossed version of $\cos \theta$, (4.45). The partial waves can then be projected out in the usual way. First,

$$f_1 = \frac{E + M_\Lambda}{2W}\left[\frac{3x_u{}^*(W - 2M_\Lambda - M^*)}{E^* + M_\Lambda} + \frac{(-W + 2M_\Lambda - M^*)}{E^* - M_\Lambda}\right]\frac{R}{u - M^{*2}} \qquad (4.50a)$$

$$f_2 = \frac{E - M_\Lambda}{2W}\left[\frac{3x_u{}^*(W + 2M_\Lambda + M^*)}{E^* + M_\Lambda} + \frac{(-W - 2M_\Lambda + M^*)}{E^* - M_\Lambda}\right]\frac{R}{u - M^{*2}}. \qquad (4.50b)$$

Then, since

$$u - M^{*2} = 2q^2\left[x_s{}^* - \cos \theta\right] \ ; \quad x_s{}^* = 1 - \frac{s + M^{*2} - \Sigma}{2q^2}, \qquad (4.51)$$

the partial wave amplitudes are

$$f_{\ell\pm} = \frac{\Gamma(Y_1{}^* \to \pi\Lambda)M^*}{q^*} \ \frac{1}{4Wq^2} \ .$$

$$\cdot \left\{ (E + M_\Lambda) \left[\frac{3x_u{}^*(W-2M_\Lambda-M^*)}{E^* + M_\Lambda} + \frac{(-W+2M_\Lambda-M^*)}{E^* - M_\Lambda} \right] Q_\ell(x_s{}^*) \right. \tag{4.52}$$

$$\left. + (E - M_\Lambda) \left[\frac{3x_u{}^*(W+2M_\Lambda+M^*)}{E^* + M_\Lambda} + \frac{(-W-2M_\Lambda+M^*)}{E^* - M_\Lambda} \right] Q_{\ell\pm1}(x_s{}^*) \right\} .$$

The partial wave amplitudes for the exchange diagrams of Figure 2.1 can all be written in the form

$$f_{\ell\pm}(W) = C \frac{1}{4Wq_iq_j} \left[\sqrt{(E_i + M_i)(E_j + M_j)}\ g(W)\ Q_\ell(x_s^e) \right.$$

$$\left. - \sqrt{(E_i - M_i)(E_j - M_j)}\,g(-W)\ Q_{\ell\pm1}(x_s^e) \right] . \tag{4.53}$$

The indices i and j are the final and initial channel numbers. C is a strength factor, which for $\pi\Sigma \rightarrow \pi\Sigma$ scattering includes a vector $\begin{pmatrix} a_2 \\ a_1 \\ a_0 \end{pmatrix}$ giving the relative strengths of the force in the various isospin states. The argument of the Q_ℓ functions, x_s^e, is determined by kinematics, including the mass of the exchanged particle e.

A convenient summary of the input amplitudes is then given by a tabulation of C, $g(W)$, and x_s^e for the

TABLE 4.1. Elements making up the Born exchange amplitudes. For use with formula (4.53). In the Y_1^* exchange in the reaction $i \longleftrightarrow j$, the symbol x_u^* stands for $[(2\omega_i^* \omega_j^* - 2\mu 2) \pm (s + M_{Y_1^*}^2 - \Sigma_{ij})]/2q_i^* q_j^*$. $\gamma(Y_1^* \rightarrow \pi\Lambda)$ is the $Y_1^* \rightarrow \pi\Lambda$ decay amplitude, whose square is the partial width, $\Gamma(Y_1^* \rightarrow \pi\Lambda)$. Similarly for $\gamma(Y_1^* \rightarrow \pi\Sigma)$. Kinematical symbols are defined in Appendix 1A.

Reaction	Exchange	Strength Factor C	g(W)	Argument of Q_ℓ Functions
$\pi\Lambda \longrightarrow \pi\Lambda$	Σ	$\dfrac{g_{\pi\Lambda\Sigma}^2}{4\pi}$	$W - 2M_\Lambda + M_\Sigma$	$x_s^\Sigma = 1 - \dfrac{s+M_\Sigma^2-\Sigma_1}{2q_1^2}$
	Y_1^*	$\dfrac{\Gamma(Y_1^* \rightarrow \pi\Lambda)\, M_{Y_1^*}}{q_1^{*}}$	$\dfrac{3x_u^*(W-2M_\Lambda-M_{Y_1^*})}{E_\Lambda^* + M_\Lambda} + \dfrac{(-W+2M_\Lambda-M_{Y_1^*})}{E_\Lambda^* - M_\Lambda}$	$x_s^{Y_1^*} = 1 - \dfrac{s+M_{Y_1^*}^2-\Sigma_1}{2q_1^2}$
$\pi\Sigma \longrightarrow \pi\Sigma$	Λ	$\begin{pmatrix}1\\-1\\1\end{pmatrix}\dfrac{g_{\pi\Lambda\Sigma}^2}{4\pi}$	$W - 2M_\Sigma + M_\Lambda$	$x_s^\Lambda = 1 - \dfrac{s+M_\Lambda^2-\Sigma_2}{2q_2^2}$
	Σ	$\begin{pmatrix}1\\1\\-2\end{pmatrix}\dfrac{g_{\pi\Sigma\Sigma}^2}{4\pi}$	$W - M_\Sigma$	$x_s^\Sigma = 1 - \dfrac{s+M_\Sigma^2-\Sigma_2}{2q_2^2}$
	Y_1^*	$\begin{pmatrix}1\\1\\-2\end{pmatrix}\dfrac{\Gamma(Y_1^* \rightarrow \pi\Sigma)M_{Y_1^*}}{2q_2^{*}}$	$\dfrac{3x_u^*(W-2M_\Sigma-M_{Y_1^*})}{E_\Sigma^* + M_\Sigma} + \dfrac{(-W+2M_\Sigma-M_{Y_1^*})}{E_\Sigma^* - M_\Sigma}$	$x_s^{Y_1^*} = 1 - \dfrac{s+M_{Y_1^*}^2-\Sigma_1}{2q_2^2}$

TABLE 4.1 - Continued

Reaction	Exchange	Strength Factor C	g(W)	Argument of Q_ℓ Functions
	Y_0^*	$\binom{1}{1}\binom{-1}{1}\dfrac{\Gamma(Y_0^*\to\pi\Sigma)M_{Y_0}^*}{3q_2^*(E_\Sigma^*+M_\Sigma)}$	$W - 2M_\Sigma - M_{Y_0}^*$	$x_s^{Y_0^*} = 1 - \dfrac{s+M_{Y_0^*}^2-\Sigma_2}{2q_2^2}$
	$\rho(\gamma_\mu$ coupling)	$\left(\begin{array}{c}-1\\1\\2\end{array}\right)\dfrac{g_{\rho\pi\pi}g_{\rho\Sigma\Sigma}}{4\pi}$	$W - M_\Sigma$	$x_s^\rho = 1 + \dfrac{m_\rho^2}{2q_2^2}$
	$\rho(\sigma_{\mu\nu}k_\nu$ coupling)	$\left(\begin{array}{c}-1\\1\\2\end{array}\right)\dfrac{g_{\rho\pi\pi}g'_{\rho\Sigma\Sigma}}{4\pi}\dfrac{1}{2M_\Sigma}$	$-2s + 4M_\Sigma W - 2/\beta_2 - m_\rho^2$	$x_s^\rho = 1 + \dfrac{m_\rho^2}{2q_2^2}$
$\pi\Lambda\to\pi\Sigma$	Σ	$\sqrt{2}\,\dfrac{g_{\pi\Lambda\Sigma}g_{\pi\Sigma\Sigma}}{4\pi}$	$W - M_\Lambda$	$x_s^\Sigma = \dfrac{(2\omega_1\omega_2-2\mu^2)-(s+M_\Sigma^2-\Sigma_{12})}{2q_1q_2}$
	Y_1^*	$-\dfrac{\gamma(Y_1^*\to\pi\Lambda)\gamma(Y_1^*\to\pi\Sigma)M_{Y_1}^*}{\sqrt{q_1^*q_2^*}}$	$\dfrac{3x_u^*(W-M_\Lambda-M_\Sigma-M_{Y_1}^*)}{\sqrt{(E_\Lambda^*+M_\Lambda)(E_\Sigma^*+M_\Sigma)}} + \dfrac{(-W+M_\Lambda+M_\Sigma-M_{Y_1}^*)}{\sqrt{(E_\Lambda^*-M_\Lambda)(E_\Sigma^*-M_\Sigma)}}$	$x_s^{Y_1^*} = \dfrac{(2\omega_1\omega_2-2u^2)-(s+M_{Y_1^*}^2-\Sigma_{12})}{2q_1q_2}$
	$\rho(\gamma_\mu$ coupling)	$-2\sqrt{2}\,\dfrac{g_{\rho\pi\pi}g_{\rho\Lambda\Sigma}}{4\pi}$	$W - \dfrac{M_\Lambda+M_\Sigma}{2}$	$x_s^\rho = \dfrac{2\omega_1\omega_2-2\mu^2+m_\rho^2}{2q_1q_2}$
	$\rho(\sigma_{\mu\nu}k_\nu$ coupling)	$-\sqrt{2}\,\dfrac{g_{\rho\pi\pi}g'_{\rho\Lambda\Sigma}}{4\pi}\dfrac{1}{M_\Lambda+M_\Sigma}$	$-2s+2(M_\Lambda+M_\Sigma)W - 2(M_\Lambda M_\Sigma-\mu^2)-m_\rho^2$	$x_s^\rho = \dfrac{2\omega_1\omega_2-2\mu^2+m_\rho^2}{2q_1q_2}$

various exchanges, Table 4.1.[23] The coupling constants which appear in some of the strength factors are defined in Table 4.2, which gives the Hamiltonian densities and vertex factors for the corresponding vertices.

We also record here the complete residue matrix R at the Σ pole in h in terms of the $\pi\Lambda\Sigma$ and $\pi\Sigma\Sigma$ coupling constants, as derived from consideration of the diagrams in Figure 4.5. With the abbreviations $g_{\pi\Lambda\Sigma} \equiv g_\Lambda$, $g_{\pi\Sigma\Sigma} \equiv g_\Sigma$, h near the pole is

$$h(W) = \frac{\begin{pmatrix} -\dfrac{g_\Lambda^2}{4\pi}\dfrac{1}{2} & \sqrt{2}\,\dfrac{g_\Lambda g_\Sigma}{4\pi}\dfrac{1}{2} \\[2em] \sqrt{2}\,\dfrac{g_\Lambda g_\Sigma}{4\pi}\dfrac{1}{2} & -2\,\dfrac{g_\Sigma^2}{4\pi}\dfrac{1}{2} \end{pmatrix}}{W - M_\Sigma} \equiv \frac{R}{W - M_\Sigma}. \tag{4.54}$$
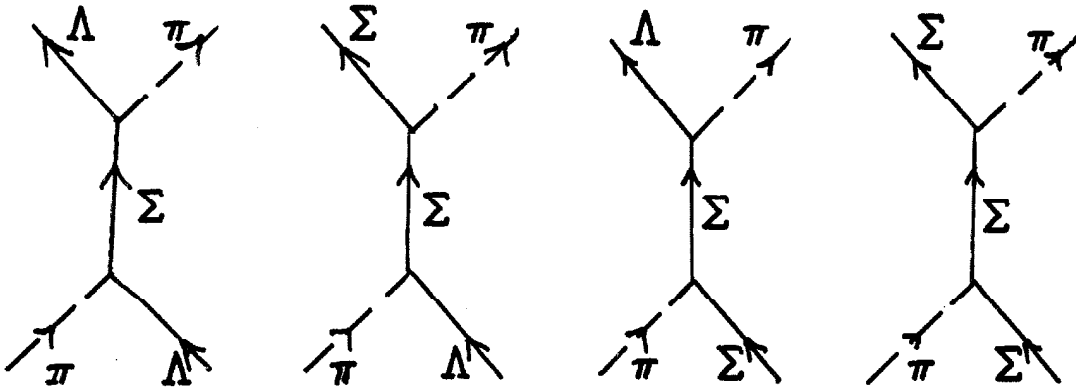

Figure 4.5. The processes corresponding to the Σ pole in the scattering matrix h.

TABLE 4.2. Definitions of the coupling constants in terms of Hamiltonian densities and vertex factors for the corresponding vertices. In the vertex pictures, the indices α, β, i, j, refer to isospin, while μ labels the 4-vector components. At the $\rho\pi\pi$ and $\rho\Sigma\Sigma(\gamma_\mu)$, $\rho\Sigma\Sigma(\gamma_\mu)'$ vertices, the ρ has been coupled to the normalized isospin current of the other particle. If the width $\Gamma(\rho \to 2\pi)$ is 100 Mev, then $g_{\rho\pi\pi}^2/4\pi = 2.0$.

Vertex	Hamiltonian Density	Picture	Vertex Factor
$\pi\Lambda\Sigma$	$H = ig_{\pi\Lambda\Sigma}(\bar{\Lambda}\gamma_5\vec{\Sigma}\cdot\vec{\pi} + \vec{\bar{\Sigma}}\cdot\vec{\pi}\gamma_5\Lambda)$		$ig_{\pi\Lambda\Sigma}\,\gamma_5\,\delta_{\ell\alpha}$
$\pi\Sigma\Sigma$	$H = g_{\pi\Sigma\Sigma}(\vec{\bar{\Sigma}}\times\gamma_5\vec{\Sigma})\cdot\vec{\pi}$		$g_{\pi\Sigma\Sigma}\,\gamma_5\,\epsilon_{\alpha\ell i}$
$\rho\pi\pi$	$H = -g_{\rho\pi\pi}\,\vec{\rho}_\mu\cdot(\vec{\pi}\times\partial_\mu\vec{\pi})$		$ig_{\rho\pi\pi}(q_i + q_f)_\mu\,\epsilon_{\ell\alpha\beta}$
$\rho\Sigma\Sigma(\gamma_\mu)$	$H = g_{\rho\Sigma\Sigma}\,\vec{\rho}_\mu\cdot(\vec{\bar{\Sigma}}\times\gamma_\mu\vec{\Sigma})$		$g_{\rho\Sigma\Sigma}\,\gamma_\mu\,\epsilon_{\ell j i}$
$\rho\Sigma\Sigma(\sigma_{\mu\nu}k_\nu)$	$H = -i\dfrac{g'_{\rho\Sigma\Sigma}}{4M_\Sigma}\vec{\rho}_\mu\cdot(\vec{\bar{\Sigma}}\times\sigma_{\mu\nu}\vec{\Sigma})\cdot(\partial_\mu\rho_\nu-\partial_\nu\rho_\mu)$		$\dfrac{g'_{\rho\Sigma\Sigma}}{2M_\Sigma}\sigma_{\mu\lambda}k_\lambda\,\epsilon_{\ell j i}$
$\rho\Lambda\Sigma(\gamma_\mu)$	$H = ig_{\rho\Lambda\Sigma}\,\vec{\rho}_\mu\cdot(\bar{\Lambda}\gamma_\mu\vec{\Sigma} + \vec{\bar{\Sigma}}\gamma_\mu\Lambda)$		$ig_{\rho\Lambda\Sigma}\,\gamma_\mu\,\delta_{\ell j}$
$\rho\Lambda\Sigma(\sigma_{\mu\nu}k_\nu)$	$H = \dfrac{g'_{\rho\Lambda\Sigma}}{2(M_\Lambda+M_\Sigma)}(\bar{\Lambda}\sigma_{\mu\nu}\vec{\Sigma} + \vec{\bar{\Sigma}}\sigma_{\mu\nu}\Lambda)\cdot(\partial_\mu\rho_\nu-\partial_\nu\rho_\mu)$		$i\dfrac{g'_{\rho\Lambda\Sigma}}{(M_\Lambda+M_\Sigma)}\sigma_{\mu\lambda}k_\lambda\,\delta_{\ell j}$

In approximating the input function $B_{ij}(W)$,
(3.25), on the basis of the Born amplitudes in Table 4.1,
it is both necessary and appropriate to improve on the
high energy behavior of $B_{ij}(W)$ by damping. In the first
place, the Y_1^* and ρ amplitudes $\dfrac{f_{p\frac{1}{2}}}{\rho_{ij}}$, because of the high
spin being exchanged, have an asymptotic behavior which
exceeds $\dfrac{1}{W}$. But $\dfrac{1}{W}$ is the least convergent behavior
possible for a true amplitude h_{ij} related to the unitary
S - matrix by (3.6) and (3.10). Thus the high spin
exchange amplitudes are plainly wrong at high energies,
and should be damped. Secondly, if the particles ex-
changed in the input graphs are all composite structures,
as we believe, then according to Reggeism the partial
wave exchange amplitudes will be tamer at high energies
than the un-Reggeized amplitudes of Table 4.1 - (4.53).
It is therefore appropriate to damp all the Born ampli-
tudes, not just those which violate unitarity, in order
to crudely represent the effects of Reggeism. The
simplest procedure is to damp all the input diagrams in
the same way, so as to introduce as few extra parameters
as possible. The most divergent exchange amplitudes are
those associated with the Y_1^* exchanges in $\pi\Lambda \longrightarrow \pi\Lambda$,
$\pi\Sigma \longrightarrow \pi\Sigma$, and $\pi\Lambda \longleftrightarrow \pi\Sigma$, which go like W at infinity. The
damping factor which will multiply all Born amplitudes

should therefore go like $\frac{1}{W^2}$ at ∞ in order to bring the Y_1^* amplitudes in line with the requirements of unitarity. It should also leave the inputs essentially unchanged in the low energy region around threshold. Lastly, it is desirable that the damping factor be singular only in places where B(W) is already supposed to be singular. (Its singularities will have to be far from $W \approx M_\Sigma$ for B(W) to be left relatively undisturbed there.)

A suitable factor by which to modify each Born amplitude in the reaction $i \leftarrow j$ is then

$$\frac{1}{1 + \frac{(W^2 - W_t^2)}{Z^2}} , \qquad (4.55)$$

where W_t is taken to be the $\pi\Lambda$ threshold $(M_\Lambda + \mu)$ for $ij = 11$, and the $\pi\Sigma$ threshold $(M_\Sigma + \mu)$ for $ij = 12, 21, 22$. For the experimental situation, $M_\Sigma > M_\Lambda$, this amounts to choosing W_t as the physical threshold for each process. One's intuitive guess is that a reasonable value for the cutoff parameter Z is something like 5 lambda masses, rather than 1 or 20. Z will have to be varied to verify that our results are qualitatively independent of it. The distant poles of the damping factor at $W = \pm i\sqrt{Z^2 - W_t^2}$

can be thought of as a very crude representation of the short-range forces we do not know how to take into account properly.

To summarize, our approximation to each of the driving functions B_{ij}, (3.25), is obtained by adding up all the amplitudes $f_{p_{\frac{1}{2}}} \equiv f_{1-}$ given in Table 4.1 - (4.53) for the reaction $i \leftarrow j$, dividing by the $p_{\frac{1}{2}}$ kinematical factor ρ_{ij}, (3.10), and multiplying by the damping factor (4.55):

$$B_{ij}(W) = \frac{\displaystyle\sum_{\substack{\text{all input} \\ \text{graphs for } i \leftarrow j}} f_{p_{\frac{1}{2}}}}{\rho_{ij}} \quad \frac{1}{1 + \dfrac{(W^2 - W_t^2)}{z^2}} \quad . \quad (4.56)$$

V. THE PLAN OF THE DYNAMICAL CALCULATIONS

The self-consistent Σ bound state that we antici-
pate getting will be characterized by three numbers: its
mass M_Σ, and its couplings to the $\pi\Lambda$ and $\pi\Sigma$ channels,
$g^2_{\pi\Lambda\Sigma}/4\pi$ and $g^2_{\pi\Sigma\Sigma}/4\pi$. These three parameters are then
to be compared with experiment. Now M_Σ is, of course,
very well established as 1193 Mev, but our knowledge of
the coupling constants is not at all precise. de Swart
and Iddings[24] have learned something about them by
simultaneously fitting hyperfragment data and the ob-
served $\Sigma^0/(\Sigma^0 + \Lambda)$ fractions in $\Sigma^- + p \rightarrow n + \Sigma^0$ (or Λ)
and in $\Sigma^- + d \rightarrow 2n + \Sigma^0$ (or Λ) with a static hyperon-
nucleon potential. In each state, this potential includes
a pion exchange contribution which depends on the
couplings of interest, and a phenomenological hard core
of (unfortunately) unknown radius. It was not possible
to determine the couplings closely, but the results
favored values in the ranges $17 < \frac{g^2_{\pi\Lambda\Sigma}}{4\pi} < 35$, $0 < \frac{g^2_{\pi\Sigma\Sigma}}{4\pi} < 3$.
However, the analysis could not rule out the possibility
that both $g^2_{\pi\Lambda\Sigma}/4\pi$ and $g^2_{\pi\Sigma\Sigma}/4\pi$ are about as large as
$g^2_{\pi NN}/4\pi$ $(= 15)$.

This ignorance about the coupling constants is
both fortunate and unfortunate. On the one hand, it will
be harder to test the numerical success of our model, but

on the other hand, the numbers we get for $g^2_{\pi\Lambda\Sigma}/4\pi$ and $g^2_{\pi\Sigma\Sigma}/4\pi$ will take on the aura of predictions.

One might ask whether the present calculation will predict the relative sign of $g_{\pi\Lambda\Sigma}$ and $g_{\pi\Sigma\Sigma}$. The answer is that this relative sign cannot be measured (This is explained in Appendix B.), so the model being developed here had better not (and does not) predict it.

The philosophy in this dynamical explanation of the Σ is to take the properties of all the other particles from experiment. For the Y_1^*, Y_0^*, and ρ, however, there are uncertainties in the experimental picture, and one must make guesses based on a combination of current theoretical ideas and any experimental information available. The uncertainties with which we have to contend are the following:

Y_1^* (1385): One can be fairly certain that the spin and parity are $3/2\,^+$. Although the data allow the assignment $5/2\,^-$ as well as $3/2\,^+$, [25] the Y_1^* mass fits so beautifully into the pattern expected for the masses of a unitary decuplet consisting of N^*(1238), Y_1^*(1385), Ξ^*(1530), and Ω^-(1686 ± 12), that it seems very likely that the Y_1^* has the same spin and parity as the N^*. Although not all experiments agree on the total width, it is reasonably safe to assume it to be 50 ± 10 Mev. [26]

However, all we know about the branching fraction $\Gamma(Y_1^* \to \pi\Sigma)/\Gamma_{total}(Y_1^*)$ is that it is not more than 8%.[27] It could be 0. Unitary symmetry predicts 7-16%, so we shall favor the experimental upper limit of 8%.

$Y_0^*(1405)$: There is almost no evidence at all on the spin-parity, which are, however, conjectured on theoretical grounds to be $\frac{1}{2}^-$. The total width is 50 Mev.[27]

$\rho(750)$: The spin-parity of 1^- is firmly established. Also, we know that $\Gamma(\rho \to 2\pi) \approx 100$ Mev, from which it follows that $g^2_{\rho\pi\pi}/4\pi = 2.0$. But the ρ-hyperon coupling strengths are not, of course, available from experiment.

What can we say about these ρ-hyperon coupling constants? Consider first the charge (γ_μ) couplings, $g_{\rho\Lambda\Sigma}$ and $g_{\rho\Sigma\Sigma}$. If we assume that the vector mesons dominate the electromagnetic charge form factors of all the baryons, and the pion form factor as well, then at zero momentum transfer the unitary symmetry coupling of the vector mesons to baryons must be pure F in order that the baryons have their observed charges, and $g_{\rho\Sigma\Sigma} = g_{\rho\pi\pi}$, while $g_{\rho\Lambda\Sigma} = 0$.[28] However, the couplings which stand in front of our partial wave amplitudes for ρ exchange correspond to a momentum transfer t on the mass shell of the

ρ, i.e., to $t = m_\rho{}^2$, not to $t = 0$. At $t = m_\rho{}^2$, $g_{\rho\Lambda\Sigma}$ may well be non-zero.

Turning to the magnetic couplings, $g'_{\rho\Lambda\Sigma}$ and $g'_{\rho\Sigma\Sigma}$, we note that something __is__ known about the related coupling $g'_{\rho NN}$, which measures the strength of the magnetic $(\sigma_{\mu\nu}k_\nu)$ coupling of ρ's to __nucleons__. Let us make the meaning of $g'_{\rho NN}$ definite by writing the magnetic ρNN interaction Hamiltonian as

$$H_{mag} = \frac{g'_{\rho NN}}{8M_N} \; \overline{N}\,\vec{\tau}\,\sigma_{\mu\nu}N \cdot (\partial_\mu\vec{\rho_\nu} - \partial_\nu\vec{\rho_\mu}), \qquad (5.1)$$

where M_N is the nucleon mass. In fitting N-N scattering with π, ρ, ω, etc. exchange, Scotti and Wong [29] found that

$$\frac{g'^2_{\rho NN}}{4\pi} = 49. \qquad (5.2)$$

Their fit, however, only determines this parameter to within a factor of about 2. They also found, again to within a factor of 2, that

$$\frac{g^2_{\rho NN}}{4\pi} = 5.1, \qquad (5.3)$$

where $g_{\rho NN}$ measures the ρ coupling to the nucleon isospin current. Specifically, $g_{\rho NN}$ is defined by writing for the ρNN charge coupling

$$H_{charge} = g_{\rho NN} \vec{\rho}_\mu \cdot i\bar{N}\gamma_\mu \frac{\vec{\tau}}{2} N .\tag{5.4}$$

A check on these numbers is provided by the e.m. form factors. The assumption that the ρ dominates both the electric and magnetic nucleon isovector form factors leads to the relation

$$\frac{g'_{\rho NN}}{g_{\rho NN}} = \mu^p_{(a)} - \mu^n_{(a)} = 3.70.\tag{5.5}$$

Here $\mu^p_{(a)}$ and $\mu^n_{(a)}$ are the proton and neutron anomalous magnetic moments, measured in units of the nuclear magneton $e/2M_N$. From (5.5) we should then have

$$\left(\frac{g'^2_{\rho NN}}{4\pi}\right) \Big/ \left(\frac{g^2_{\rho NN}}{4\pi}\right) = \frac{70}{5.1} ;\tag{5.6}$$

the Scotti and Wong ratio of $49/5.1$ is crudely consistent with this.

Once $g'_{\rho NN}$ is known, the desired couplings $g'_{\rho\Lambda\Sigma}$ and $g'_{\rho\Sigma\Sigma}$ may be related to it through unitary symmetry. We assume that the $\sigma_{\mu\nu}k_\nu$ coupling of the vector mesons to baryons follows the pattern prescribed by SU_3.[30] Unfortunately, there are two possible types of coupling, "F" and "D", so that the general unitary invariant coupling has the form (omitting factors such as $\sigma_{\mu\nu}k_\nu$)

$$H = G\left[d(\bar{B}VB)_{\substack{D-type\\pattern}} + f(\bar{B}VB)_{\substack{F-type\\pattern}}\right]; \quad d + f = 1. \qquad (5.7)$$

G functions as a strength parameter, while f and d indicate the relative proportions of the two types of coupling present. B, V, and $\bar{B}$ stand for baryon, vector meson, and anti-baryon; $(\bar{B}VB)$ is actually a long string of terms of the form $(\bar{p}\rho^0 p + \frac{2}{\sqrt{3}} \bar{\Sigma}^0 \rho^0 \Lambda - \frac{1}{\sqrt{3}} \bar{p}K^{*+} \Lambda + \ldots)$.

By referring to an explicit representation of the pattern schematized in (5.7),[30] one finds that $g'_{\rho NN}$, $g'_{\rho\Lambda\Sigma}$, and $g'_{\rho\Sigma\Sigma}$, as I defined them, are related to the parameters of (5.7) by

$$g'_{\rho NN} = 2G(d + f) = 2G \qquad (5.8a)$$

$$g'_{\rho\Lambda\Sigma} = \frac{2}{\sqrt{3}} Gd \qquad (5.8b)$$

$$g'_{\rho\Sigma\Sigma} = 2Gf \; . \tag{5.8c}$$

From Scotti and Wong's results, we can estimate that

$$\frac{G^2}{4\pi} = \frac{1}{4} \frac{g'^2_{\rho NN}}{4\pi} = \frac{1}{4} \, (49) = 12.25 \; . \tag{5.9}$$

The d/f mixing ratio may be estimated from the fact that the nucleon isoscalar anomalous magnetic moment is very small. If we take this moment to be zero, the assumption that the vector mesons dominate the baryon form factors then requires that the magnetic coupling $g'_{\omega NN}$ of the ω meson to nucleons vanish. Since

$$g'_{\omega NN} \propto - \frac{1}{\sqrt{3}} \, d + \sqrt{3}f \; ,$$

we have

$$d/f = 3 \; . \tag{5.10}$$

Combining the strength of (5.9) and the mixing ratio of 3, we come up with

$$\frac{g'_{\rho\Sigma\Sigma}}{4\pi} = 3.06 \tag{5.11a}$$

$$\frac{g'^{2}_{\rho\Lambda\Sigma}}{4\pi} = 9.18. \qquad (5.11b)$$

Apart from sign, then, the coupling combinations which
appear in our "magnetic ρ graphs" are ($g^{2}_{\rho\pi\pi}/4\pi = 2.0$)

$$\frac{g_{\rho\pi\pi}g'_{\rho\Sigma\Sigma}}{4\pi} = 2.48 \qquad (5.12a)$$

$$\frac{g_{\rho\pi\pi}g'_{\rho\Lambda\Sigma}}{4\pi} = 4.27. \qquad (5.12b)$$

From this discussion it is clear that although
we have some ideas on the ρ couplings, we have no definite
knowledge. The same is true of the Y_1^* branching
fraction. Therefore, the procedure followed in the
dynamical calculations was to vary all of these para-
meters, favoring values near the estimates above, and see
how the self-consistent solution depends on them. In
this way one can study in detail the influence of various
kinds of input forces on the self-consistent results, and
find out to what extent the main conclusions one would like
to draw are independent of the precise values of experi-
mental unknowns.

ρ exchange in $\pi\Sigma\to\pi\Sigma$, and all the input graphs
for $\pi\Lambda\leftrightarrow\pi\Sigma$, involve different vertices at the two sides
of the diagram (see Fig. 2.1), so that relative signs of
coupling constants are required to determine the signs of
these graphs. Thus, for example, we need the signs of
$g_{\rho\pi\pi}g_{\rho\Sigma\Sigma}/4\pi$, and $\gamma(Y_1^*\to\pi\Lambda)\gamma(Y_1^*\to\pi\Sigma)$, which we wouldn't
know even if the Y_1^* branching ratio had been accurately
determined. All these required signs are provided by
unitary symmetry combined with considerations of form
factors. And although unitary symmetry and the model in
which the vector mesons dominate the form factors are
only approximate, so that magnitudes predicted by these
theories are not accurate, the sign predictions are
probably quite reliable; the theories would have to be
very crude for them to be wrong.

The matter of signs in the $\pi\Lambda\leftrightarrow\pi\Sigma$ transition
amplitude deserves some explanation. Because the initial
and final states are different and involve independent
phase conventions, the overall sign of the transition
amplitude $h_{12} = h_{21}$ has no significance. However, the
relative signs of the $\pi\Lambda\leftrightarrow\pi\Sigma$ input graphs obviously do
make a difference, because these graphs have to be added
together. The relative signs of these graphs depend on
the signs of 4-way products of coupling constants:

$\text{sign}(g_{\pi\Lambda\Sigma}g_{\pi\Sigma\Sigma} \gamma(Y_1^* \to \pi\Lambda)\gamma(Y_1^* \to \pi\Sigma))$, and sign
$(g_{\pi\Lambda\Sigma}g_{\pi\Sigma\Sigma}g_{\rho\pi\pi}g'_{\rho\Lambda\Sigma})$ (assuming that $g_{\rho\Lambda\Sigma} = 0$). Note that,
unlike $g_{\pi\Lambda\Sigma}g_{\pi\Sigma\Sigma}$, whose sign is a matter of convention,
these products involve every particle an <u>even</u> number of
times. To get the signs of the 4-way products, we first
observe that if the ρ dominates both the π form factor
and the N isovector charge form factor, then sign
$(g_{\rho NN}/g_{\rho\pi\pi}) = +$. Then, from the assumption that the ρ
dominates both the electric and magnetic N isovector form
factors, sign $(g'_{\rho NN}/g_{\rho NN}) = +$, (5.5). The required sign
involving ρ's can therefore be replaced by sign
$(g_{\pi\Lambda\Sigma}g_{\pi\Sigma\Sigma}g'_{\rho NN}g'_{\rho\Lambda\Sigma})$. The unitary symmetry patterns for
the coupling of the pseudoscalar mesons, the vector mesons,
and the 3/2 $^+$ baryon decuplet to the 1/2 $^+$ baryon octet
can now be used to determine both required signs. This
is accomplished by choosing a set of conventions and then
picking off the signs of the individual factors in each
4-way product, one-by-one. In doing this, one must be
extremely careful to keep all the conventions consistent,
so that they will cancel out when the 4-way products are
formed.[31] The determination of sign $(g_{\pi\Lambda\Sigma}g_{\pi\Sigma\Sigma}g'_{\rho NN}g'_{\rho\Lambda\Sigma})$
involves two mixing ratios: d/f for the magnetic vector
meson-baryon coupling, which we have decided is positive,

(5.10), and d/f for the pseudoscalar meson-baryon coupling, which is thought to be positive (for the phase convention of reference 30) from the dynamical considerations of various authors, and from the experimental estimates for $g_{\pi\Lambda\Sigma}$ and $g_{\pi\Sigma\Sigma}$.[32] Sign $(g_{\pi\Lambda\Sigma}g_{\pi\Sigma\Sigma}\ \gamma(Y_1^*\to\pi\Lambda)\gamma(Y_1^*\to\pi\Sigma))$ depends only on the latter mixing ratio, the unitary symmetric coupling of the baryon decuplet to the baryon octet being unique. Given the mixing ratios, we conclude that

$$\text{sign}\ (g_{\pi\Lambda\Sigma}g_{\pi\Sigma\Sigma}\gamma(Y_1^*\to\pi\Lambda)\gamma(Y_1^*\to\pi\Sigma)) = +, \qquad (5.13a)$$

and

$$\text{sign}\ (g_{\pi\Lambda\Sigma}g_{\pi\Sigma\Sigma}g_{\rho\pi\pi}g'_{\rho\Lambda\Sigma}) = +. \qquad (5.13b)$$

In the ρ meson exchanges in $\pi\Sigma\to\pi\Sigma$, $\text{sign}(g_{\rho\pi\pi}g'_{\rho\Sigma\Sigma})$ = sign $(g'_{\rho NN}g'_{\rho\Sigma\Sigma})$ from form factors, and from SU_3 the latter sign is +. The remaining sign $(g_{\rho\pi\pi}g_{\rho\Sigma\Sigma})$ has already been said to be +.

ARE THE FORCES ATTRACTIVE?

The character of the forces in the $p_{\frac{1}{2}}$, $I = 1$ state, in the $\pi\Lambda$ or $\pi\Sigma$ channel, may be crudely estimated by looking at the elastic Born amplitudes at physical threshold. Except for a positive kinematical factor, the contribution (4.56) of each exchange diagram to the input function B_{ii} is just $(\sin \delta e^{i\delta})_{p_{\frac{1}{2}}, I = 1}$. Since a positive phase shift means that the wave function is being sucked in by the potential, a positive contribution to the threshold value of B_{ii} corresponds to an attractive force in channel i.

The threshold contributions, calculated from Table 4.1 for the experimental masses and for coupling strengths typical of those which were involved in the dynamical calculations, are given in Table 5.1. We see that in both channels the input forces add up to a net attraction. The existence of a bound state is thus a strong possibility; the dynamical calculations will show whether one is actually produced or not.

A more complete picture of all the input amplitudes, including those for $\pi\Lambda\leftrightarrow\pi\Sigma$, is given in Figs. 5.1 - 5.3.
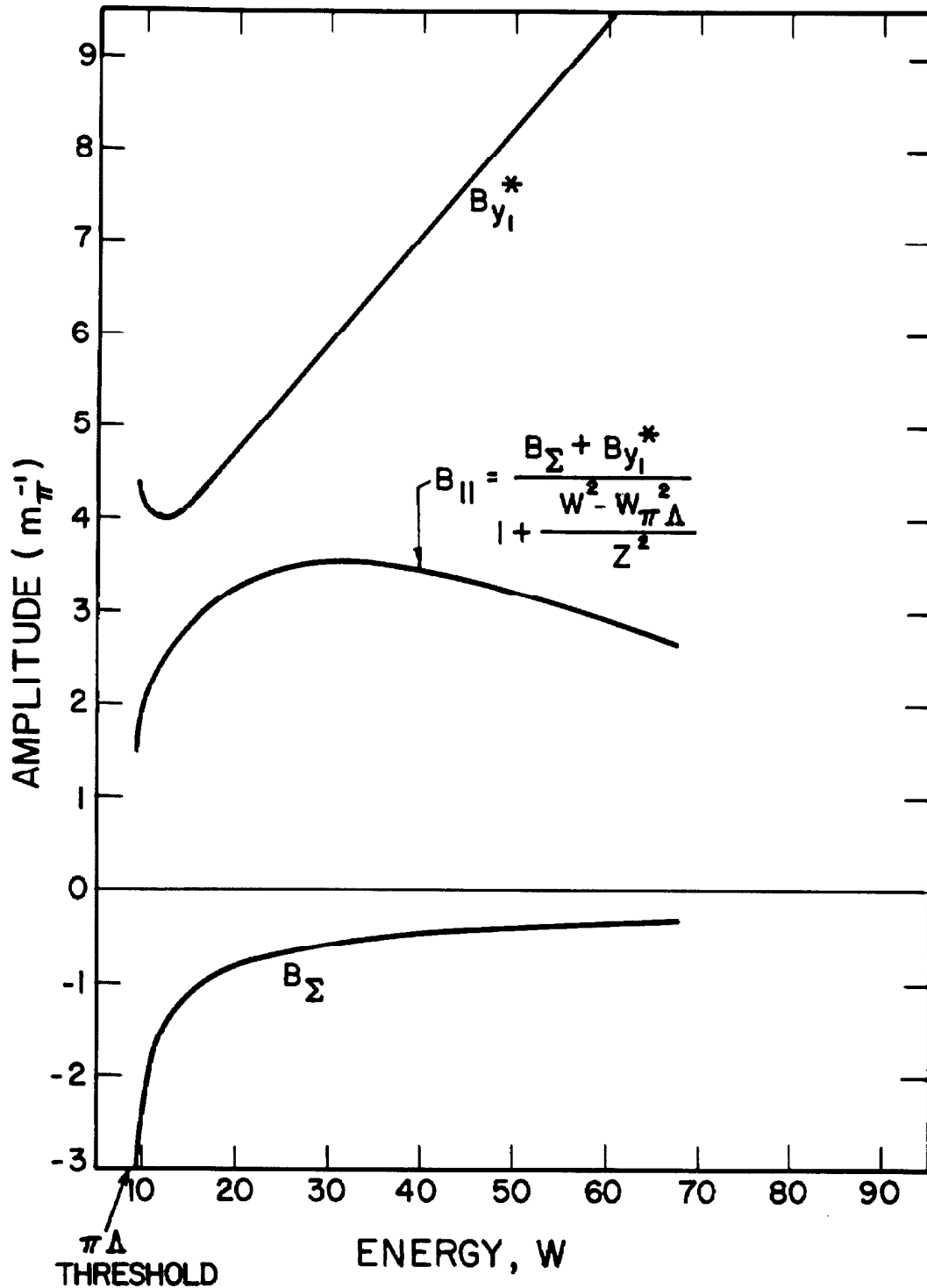
Figure 5.1. The $\pi\Lambda \to \pi\Lambda$ input Born amplitudes. B_{11} is the total damped contribution of the two exchange graphs, as per (4.56). B_Σ and $B_{Y_1^*}$ are the individual contributions, undamped. The curves were computed with the experimental masses, the couplings given in Table 5.1, and the cutoff $Z = 5M_\Lambda$.

Figure 5.2a

Figure 5.2, The $\pi\Sigma \to \pi\Sigma$ input Born amplitudes.

Figure 5.3. The $\pi\Lambda \longrightarrow \pi\Sigma$ input Born amplitudes.

TABLE 5.1. The input forces in the $\pi\Lambda$ and $\pi\Sigma$ channels, in the $p_{\frac{1}{2}}$, $I = 1$ state, at the physical thresholds. The numbers are based on the experimental masses, in pion mass units, and coupling strengths typically involved in the dynamical calculations.

$\pi\Lambda$ channel

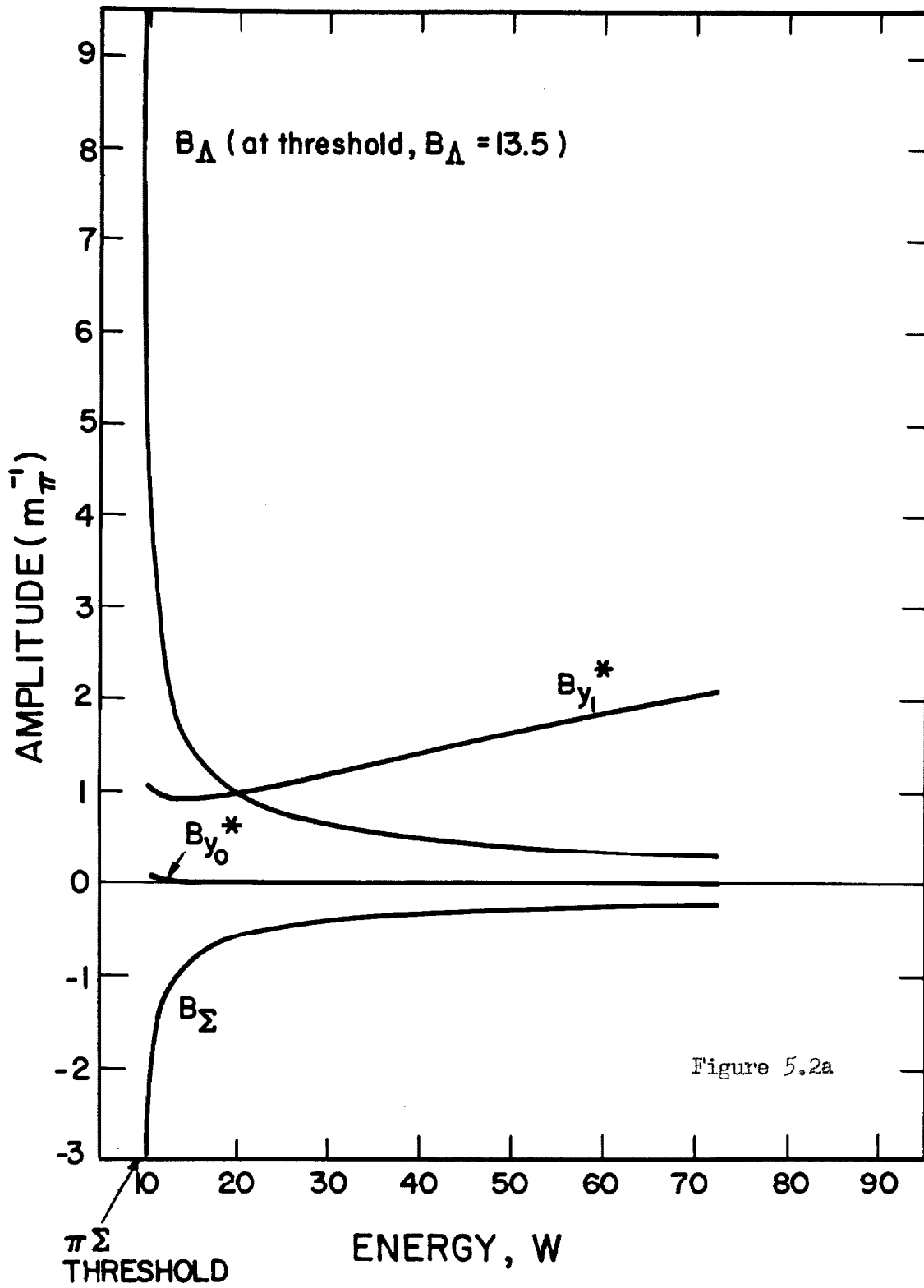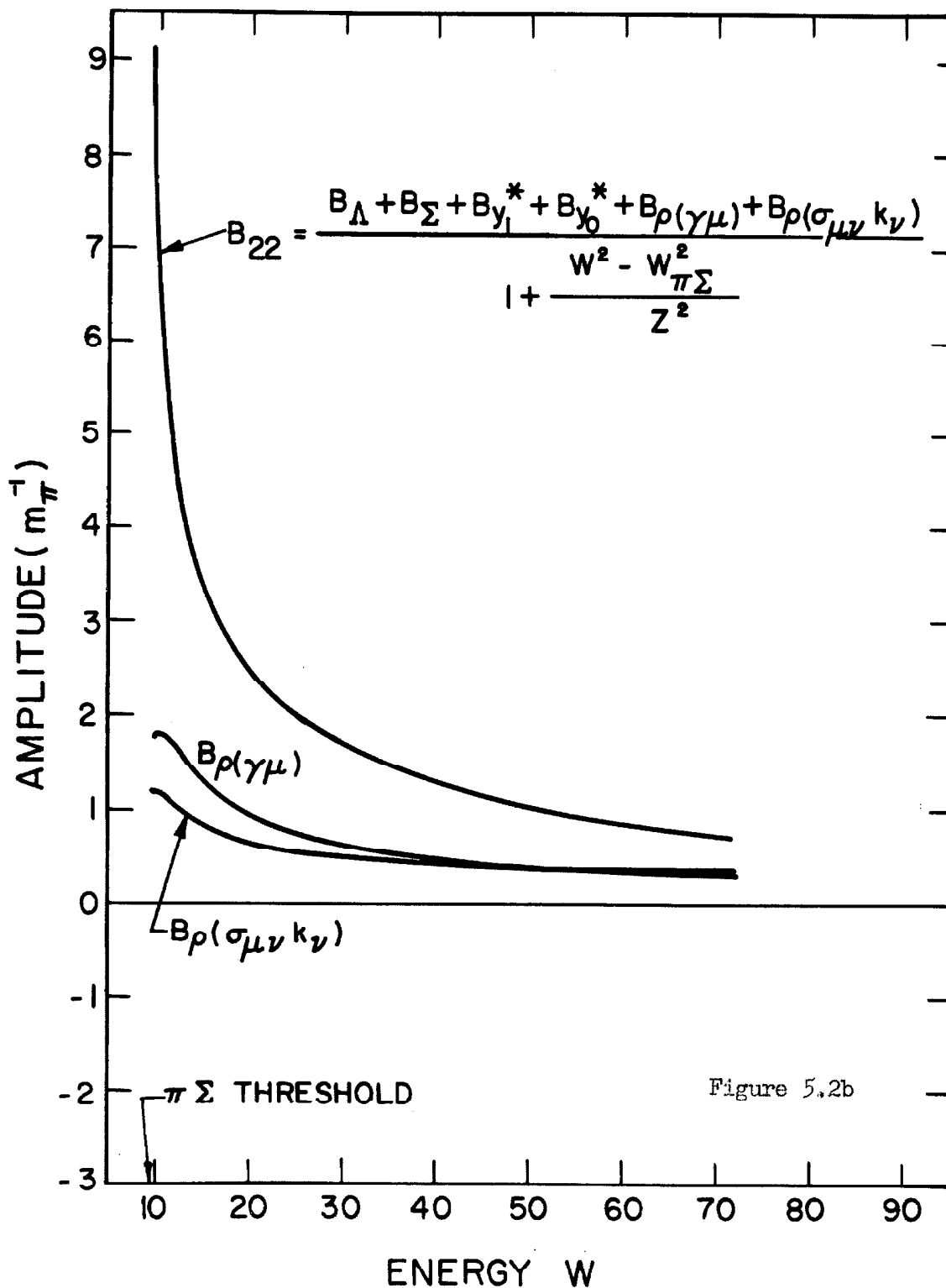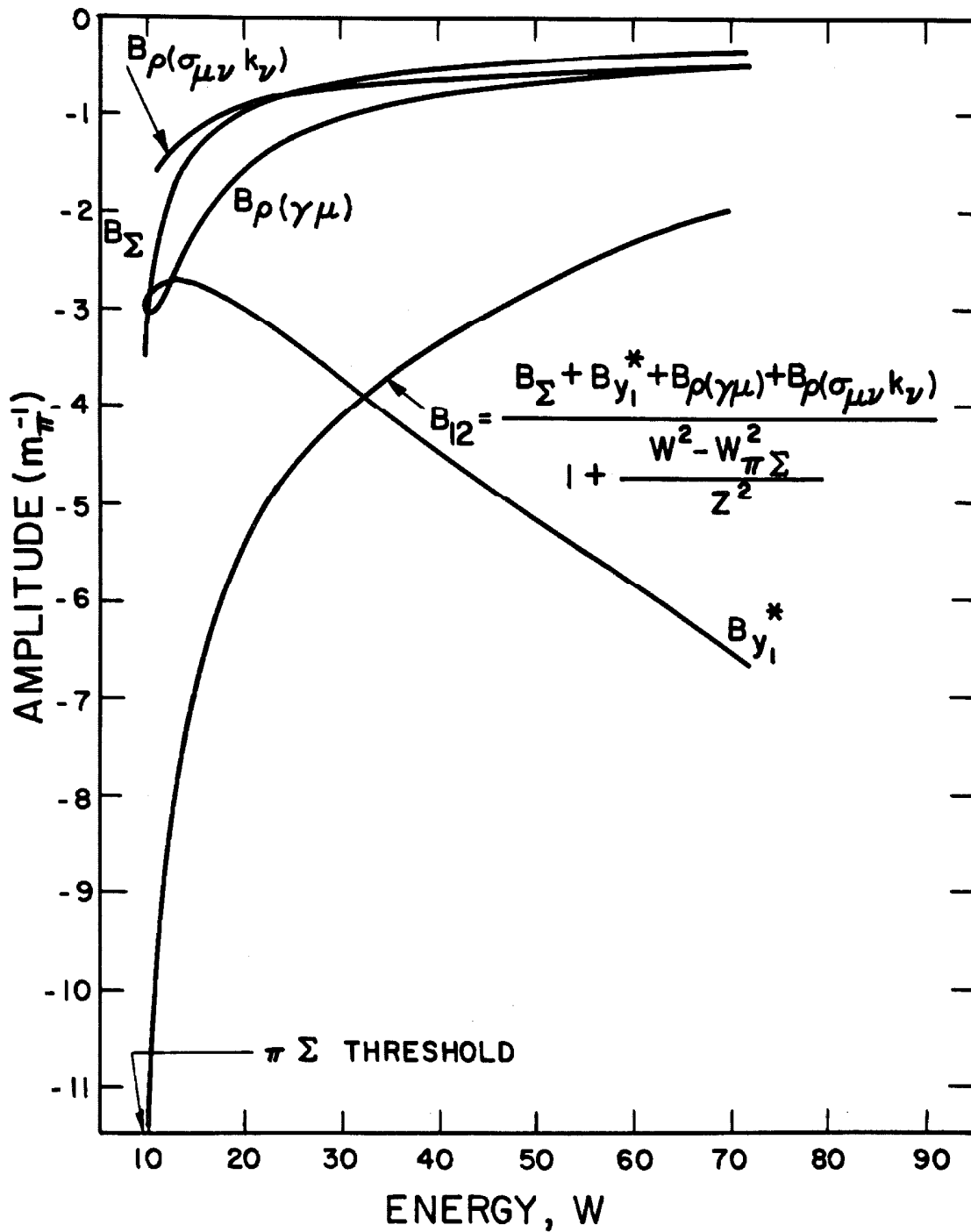| Exchange	Contribution to B_{11} at $\pi\Lambda$ Threshold	Which Equals	When
Σ	$-.111 \dfrac{g^2_{\pi\Lambda\Sigma}}{4\pi}$	-3.32	$\dfrac{g^2_{\pi\Lambda\Sigma}}{4\pi} = 30$
Y_1^*	$+14.1\ \Gamma(Y_1^* \to \pi\Lambda)$	$+4.70$	$\Gamma(Y_1^* \to \pi\Lambda) = 46$ Mev

Total : Attractive

$\pi\Sigma$ channel

Exchange	Contribution to B_{22} at $\pi\Sigma$ Threshold	Which Equals	When
Λ	$+.450 \dfrac{g^2_{\pi\Lambda\Sigma}}{4\pi}$	$+13.5$	$\dfrac{g^2_{\pi\Lambda\Sigma}}{4\pi} = 30$
Σ	$-.187 \dfrac{g^2_{\pi\Sigma\Sigma}}{4\pi}$	-3.74	$\dfrac{g^2_{\pi\Sigma\Sigma}}{4\pi} = 20$
Y_1^*	$+40.7\ \Gamma(Y_1^* \to \pi\Sigma)$	$+1.18$	$\Gamma(Y_1^* \to \pi\Sigma) = 4$ Mev
Y_0^*	$+.245\ \Gamma(Y_0^* \to \pi\Sigma)$	$+.09$	$\Gamma(Y_0^* \to \pi\Sigma) = 50$ Mev
$\rho(\gamma_\mu)$	$+.862 \dfrac{g_{\rho\pi\pi}g_{\rho\Sigma\Sigma}}{4\pi}$	$+1.72$	$\dfrac{g_{\rho\pi\pi}g_{\rho\Sigma\Sigma}}{4\pi} = 2.0$
$\rho(\sigma_{\mu\nu}k_\nu)$	$+.490 \dfrac{g_{\rho\pi\pi}g'_{\rho\Sigma\Sigma}}{4\pi}$	$+1.22$	$\dfrac{g_{\rho\pi\pi}g'_{\rho\Sigma\Sigma}}{4\pi} = 2.5$

Total: Attractive

As indicated in Fig. 2.1, the f^o resonance at
1250 Mev was initially considered for inclusion as a
force carrier. This particle would have been awkward
to handle, however, because of the controversy over its
quantum numbers, and the complete ignorance of the $f^o_{\Lambda\Lambda}$
and $f^o_{\Sigma\Sigma}$ coupling strengths. Assuming the f^o to be 2^+,
$I = 0$, I computed the f^o exchange amplitudes, and found
that for generous estimates of the $f^o_{\Lambda\Lambda}$ and $f^o_{\Sigma\Sigma}$ coupling
constants, the f^o forces were not large enough to have
any substantial effect on the numerical results. So the
f^o was dropped.

From Table 5.1 it is also apparent that the Y_o^*
force is negligible, if the Y_o^* really has $J^\pi = \frac{1}{2}^-$, as
has been assumed in calculating the force. The Y_o^* was
actually retained because it happened to have been in-
cluded in the original computer program, but it is of no
consequence.

In the search for a self-consistent bound state,
the properties of all particles other than the Σ are to
be kept fixed. In the case of the Y_1^* (and the unim-
portant Y_o^*), however, the question arises whether one
should hold fixed the $\pi\Sigma$ decay width, or the $Y_1^*_{\pi\Sigma}$
"coupling constant." If one were doing the ideal grand
bootstrap, the properties of all the particles would be

varied, and a simultaneous self-consistent solution
sought. Suppose that the approximate self-consistent
solution involved a Y_1^* with the correct mass, but a Σ
which is 100 Mev too light. The phase space available
to the Y_1^* for $\pi\Sigma$ decay would then be considerably greater
than it is in "real life", because of the (momentum)[3]
dependence of p - wave phase space near threshold. One
would guess that the $Y_1^*\pi\Sigma$ coupling constant would not
be as far away from reality as the phase space, so that
the Y_1^* of the bootstrap would have a much greater partial
width $\Gamma(Y_1^* \to \pi\Sigma)$ than in actuality. It therefore seemed
more sensible in the present, more restricted, bootstrap
to hold the $Y_1^*\pi\Sigma$ (and the $Y_0^*\pi\Sigma$) coupling strength,
rather than the decay width, constant.

Suitable coupling constants were defined by
taking for the $Y_1^*\pi\Sigma$ vertex a factor
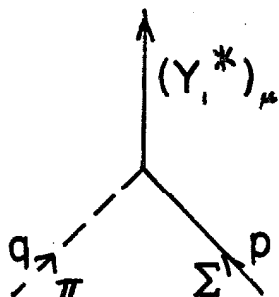
$$\frac{g_{Y_1^*\pi\Sigma}}{\mu}\,(q-p)_\mu \quad,$$

and for the $Y_0^*\pi\Sigma$ vertex a factor of
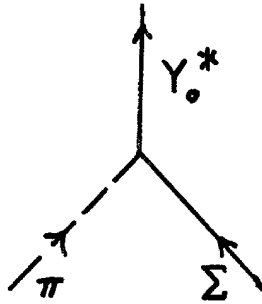
$$g_{Y_0^*\pi\Sigma} \, .$$

(The wave function for the spin 3/2 Y_1^* is a combination Dirac spinor - 4 vector, hence the 4-vector index "μ" in the vertex picture.) The relation between these couplings and the corresponding widths is, apart from constants which do not depend on the variable Σ mass,

$$\Gamma(Y_1^* \to \pi\Sigma) \propto \frac{g^2_{Y_1^*\pi\Sigma}}{4\pi} \quad q^{*3} \; (E^* + M_\Sigma) \tag{5.14a}$$

$$\Gamma(Y_0^* \to \pi\Sigma) \propto \frac{g^2_{Y_0^*\pi\Sigma}}{4\pi} \quad q^* \; (E^* + M_\Sigma) \, . \tag{5.14b}$$

In each of these expressions, q^* and E^* are the c.m. momentum and Σ energy, respectively, in the $\pi\Sigma$ channel when the total c.m. energy W is at the position of the relevant resonance. When varying the Σ mass in the dynamical calculations, we will therefore hold fixed the quantities

$$\frac{\Gamma(Y_1^* \rightarrow \pi\Sigma)}{q^{*3} \ (E^* + M_\Sigma)} \tag{5.15a}$$

$$\frac{\Gamma(Y_0^* \rightarrow \pi\Sigma)}{q^* \ (E^* + M_\Sigma)} \quad . \tag{5.15b}$$

VI. NUMERICAL PROCEDURES

The searches for self-consistent bound states corresponding to various combinations of the experimentally uncertain parameters were carried out numerically, using the California Institute of Technology's IBM 7040-7090 computer system. After the first s.c. (self-consistent) solution was found, the experimental parameters were varied slowly, so that one would always have a rough idea where the new s.c. solution would lie. This new s.c. point was then pinned down by calculating the output Σ mass and couplings, M_Σ^{out}, $G_\Lambda^{out} \equiv \dfrac{g^2_{\pi\Lambda\Sigma}}{4\pi}$, $G_\Sigma^{out} \equiv \dfrac{g^2_{\pi\Sigma\Sigma}}{4\pi}$, for each of 8 or more combinations of the corresponding inputs, M_Σ^{in}, G_Λ^{in}, G_Σ^{in}, and then using linear interpolation. A typical pass at the computer would involve the calculation of the outputs for about 4 combinations of the inputs. The program would then automatically decide on and perform any interpolations which might be appropriate, including interpolations between the latest results and the results of previous passes, the latter having been stored within the computer system.

To find the 3 outputs for a given set of inputs, the computer must:

1. Calculate the Born functions of Table 4.1.

2. Put them together to make the kernel of the integral equation for N, (3.29).

3. Solve this equation.

4. Integrate over N to get D, according to (3.27).

5. Search for a zero of the determinant of D in the region between $W = 0$ and the lower of the two thresholds.

6. If there is a zero, locate it precisely, and calculate the output couplings, using (3.35), (3.38), and (4.54).

Almost all the computing time is spent in solving the integral equation. The integrals over W' occurring there, which are all of the form

$$\int_{-\infty}^{-W_{\pi\Lambda}} + \int_{W_{\pi\Lambda}}^{\infty} \quad , \text{ or } \quad \int_{-\infty}^{-W_{\pi\Sigma}} + \int_{W_{\pi\Sigma}}^{\infty} \quad , \text{ are transformed into}$$

integrals from -1 to 1 by setting $x = \frac{W_{\pi\Lambda}}{W'}$, or $x = \frac{W_{\pi\Sigma}}{W'}$,

whichever is appropriate. From the integral equation

it follows that if $B \sim \frac{1}{W}$ at ∞, then $N \sim \frac{1}{W}$ at ∞ also, so

that the integrands in the integral equation go like $\frac{1}{W'^2}$.

Our particular change of variable results in an integrand

which is constant on either side of $x = 0$, which is

advantageous for numerical purposes.

Now a linear integral equation of the form

$$f(x) = \emptyset(x) + \int_{-1}^{1} K(x,x') \, f(x') dx'$$

for the unknown $f(x)$ in terms of the known $\emptyset(x)$ and

$K(x,x')$ can be approximated as

$$f(x) = \emptyset(x) + \sum_{j=1}^{n} h_j \, K(x,x_j) f(x_j)$$

by writing for the integral a Simpson's rule sum over

n mesh points, using the weight factors h_j from Simpson's

rule. In particular, this approximate equation is true

for x equal to any one of the mesh points x_i:

$$f(x_i) = \emptyset(x_i) + \sum_{j=1}^{n} h_j K(x_i,x_j) f(x_j) \; ; \; i=1,n. \quad (6.1)$$

But this is just a system of n linear equations for the n unknown $f(x_i)$, which can be solved by matrix inversion.

Our "N equation" is actually a system of four coupled integral equations for the four N_{ij}, but these equations can also be transformed into one big system of linear algebraic equations by applying Simpson's rule. The actual procedure was to make a <u>matrix</u> equation by grouping all the numbers representing N into a 2n x 2 matrix of the form

$$
\mathcal{N} = \begin{pmatrix} \begin{pmatrix} \uparrow \\ N_{11} \\ \downarrow \end{pmatrix} & \begin{pmatrix} \uparrow \\ N_{12} \\ \downarrow \end{pmatrix} \\ \begin{pmatrix} \uparrow \\ N_{21} \\ \downarrow \end{pmatrix} & \begin{pmatrix} \uparrow \\ N_{22} \\ \downarrow \end{pmatrix} \end{pmatrix} 2n \qquad . \qquad\qquad (6.2)
$$

Here the column vector

$$
\begin{pmatrix} \uparrow \\ N_{11} \\ \downarrow \end{pmatrix} ,
$$

for example, is the collection of the n numbers representing the function $N_{11}(W)$ at the n sample points where it is used in the integrals. The input B is made into a similar 2n x 2 matrix $\mathcal{B}$.

In analogy to the original 2 x 2 input matrix

$$B = \begin{pmatrix} B_{11}(W) & B_{12}(W) \\ B_{21}(W) & B_{22}(W) \end{pmatrix}$$

in channel space, we define a 2 x 2 kernel matrix $K(W,W')$ by

$$K_{ik}(W,W') = \frac{1}{\pi} \left[B_{ik}(W') - \frac{W-W_0}{W'-W_0} B_{ik}(W) \right] \frac{\Theta_k(W')}{W'-W} . \qquad (6.3)$$

Out of this matrix we then make a $2n \times 2n$ matrix

$$\mathcal{K} = \begin{pmatrix} \begin{pmatrix} K_{11} & \\ & \end{pmatrix} & \begin{pmatrix} & K_{12} \\ & \end{pmatrix} \\ \begin{pmatrix} K_{21} & \\ & \end{pmatrix} & \begin{pmatrix} & K_{22} \\ & \end{pmatrix} \end{pmatrix} \begin{matrix} n \\ \\ n \end{matrix} , \qquad (6.4)$$

in which the submatrix

$$\begin{pmatrix} & K_{12} \\ & \end{pmatrix} ,$$

for instance, is the collection of numbers representing $K_{12}(W,W')$ with W and W' running over the n sample points (W varies as you go down, W' as you go across). The integral equation for N, (3.29), is then approximately equivalent to the matrix equation[33]

$$\eta = \mathcal{B} + \mathcal{K}\eta,$$ (6.5)

where we have absorbed factors coming from the change of variable and from Simpson's rule into $\mathcal{K}$, and the usual rules of matrix multiplication are to be understood.

To solve (6.5), one must invert the matrix $\mathcal{M} = (\mathcal{I} - \mathcal{K})$, $\mathcal{I}$ being the 2n x 2n unit matrix. By varying the number of sample points, it was found that for most sets of inputs, a 76 x 76 matrix $\mathcal{M}$ is adequate for achieving 2% numerical accuracy in the output Σ mass and couplings. In rare cases, where conditions weren't too stable, a 100 x 100 matrix was used instead.

At this point one should perhaps mention the vital statistics. The calculation of M_Σ^{out}, G_Λ^{out}, G_Σ^{out} from a given set of inputs, using a 76 x 76 matrix, took about one minute on the 7090. The cost of computer time for the entire project was $2000.

VII. RESULTS

The dynamical calculations were begun with the "auxiliary parameters" (the experimentally unknown properties of the Y_1^* and ρ, and the cutoff Z) chosen as in Table 7.1. Except that the magnetic ρ - baryon couplings were initially turned off to cut down on the number of unknown parameters for the time being, the choices given in Table 7.1 represent our best guesses about the ρ and the Y_1^*. The remaining experimental inputs, which are well established and were used throughout the calculations, are collected in Table 7.2.

Given the initial auxiliary parameters, the first thing to see is whether reasonable values for M_Σ^{in}, G_Λ^{in}, and G_Σ^{in} do in fact lead to a bound state. It was found that they do! Next, one tries to vary the inputs until $(M_\Sigma^{out}, G_\Lambda^{out}, G_\Sigma^{out}) = (M_\Sigma^{in}, G_\Lambda^{in}, G_\Sigma^{in})$. A suitable procedure is to use several values of M_Σ^{in}, recording for each the value of M_Σ^{out} when $G_\Lambda^{out} = G_\Lambda^{in}$ and $G_\Sigma^{out} = G_\Sigma^{in}$, and then interpolate in the mass variable to find the fully self-consistent point. Following this method, I found that for each of a set of values of M_Σ^{in} exhausting the allowed range ($M_\Lambda - \mu$ to $M_\Lambda + \mu$), the M_Σ^{out}

TABLE 7.1. The initial choice of the auxiliary para-
meters. A listing of 8% for the Y_1^* branching fraction
means that as the Σ mass is varied, the Y_1^* "coupling",
(5.15a), is held fixed at a value corresponding to a
branching fraction of 8% when M_Σ has its experimental
value.

$$Z = 5M_\Lambda \qquad\qquad \frac{\Gamma(Y_1^* \rightarrow \pi\Sigma)}{\Gamma_{total}(Y_1^*)} = 8\%$$

$$\frac{g_{\rho\pi\pi}g_{\rho\Sigma\Sigma}}{4\pi} = 2.0 \qquad\qquad \frac{g_{\rho\pi\pi}g_{\rho\Lambda\Sigma}}{4\pi} = 0$$

$$\frac{g_{\rho\pi\pi}g'_{\rho\Sigma\Sigma}}{4\pi} = 0 \qquad\qquad \frac{g_{\rho\pi\pi}g'_{\rho\Lambda\Sigma}}{4\pi} = 0$$

TABLE 7.2. Well-established experimental numbers used
in the dynamical calculations. The mass of the pion
triplet, taken as 138 Mev, was used as the unit of mass.
The Σ mass of 1193 Mev is, of course, not included in
the table because M_Σ is to be "predicted" by the self-
consistency requirements.

Particle	Mass(Mev)	Total Width(Mev)
π	138	--
Λ	1115	--
Y_1^*	1385	50
Y_0^*	1405	50
ρ	750	100

corresponding to self-consistent couplings for that M_Σ^{in} was about 20% below M_Σ^{in}. Thus there is no self-consistent solution in the region we are allowed to search for this set of auxiliary parameters. (A bold extrapolation of the results suggests, however, that there is a self-consistent solution somewhere around 600 Mev.)

It was then discovered that, with all other inputs fixed, increases in $g_{\rho\Lambda\Sigma}$ with sign $(g_{\pi\Lambda\Sigma}g_{\pi\Sigma\Sigma}g_{\rho\pi\pi}g_{\rho\Lambda\Sigma}) = +$ produced increases in the output mass, without having much effect on the output couplings. $g_{\rho\Lambda\Sigma}$ was therefore turned on quite strongly in hopes of obtaining a self-consistent solution within the accessible mass region. And indeed, it was found that for

$$\frac{g_{\rho\pi\pi}g_{\rho\Lambda\Sigma}}{4\pi} = 2.5,$$

and the remaining parameters as in Table 7.1, there is a self-consistent bound state, with

$$M_\Sigma = 1158 \text{ Mev}$$
$$G_\Lambda = 40.1 \qquad\qquad (7.1)$$
$$G_\Sigma = 22.1 \quad .$$

(Let us adopt the convention that sign $(g_{\pi\Lambda\Sigma}g_{\pi\Sigma\Sigma}) = +$,
so that meaningful signs such as that of $g_{\pi\Lambda\Sigma}g_{\pi\Sigma\Sigma}g_{\rho\pi\pi}g_{\rho\Lambda\Sigma}$
may be indicated by writing $\dfrac{g_{\rho\pi\pi}g_{\rho\Lambda\Sigma}}{4\pi}$ as a positive or
negative number.)

Although we can expect departures from the value
$g_{\rho\Lambda\Sigma} = 0$ suggested by unitary symmetry for zero momentum
transfer, a value of 2.5 for $g_{\rho\pi\pi}g_{\rho\Lambda\Sigma}/4\pi$ seems rather
large, so that one would hope that adjustments of the
other parameters would allow $g_{\rho\Lambda\Sigma}$ to be cut back without
having the self-consistent solution slide down out of
range.

Before this question was investigated, however,
a measure was taken of the cutoff sensitivity of our
results. With the Y_1^* and ρ parameters fixed, the cut-
off Z was varied from 3.0 M_Λ to 6.5 M_Λ, and the corre-
sponding variation in the self-consistent solution (7.1)
was found (Fig. 7.1). While G_Λ is quite sensitive to
the cutoff, M_Σ and G_Σ vary by only about 10% as Z runs
from 3.5 M_Λ to 6.0 M_Λ. However, for Z = 3.0 M_Λ or Z =
6.5 M_Λ, there is no self-consistent solution in the
allowed window from 975 Mev to 1255 Mev. Thus our results
are certainly not entirely cutoff-independent, but a
satisfactory self-consistent solution definitely does
exist for Z throughout the reasonable range from 3.5 to

$6\,M_\Lambda$.

The variations of the Y_1^* and ρ properties were now begun. To get some idea of the effect of each experimental unknown on the self-consistent bound state, the parameters were varied more or less one at a time, using the values of Table 7.1, with $g_{\rho\pi\pi}g_{\rho\Lambda\Sigma}/4\pi$ replaced by 2.5, as a "central point." Besides this, an effort was made to find a set of parameters all close to the "best guesses" of Section V which leads to an s.c. solution in the accessible region. The cutoff Z was kept at $5M_\Lambda$ throughout.

Table 7.3a shows the effects of varying $g_{\rho\Sigma\Sigma}$ and $g_{\rho\Lambda\Sigma}$. Both M_Σ and G_Σ are quite insensitive to $g_{\rho\Sigma\Sigma}$, but M_Σ depends enough on $g_{\rho\Lambda\Sigma}$ to make it impossible to decrease $g_{\rho\pi\pi}g_{\rho\Lambda\Sigma}/4\pi$ much below 1.5. Table 7.3a also gives the value of $g^2_{\rho NN/4\pi}$, and the d/f ratio for the vector meson-baryon γ_μ-type coupling, which correspond according to unitary symmetry to each set of values for $g_{\rho\Sigma\Sigma}$ and $g_{\rho\Lambda\Sigma}$. The ρNN coupling is to be compared with the indication from N-N scattering that $g^2_{\rho NN/4\pi} = 5$, (5.3).

In the $g_{\rho\Sigma\Sigma}$ variations an interesting phenomenon was found which emphasizes that a bound state, once it exists, may greatly modify the effects expected of a
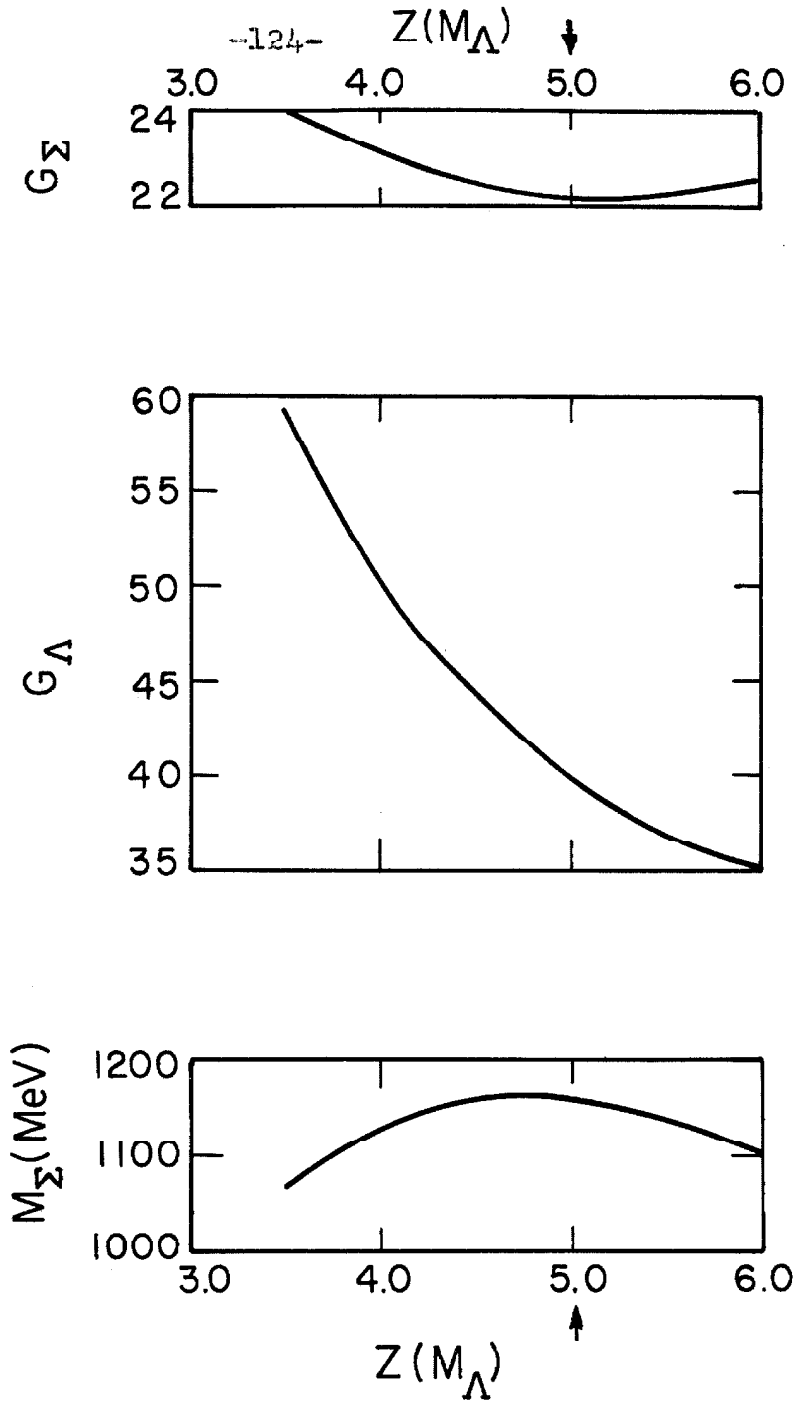
Figure 7.1. Sensitivity of the self-consistent Σ to the cutoff Z. "Experimental" inputs were $\Gamma(Y_1^* \Longrightarrow \pi\Sigma)/\Gamma_{total}(Y_1^*) = 8\%$, $g_{\rho\pi\pi}g_{\rho\Sigma\Sigma}/4\pi = 2$, $g_{\rho\pi\pi}g_{\rho\Lambda\Sigma}/4\pi = 2.5$, magnetic ρ couplings turned off. $Z = 5M_\Lambda$ is the standard cutoff used throughout the dynamical calculations.

TABLE 7.3. Self-consistent point as a function of the
experimental unknowns. The values of the inputs that
were kept fixed in obtaining each part of the table are
indicated beneath it. The decreases in $g_{\rho\Lambda\Sigma}$ in tables
(a) and (b) were made both to keep the s.c. point within
the accessible region (975 Mev to 1255 Mev) and to see
how small $g_{\rho\Lambda\Sigma}$ could be made. Table (a) gives the mixing
ratio and ρ_{NN} coupling which correspond, according to
unitary symmetry, to each combination of $g_{\rho\Sigma\Sigma}$ and $g_{\rho\Lambda\Sigma}$.

Self-Consistent Point

$\dfrac{g_{\rho\pi\pi}g_{\rho\Sigma\Sigma}}{4\pi}$	$\dfrac{g_{\rho\pi\pi}g_{\rho\Lambda\Sigma}}{4\pi}$	M_Σ(Mev)	G_Λ	G_Σ	d/f	$\dfrac{g_{\rho NN}^2}{4\pi}$
2.0	2.5	1158	40.1	22.1	2.16	20
2.5	2.5	1190	35.4	22.8	1.73	23
3.0	2.5	1222	31.2	23.6	1.45	27
3.0	1.5	1085	32.5	21.5	.86	16
3.5	1.5	1122	29.4	22.9	.74	19
4.0	1.5	1163	26.9	24.4	.65	22

$$\frac{\Gamma(Y_1^* \to \pi\Sigma)}{\Gamma_{total}(Y_1^*)} = 8\% \; ; \qquad \text{magnetic } \rho \text{ couplings turned off.}$$

(a)

TABLE 7.3 - Continued

$\dfrac{\Gamma(Y_1^* \rightarrow \pi\Sigma)}{\Gamma_{total}(Y_1^*)}$	$\dfrac{g_{\rho\pi\pi}g_{\rho\Lambda\Sigma}}{4\pi}$	Self-Consistent Point		
		M_Σ (Mev)	G_Λ	G_Σ
8%	2.5	1158	40.1	22.1
4%	2.5	1191	32.5	21.0
2%	2.5	1234	26.7	20.1
2%	1.5	1077	30.0	17.8
0%	1.5	1175	25.5	15.2

$$\frac{g_{\rho\pi\pi}g_{\rho\Sigma\Sigma}}{4\pi} = 2 \; ; \quad \text{magnetic } \rho \text{ couplings off.}$$

(b)

$\dfrac{g_{\rho\pi\pi}g'_{\rho\Sigma\Sigma}}{4\pi}$	$\dfrac{g_{\rho\pi\pi}g'_{\rho\Lambda\Sigma}}{4\pi}$	Self-Consistent Point		
		M_Σ (Mev)	G_Λ	G_Σ
0	0	1158	40.1	22.1
2.48	0	1144	35.8	24.5
2.48	2.0	1159	42.3	26.0
2.48	3.5	1177	48.0	26.7

$$\frac{\Gamma(Y_1^* \rightarrow \pi\Sigma)}{\Gamma_{total}(Y_1^*)} = 8\% \; ; \quad g_{\rho\pi\pi}g_{\rho\Sigma\Sigma}/4\pi = 2$$

$$g_{\rho\pi\pi}g_{\rho\Lambda\Sigma}/4\pi = 2.5$$

(c)

given input Born amplitude on the basis of Table 5.1.
ρ exchange with γ_μ coupling in the $\pi\Sigma$ channel has a
positive sign, so one would expect that if this ρ force
is strengthened by increasing $g_{\rho\pi\pi}g_{\rho\Sigma\Sigma}/4\pi$, leaving all
other inputs (including M_Σ^{in}, G_Λ^{in}, G_Σ^{in}) fixed, the output
mass would <u>decrease</u>. Instead, it increases! This
effect may be due to the fact that we are dealing with
a multi-channel system, but it could also occur in a
one channel situation. The effective input to the D
dispersion relation, which determines where the bound
state will lie through the condition determinant $(D) = 0$,
is N. N, in turn, is the raw input B <u>modified by D</u>
according to disc N = (discB)D. If the D matrix is very
different from I at the cuts of B, as it certainly is
for those cuts near the bound state, then the effective
input force represented by N can be rather different
from the original input B. It is perfectly possible
for an attraction to be turned into a repulsion.

Next the Y_1^* branching fraction was varied down
from its upper limit of 8% to 0(Table 7.3b). The s.c.
point depends only weakly on the branching fraction,
and any value between the experimental limits of 0%
and 8% can be very comfortably tolerated by our model.

Finally, the magnetic ρ couplings were turned on (Table 7.3c). Neither of these parameters has very much effect on the s.c. point either, except that when $g_{\rho\pi\pi}g'_{\rho\Lambda\Sigma}/4\pi$ was increased to 4.0, the behavior of the determinant of D started getting wild. This made it necessary to use bigger matrices in the numerical calculations, and the search for a self-consistent solution was abandoned as not being worth the money.

Several attempts were made to find acceptable combinations of the other parameters that would make it possible to knock $g_{\rho\pi\pi}g_{\rho\Lambda\Sigma}/4\pi$ down, but these never succeeded in decreasing this coupling below 1 without having the s.c. mass go below 975 Mev. 1, on the other hand, is not implausibly large; then too, not every conceivable combination was tried. Except for $g_{\rho\Lambda\Sigma}$, it was easy to put all the unknowns simultaneously near their guessed values and obtain a satisfactory self-consistent solution. For example,

$$\frac{\Gamma(Y_1^* \to \pi\Sigma)}{\Gamma_{total}(Y_1^*)} = 8\%$$

$$\frac{g_{\rho\pi\pi}g_{\rho\Sigma\Sigma}}{4\pi} = 2 \qquad\qquad \frac{g_{\rho\pi\pi}g_{\rho\Lambda\Sigma}}{4\pi} = 1.5$$

$$\frac{g_{\rho\pi\pi}g'_{\rho\Sigma\Sigma}}{4\pi} = 2.5 \qquad \frac{g_{\rho\pi\pi}g'_{\rho\Lambda\Sigma}}{4\pi} = 2.5$$

leads to an s.c. point with

$$M_\Sigma = 1045 \text{ Mev}$$
$$G_\Lambda = 44.3 \qquad\qquad (7.2)$$
$$G_\Sigma = 24.1.$$

VIII. CONCLUSIONS AND REMARKS

What can we say, now, about the Σ and about the method we have used? The method has two main difficulties: a computational complexity which limits one, in practice, to two channels, and a dependence on experimental quantities which aren't always very well known. On the other hand, our results were quite insensitive to the experimental unknowns, nor was the dependence on the cutoff very serious. Thus, in situations where it is sufficient to consider just one or two channels, and where the unknown parameters are either very few or not very influential, the techniques we have employed are quite adequate for testing the hypothesis that some particle is composite. It would clearly be advantageous, however, to have a computational scheme capable of handling many channels at a time, without grossly mistreating each one, and capable of simultaneously predicting the masses and couplings of several particles by the self-consistency requirement.

Now how about the Σ? Is it composite? Our results strongly suggest that it is. After all, we were able to obtain self-consistent dynamical Σ's

with reasonable masses and couplings for quite a wide range of values for the unknown parameters. The fact that we did not succeed in finding a self-consistent solution in the accessible mass range for $g_{\rho\Lambda\Sigma} = 0$ cannot be taken too seriously. For $g_{\rho\Lambda\Sigma} = 0$ <u>did</u> lead to output bound states, even though the output and input Σ parameters did not exactly match within the mass "window." Perhaps if one were to include some of the omitted effects, such as the $\overline{K}N$ channel or the higher resonance exchanges, this situation would be cleaned up. Then too, perhaps $g_{\rho\pi\pi}g_{\rho\Lambda\Sigma}/4\pi$ actually isn't very small.

Until not so long ago the relative $\Sigma\Lambda$ parity was an open question, and one might ask whether our model is capable of predicting this parity. Would our calculation have worked if we had assumed all other particles with their experimental properties, but then tried to make a "Σ" <u>with $J^\pi = \frac{1}{2}^-$</u> out of $\pi\Lambda$ and π"Σ"? In an effort to answer this question, the changes induced in the elastic Born amplitudes of Table 4.1 by a reversal of the Σ parity were figured out, and a new "threshold force" table analogous to Table 5.1 was prepared. Of course, the Born amplitudes were this time evaluated in the $s_{\frac{1}{2}}$ $\pi\Lambda$ state, and the $p_{\frac{1}{2}}$, $I = 1$ $\pi\Sigma$ state, where a $\frac{1}{2}^-$, $I = 1$ Σ would appear. In estimating the force strengths, the

Σ couplings were taken to be $g^2_{\pi\Lambda\Sigma}/4\pi = \frac{1}{2}$, $g^2_{\pi\Sigma\Sigma}/4\pi = 20$. These values represent a possible fit to the data on hyperfragments and $\Sigma^- + p$ reactions with the assumption of odd Σ parity.[34]

In the $\pi\Lambda$ channel, the forces turn out to be repulsive, although if we had taken $g^2_{\pi\Lambda\Sigma}/4\pi = 1$, we would have gotten attraction. In the $\pi\Sigma$ channel, there is an unambiguous huge attraction. Although a repulsion in one channel and a huge attraction in the other is certainly a strange looking situation, we cannot come to any definite conclusions on the basis of these considerations alone. To rule out odd $\Sigma\Lambda$ parity, we would have to show that the detailed dynamical calculations based on this assumption fail, or that odd $\Sigma\Lambda$ parity leads to repulsive forces in the $3/2^+$, $I = 1$ state where the Y_1^* resonance exists, etc.

Finally, we speculate on whether dynamical treatments of the Λ and the Y_1^* similar to that just given for the Σ, and based on the same channels and forces, are likely to work. Because of isospin, the Λ cannot be made out of π and Λ, so we would look for the Λ only in the $p_{\frac{1}{2}}$, $I = 0$ $\pi\Sigma$ state. With reasonable estimates for the couplings, the exchange amplitudes of Table 4.1

add up to a weak repulsion in this state at threshold.
This repulsion involves a contribution from Λ exchange,
however, and since the Λ force drops off very fast with
increasing energy above threshold (Fig. 5.2), the sum
of the forces will quickly turn into an attraction.
Thus a Λ bootstrap based on the $\pi\Sigma$ channel would probably
work, and may be attempted shortly.

The Y_1^* (1385) appears in the $P_{3/2}$, $I = 1$ $\pi\Lambda$
and $\pi\Sigma$ states. Estimating the forces as before, we find
at threshold an attraction in the $\pi\Lambda$ channel and a
repulsion in the $\pi\Sigma$ channel. But the latter is due
mostly to Λ exchange, and so the force in the $\pi\Sigma$ channel
will become only weakly repulsive, or even attractive,
not far above threshold. Since,experimentally, the Y_1^*
seems to couple much more strongly to the $\pi\Lambda$ channel
than to the $\pi\Sigma$, one might reasonably suppose that this
particle can be well understood in terms of the $\pi\Lambda$
channel alone. However, it would be nice if we could
explain the small branching fraction of the Y_1^*, and
for this reason dynamical calculations taking into
account both the $\pi\Lambda$ and $\pi\Sigma$ channels are planned.

APPENDIX A: SYMBOLS AND KINEMATICS

The following kinematical symbols have been employed.

μ = pion mass

M_Λ = Λ mass = M_1

M_Σ = Σ mass = M_2

$M_{Y_1^*}$ = Y_1^* mass

$M_{Y_0^*}$ = Y_0^* mass

m_ρ = ρ mass

$\pi\Lambda$ channel = channel 1

$\pi\Sigma$ channel = channel 2

Σ_i = $2(M_i^2 + \mu^2)$;   i = 1,2

$\sqrt{\beta}i$ = $(M_i^2 - \mu^2)$; i = 1,2

Σ_{ij} = $2\mu^2 + M_i^2 + M_j^2$; i,j = 1,2

W = total center-of-mass energy

s = W^2

q = pion 4-momentum, or magnitude of center of mass momentum, depending on context

E = baryon energy, usually in c.m.

ω = pion energy, usually in c.m.

θ = barycentric scattering angle

q, E, and ω will generally be indexed. When the letters
i and f are used together as indices, as in $q_i + q_f$, they
refer to the initial and final states of the reaction in
question. But when the letters i and j occur, together
or singly, they are channel numbers taking on the values
1(πΛ channel) and 2(πΣ channel). The indexed quantities
then stand for the center-of-mass variables in the
appropriate channel.

The various c.m. variables in channel i are re-
lated to the c.m. energy W by

$$4q_i^2 = s - \Sigma_i + \vartheta_i/s$$

$$(E_i \pm M_i) = \frac{(W \pm M_i)^2 - \mu^2}{2W}$$

$$E_i + \omega_i = W.$$

In a reaction in which the initial and final
pion 4-momenta are q_i and q_f, and the corresponding
baryon momenta p_i and p_f, the usual invariants are

$$s = -(q_i + p_i)^2$$

$$t = -(q_i - q_f)^2$$

$$u = - (q_i - p_f)^2 .$$

If the final and initial channels of the reaction are i and j, the invariants are related by

$$s + t + u = \Sigma_{ij} .$$

In terms of the c.m. variables,

$$s = W^2$$

$$t = -2q_i q_j \left(\frac{2\omega_i \omega_j - 2\mu^2}{2q_i q_j} - \cos \theta \right)$$

$$u = \Sigma_{ij} - s + 2q_i q_j \left(\frac{2\omega_i \omega_j - 2\mu^2}{2q_i q_j} - \cos \theta \right) .$$

For exchange of a particle of mass m_e in the t or u channel, the characteristic denominators are

$$t - m_e^2 = -2q_i q_j \left[\frac{2\omega_i \omega_j - 2\mu^2 + m_e^2}{2q_i q_j} - \cos \theta \right]$$

$$u - m_e^2 = 2q_i q_j \left[\frac{(2\omega_i \omega_j - 2\mu^2) - (s + m_e^2 - \Sigma_{ij})}{2q_i q_j} - \cos \theta \right]$$

Channel indices are sometimes omitted from c.m. quantities such as q_i, E_i, Σ_i when a reaction involving only one channel is being discussed. In describing diagrams with a resonance as an intermediate particle, we use q^*, E^*, and ω^* to denote the values of q, E, and ω when W equals the resonance mass.

The convention used for scalar products between 4-vectors is

$$p \cdot q = (\vec{p}, ip_0) \cdot (\vec{q}, iq_0) = \vec{p} \cdot \vec{q} - p_0 q_0 \ .$$

Our Dirac spinors for the Λ or Σ in spin state r obey $(\not{p} = \gamma_\mu p_\mu)$

$$(\not{p} - iM_\Lambda) \ u_\Lambda^{(r)}(\vec{p}) = 0,$$

$$(\not{p} - iM_\Sigma) \ u_\Sigma^{(r)}(\vec{p}) = 0,$$

and are normalized to

$$\bar{u}u = 1.$$

Our Hermitean γ-matrices satisfy

$$\gamma_\mu \gamma_\nu + \gamma_\nu \gamma_\mu = 2 \, \delta_{\mu\nu} \; ; \; \mu, \; \nu = 1,4.$$

In terms of the γ_μ, we define

$$\gamma_5 = \gamma_1 \gamma_2 \gamma_3 \gamma_4 \, ,$$

and

$$\sigma_{\mu\nu} \equiv \frac{\gamma_\mu \gamma_\nu - \gamma_\nu \gamma_\mu}{2i} \quad .$$

APPENDIX B: RELATIVE SIGNS

OF COUPLING CONSTANTS

The sign of any product of coupling constants
which mentions one or more particles an odd number of
times depends on conventions. For example, the sign of
$g_{\pi\Lambda\Sigma}g_{\pi\Sigma\Sigma}$ is not independent of conventions, in the way
that the relative sign of the electric charges of the
proton and electron (i.e., sign $(g_{\gamma pp}g_{\gamma ee})$) is, simply
because what one person calls "Λ" another may call "$-\Lambda$".
Of course, the product $g_{\pi\Lambda\Sigma}g_{\pi\Sigma\Sigma}$ can enter into more
involved combinations, such as $g_{\pi\Lambda\Sigma}g_{\pi\Sigma\Sigma}g_{\rho\pi\pi}g_{\rho\Lambda\Sigma}$, whose
signs are independent of conventions.

APPENDIX C: UNITARY SYMMETRY

AND MANY CHANNELS

Since the p and n are essentially the same
particle in two different charge states, and similarly
the π^+, π^0, and π^- are basically identical, it would
be nonsensical to construct a dynamical model of the p
which pictures this particle as a $\pi^0 p$ bound state, but
ignores the fact that it can also be made up out of
$\pi^+ n$. Now from the point of view of unitary symmetry, the
π and N are both parts of octets, so it would seem that
a bootstrap treatment of the N based on the πN channel
should include the ηN, $K\Lambda$, and $K\Sigma$ channels as well,
since the relationship between these channels and πN is
analogous to that between $\pi^+ n$ and $\pi^0 p$. The analogy is
not that good quantitatively, however, because the mass
splittings in a unitary supermultiplet are far greater
than those characteristic of an isospin multiplet. In
the N bootstrap, the influence of the ηN, $K\Lambda$, and $K\Sigma$
channels is depressed by the fact that their thresholds
are all 400 Mev to 600 Mev above that for πN (see Table
C.1), the nucleon bound state being below all the thres-
holds. Thus, there may be some grounds for neglecting

the ηN, $K\Lambda$, $K\Sigma$ channels; indeed, calculations involving this approximation have worked rather well. [13]

It is unfortunate that we have as yet no quick yet quantitative way of estimating the importance of a channel without actually including it in a full-fledged dynamical treatment; we can only make guesses based on meager experience. Considering only those channels which are related by unitary symmetry to the lowest in each case, Table C.1 is a crude attempt to compare the importance of higher channels in dynamical models of the N, Λ, Σ, and Ξ (the members of the $\frac{1}{2}^+$ baryon octet). For each particle, the table shows the separations between the higher thresholds and the lowest, and compares the strengths with which the particle couples to normalized isospin states in each of the channels. These couplings have been estimated by using, unmodified, the coupling pattern which holds in the limit of exact unitary symmetry.

One thing which stands out in Table C.1 is the relative unimportance of the higher channels in a dynamical model of the N, as contrasted with the situation for the Ξ, where the higher thresholds are both nearer and more strongly coupled. (Note also the in-

teresting fact that in both cases the coupling to the second lowest channel is very weak.) This is consistent with the fact that a single-channel bootstrap of the N works nicely, while a Ξ-strap based only on the $\pi\Xi$ channel would not work at all.

The Σ, with which we are dealing here in detail, is somewhere between the N and the Ξ. The first channel we have omitted, $\bar{K}N$, is probably not negligible, as has been said before. On the other hand, we have argued that inclusion of the $\bar{K}N$ channel would not destroy the Σ bound state we have found, so now we ask about the still higher channels, $\eta\Sigma$ and $K\Xi$. With respect to the separation between their thresholds and that of $\pi\Lambda$, these channels are comparable to the higher channels in the N problem. The couplings to $\eta\Sigma$ and $K\Xi$ are, however, rather larger than the corresponding couplings in the N case, though not quite as large as those for the Ξ. Thus, on the basis of the numbers in Table C.1 alone, one cannot say whether $\eta\Sigma$ and $K\Xi$ are more like the (apparently) relatively unimportant higher channels for the N, or the important higher ones for the Ξ.

It should be realized that while the considerations above are natural from the point of view of unitary

symmetry, the numbers in Table C.1 are not necessarily
the most relevant ones in deciding which channels should
be included and which can be left out. In the case of
the nucleon, for instance, the next two-particle channel
above πN is πN^*, and not any of the channels listed in
the table. From the large N^* width, the $N\pi N^*$ coupling
is evidently not small, so if one is wondering whether
a second channel should be included in an N-strap, he
should probably worry first about πN^*, not ηN, $K\Lambda$, or
$K\Sigma$. There is nothing in the dynamical equations which
can make a channel more important just because it is
related, according to unitary symmetry, to the lowest
channel.

TABLE C.1. Comparison of importance of higher channels for N, Λ, Σ, and Ξ. For each particle, the "Threshold Distance" column lists the distance from the lowest threshold to each of the higher ones. The couplings of each particle to normalized isospin states in the relevant channels have been estimated assuming two alternative plausible values for the f/d mixing ratio. The couplings are always normalized so that the lowest channel couples in with unit strength.

N

Channel	Threshold Distance (Mev)	Coupling (f/d=1/3)	Coupling (f/d=1/2)
πN	—	1	1
ηN	410	0	.11
KΛ	535	.5	.55
KΣ	610	.5	.33

Λ

Channel	Threshold Distance (Mev)	Coupling (f/d=1/3)	Coupling (f/d=1/2)
πΣ	—	1	1
K̄N	110	.82	1.02
ηΛ	335	.58	.58
KΞ	490	0	.20

TABLE C.1.- Continued

$$\underline{\Sigma}$$

Channel	Threshold Distance (Mev)	Coupling (f/d=1/3)	Coupling (f/d=1/2)
$\pi\Lambda$	-	1	1
$\pi\Sigma$	75	.82	1.22
$\overline{K}N$	185	.82	.61
$\eta\Sigma$	485	1	1
$K\Xi$	565	1.64	1.83

$$\underline{\Xi}$$

Channel	Threshold Distance (Mev)	Coupling (f/d=1/3)	Coupling (f/d=1/2)
$\pi\Xi$	-	1	1
$\overline{K}\Lambda$	155	0	.33
$\overline{K}\Sigma$	230	2	3
$\eta\Xi$	410	1	1.67

FOOTNOTES

1. F. Zachariasen, Phys. Rev. Letters 7, 112 (1961), and erratum, p.278.

2. E. Abers, thesis (unpublished), and M. Der-Sarkissian, private communication.

3. R. H. Dalitz, Strange Particles and Strong Interactions (Oxford, Bombay, 1962), pp.88-91.

4. H. Courant, et.al., Phys. Rev. Letters 10, 409 (1963), M. Watson, et.al., Phys. Rev. 131, 2248 (1963), and E. Beall, et.al., Phys. Rev. Letters 8, 75 (1962).

5. The general kinematics of $\pi\Lambda - \pi\Sigma$ scattering is given in R. Hwa and D. Feldman, Ann. of Phys. 21, 453 (1963). Except for there being two channels, the present situation is identical to that in the more familiar case of pion nucleon scattering, treated in G. Chew, M. Goldberger, F. Low, and Y. Nambu, Phys. Rev. 106, 1337 (1957).

6. Our kinematical symbols, as well as the principal relations between them, are summarized in Appendix A.

7. See, for example, S. Mandelstam, Phys. Rev. Letters 4, 84 (1960). The demonstrations in the literature will, in general, refer to amplitudes related to the partial wave S - matrix by different kinematical factors from the ones chosen here. The kinematical factors make no difference in the analytic continuation down below the physical region, so long as one is careful to work with amplitudes, such as our h_{ij}, which do not have kinematical branch points at the higher thresholds.

8. S. Frautschi and J. Walecka, Phys. Rev. 120, 1486 (1960).

9. R. Hwa and D. Feldman, reference 5. For discussion of anomalous thresholds, see R. Karplus, C. Sommerfield, and E. Wichmann, Phys. Rev. $\underline{114}$, 376 (1959), and S. Mandelstam, reference 7.

10. J. Bjorken, Phys. Rev. Letters $\underline{4}$, 473 (1960), and G. Chew and S. Mandelstam, Phys. Rev. $\underline{119}$, 467 (1960).

11. G. Chew, $\underline{S - Matrix\ Theory\ of\ Strong\ Interactions}$ (Benjamin, New York, 1961), p. 48.

12. R. Warnock, Bull. Am. Phys. Soc. $\underline{9}$, 116 (1964).

13. E. Abers and C. Zemach, Phys. Rev. $\underline{131}$, 2305 (1963).

14. J. Bjorken and M. Nauenberg, Phys. Rev. $\underline{121}$, 1250 (1960).

15. For an explication and application of the determinantal method, see F. Zachariasen and C. Zemach, Phys. Rev. $\underline{128}$, 849 (1962).

16. It is fairly evident that the unitarity condition as it stands is no longer true. For example, if one makes a perturbation expansion of h in powers of the coupling constant, $h = h^{(0)} + h^{(2)} + \ldots$, then (3.12) says that Im $h^{(2)} = 0$ down to the $\pi\Lambda$ threshold. But when a cut from Λ exchange, which is a second-order process, moves above the $\pi\Lambda$ threshold, this statement is manifestly false.

17. Generally speaking, the cut for a given exchange process moves to the right when either the external masses are increased, or the exchanged mass is decreased.

18. Nor does this crossing occur when the masses are related by the triangle condition $M_\Sigma^2 = M_\Lambda^2 + \mu^2$ commonly associated with anomalous thresholds.

19. Note that the troublesome singularity appears only in B_{22} ($\pi\Sigma \to \pi\Sigma$); no overlaps will occur in the other amplitudes.

20. Furthermore, the extended ND^{-1} method still guarantees that in approximate calculations the results will have the proper symmetry and threshold behavior, and be independent of the subtraction point, and that the output coupling constants will be real.

21. For spin 1 and spin 3/2 exchanges, an integral as in (3.25) over the discontinuities of the partial wave Born amplitude would not converge. In such cases, even the partial wave projection of the on-shell parts of A and B would not be a suitable contribution to the approximate $B_{ij}(W)$, and a damped version of this projection is taken instead.

22. The Y_1^* (1385) will be assumed to be $3/2^+$, as discussed in Section V.

23. f^0 exchange is not included in Table 4.1 because the small f^0 forces were neglected in the dynamical calculations, as discussed in Section V.

24. J. de Swart and C. Iddings, Phys. Rev. 128, 2810 (1962), and Phys. Rev. 130, 319 (1963). This work is discussed by R. H. Dalitz in the report of the 1962 International Conference on High-Energy Physics at CERN.

25. J. Shafer and D. Huwe, Phys. Rev. (to be published), and J. Shafer, J. Murray, and D. Huwe, Phys. Rev. Letters 10, 179 (1963).

26. A. H. Rosenfeld, private communication.

27. W. H. Barkas and A. H. Rosenfeld, Lawrence Radiation Lab. Report UCRL - 8030 Rev. (April, 1963 edition).

28. $g_{\rho\Sigma\Sigma} = g_{\rho\pi\pi}$, $g_{\rho\Lambda\Sigma} = 0$ also follows from Sakurai's hypothesis that the ρ couples universally to the isospin current.

29. A. Scotti and D. Wong, Phys. Rev. Letters 10, 142 (1963).

30. The meson octet-baryon octet coupling patterns
may be found in the back of J. J. Sakurai, "New
Mesons and Resonances in Strong Interaction
Physics - Theoretical," <u>Proceedings of the Inter-
national School of Physics "Enrico Fermi"</u>
(Varenna, Italy).

31. The author wishes to thank Dr. Y. Hara for pro-
viding a set of coupling patterns based on con-
sistent conventions for comparison purposes.

32. See, for example, R. H. Dalitz, Phys. Letters <u>5</u>,
53 (1963), and A. Martin and K. Wali, Phys. Rev.
<u>130</u>, 2455 (1963).

33. By contrast, the system of equations (6.1) for a
single integral equation have the form, in matrix
language: column vector = column vector + matrix.
column vector.(6.5), in which everything is a
multi-columned matrix, is a trivial generalization
of this.

34. J. de Swart and C. Iddings, Phys. Rev. <u>130</u>, 319
(1963).